Exact and approximate epidemic models on networks: theory and applications

Michael Taylor

Doctor of Philosophy
University of Sussex
December 2012

Declaration

I declare that this thesis was composed by myself and that the work contained therein is my own, except where explicitly stated otherwise in the text.

(*Michael Taylor*)

To Dad with much love

Abstract

This thesis is concerned with modelling the spread of diseases amongst host populations and the epidemics that result from this process. We are primarily interested in how networks can be used to model the various heterogeneities observable in real-world populations.

Firstly, we start with the full system of Kolmogorov/master equations for a simple Susceptible-Infected-Susceptible (SIS) type epidemic on an arbitrary contact network. From this general framework, we rigorously derive sets of ODEs that describe the exact dynamics of the expected number of individuals and pairs of individuals.

We proceed to use moment closure techniques to close these hierarchical systems of ODEs, by approximating higher order moments in terms of lower order moments. We prove that the simple first order mean-field approximation becomes exact in the limit of a large, fully-connected network. We then investigate how well two different pairwise approximations capture the topological features of theoretical networks generated using different algorithms.

We then introduce the effective degree modelling framework and propose a model for SIS epidemics on dynamic contact networks by accounting for random link activation and deletion. We show that results from the resulting set of ODEs agrees well with results from stochastic simulations, both in describing the evolution of the network and the disease. Furthermore, we derive an analytic calculation of the stability of the disease-free steady state and explore the validity

of such a measure in the context of a dynamically evolving contact network.

Finally, we move on to derive a system of ODEs that describes the interacting dynamics of a disease and information relating to the disease. We allow individuals to become responsive in light of received information and, thus, reduce the rate at which they become infected. We consider the effectiveness of different routes of information transmission (such as peer-to-peer communication or mass media campaigns) in slowing or preventing the spread of a disease.

Finally, we use a range of modelling techniques to investigate the spread of disease within sheep flocks. We use field data to construct weighted contact networks for flocks of sheep to account for seasonal changes of the flock structure as lambs are born and eventually become weaned. We construct a range of network and ODE models that are designed to investigate the effect of link-weight heterogeneity on the spread of disease.

Acknowledgements

First and foremost, I would like to humbly thank my PhD supervisor Dr Istvan Kiss. Without his constant support, guidance, encouragement, passion, expertise and understanding, this thesis would not exist. It has been an honour to be your first PhD student, and I know that there will be many more grateful students similarly acknowledging your support for many years to come.

I would also like to thank all the academics with whom I have had the privilege to collaborate and work over the last few years. In particular, I would like to thank Thomas House, Timothy Taylor, David Schley, Darren Green, Vasilis Hatzopoulos and Péter Simon for all their crucial contributions.

I am also very grateful to the Engineering and Physical Sciences Research Council for the financial support that has made this work possible.

My time at the University of Sussex would not have been as enjoyable and rewarding if not for the enthusiasm and hard work of both the mathematics faculty and also all the fantastic staff who help make the University the stimulating place it is. I would like to offer special thanks to Dorothy for many a relaxing lunchtime stroll to feed the ducks and chew the cud.

This thesis is, in some ways, the culmination of over ten years of University life and education. Along the way there have been many people who have helped keep me going, but I would like to offer special thanks to two people in particular. Firstly, without the humour, help and compassion of Dr Charles Fall, I would never have achieved as highly as I did in my undergraduate degree. Without that

success and the confidence that came with it, I would most likely not be writing this today. I would also like to thank Dr Jon Pitchford for running the excellent MRes course *Mathematics in the Living Environment* at the University of York. It was the most stimulating and inspiring course, and left with me a real passion for how mathematics can help us to understand the complex processes of the real world.

Outside of the academic world, I owe so much to my wonderful, amazing friends. There are far too many to name check here, but you know who you are and I love you all very much!

Finally, I need to thank my family. Firstly, my sisters Rebecca and Laura, for putting up with the odd grump or two over the years. Secondly, my Mum for everything, always. And, finally, my Dad, for being my best friend and for making me laugh so very much. I am so grateful to have such a wonderful family. These things don't come for free, they require the love and dedication of every single one of us, so thank you all, and I love you lots.

Contents

List of Figures

List of publications and author contributuons

1. P. L. Simon, M. Taylor, and I. Z. Kiss. Exact epidemic models on graphs using graph automorphism driven lumping. *J. Math. Biol.*, 62:479–508, 2011.

    - **P. L. Simon** worked on the derivation of population level ODEs from Markovian master equations, helped prove that the mean field equations equations became exact in the limit of a large, fully connected network, developed the method of graph automorphism driven lumping and wrote much of the text.
    - **M. Taylor** worked on the derivation of population level ODEs from Markovian master equations, helped prove that the mean field equations equations became exact in the limit of a large, fully connected network and wrote some of the text.
    - **I. Z. Kiss** worked on the derivation of population level ODEs from Markovian master equations, helped prove that the mean field equations equations became exact in the limit of a large, fully connected network, developed the method of graph automorphism driven lumping and supervised the work of Taylor.
    - *This paper informs the content of Chapters 2 and 3 of this thesis.*

2. V. Hatzopoulos, M. Taylor, P. L. Simon, and I. Z. Kiss. Multiple sources and routes of information transmission: Implications for epidemic dynamics. *Math. Biosci.*, 231:197–209, 2011.

    - **V. Hatzopoulos** coded and performed the simulations, helped develop the R_0 calculations produced the figures and wrote much of the text.
    - **M. Taylor** derived the pairwise ODEs and wrote some of the text.
    - **P. L. Simon** developed the R_0 calculations.
    - **I. Z. Kiss** developed the R_0 calculations, wrote some of the text and supervised the work of Hatzopolous and Taylor.
    - *This paper informs the content of Chapter 5 of this thesis.*

3. M. Taylor, P. L. Simon, D. M. Green, T. House, and I. Z. Kiss. From Markovian to pairwise epidemic models and the performance of moment closure approximations. *J. Math. Biol.*, 64:1021–1042, 2012.

    - **M. Taylor** derived the ODEs from the master equations, employed the various moment closures, coded and performed the necessary simulations, produced the figures and wrote most of the text.
    - **P. L. Simon** helped derive the ODEs from the master equations.
    - **D. M. Green** provided the various theoretical contact networks used in the simulations.
    - **T. House** derived the Improved Pairwise Approximation and provided some of the text.
    - **I. Z. Kiss** helped derive the ODEs from the master equations and supervised the work of Taylor.
    - *This paper informs the content of Chapters 2 and 3 of this thesis.*

4. M. Taylor, T. J. Taylor, and I. Z. Kiss. Epidemic threshold and control in a dynamic network. *Phys. Rev E*, 85:016103, 2012.

    - **M. Taylor** derived the dynamic effective degree model, coded and performed the necessary simulations, derived the next generation R_0 calculation, produced the figures and wrote the text.
    - **T. J. Taylor** helped derive the dynamic effective degree model and helped develop the next generation R_0 calculation.
    - **I. Z. Kiss** helped derive the dynamic effective degree model and supervised the work of Taylor and Taylor.
    - *This paper informs the content of Chapter 4 of this thesis.*

5. D. Schley, S. Whittle, M. Taylor, and I. Z. Kiss. Models to capture the potential for disease transmission in domestic sheep flocks. *Prev. Vet. Med.*, 106:174–184, 2012.

    - **D. Schley** supervised the collection of all the raw field-data, helped produce some of the figures, helped run the simulations, wrote much of the text and supervised the work of Whittle.
    - **S. Whittle** helped collect the field data and was involved in the simulations and write up.
    - **M. Taylor** derived and solved the network and ODE models, made all analytic calculations produced the figures and wrote some of the text.
    - **I. Z. Kiss** helped derive the network and ODE models and supervised the work of Taylor.
    - *This paper informs the content of Chapter 6 of this thesis.*

Chapter 1

Introduction

1.1 Background

The Greek physician Galen (c.129-c.216 AD), who was greatly influenced by the rational, patient-based approach to medicine pioneered by Hippocrates, became the most trusted health advisor in the Roman Empire. On the matter of dealing with plague, he is thought to have advised 'Cito, Longe, Tarde', which translates as 'Leave quickly, go far away, come back slowly'. This advice was still the most prevalent attitude when the plague epidemics of the 14^{th} century swept through Europe. The novel response of the wealthy merchants of Venice to the spread of plague was to force trading vessels to remain at anchor for 30 days prior to docking. This was later increased to 40 days and, thus, the modern word 'quarantine' was born from the Italian 'quaranta' [37]. This intuitive response to an epidemic remains a valid public health response to this day, but is disruptive and controversial. Over the last 30 years or so, real advances have been made in the understanding of how infectious diseases spread through populations, with contributions not just from the medical fraternity, but also with crucial contributions from fields such as sociology, mathematics, computer science and physics. For example, there has been much inter-disciplinary research published in response to recent outbreaks of Foot and Mouth disease [31, 65], SARS [3, 107] and Influenza

[32, 50].

Epidemiological control of infectious diseases falls broadly into two categories: developing vaccines and cures to directly combat the spread of disease at the level of the pathogen, or disrupting the contact networks or transmission vectors along which the pathogen spreads to indirectly combat the disease at the level of the hosts. This thesis is concerned with the second of these responses; in particular, it is concerned with how the structures of host populations can help or hinder the spread of a disease. Networks readily lend themselves to such study, as the connections between individuals naturally define a network. In this introductory chapter, we take a brief look at the development of mathematical epidemiology and how these advances have been used to help model the spread of diseases. We then look at some general modelling methods that will be used throughout this thesis and, finally, we give a brief overview of the following chapters.

1.2 Mathematical epidemiology

1.2.1 Compartmental disease models

The vast majority of epidemiological models are based on splitting the population into compartments based on the disease status of each individual, a technique that can be traced back to early work by Kermack & McKendrick [70] and, more recently, to that of Anderson & May [4]. The number of compartments and the way in which individuals move from one compartment to another depend upon the nature of the disease being modelled. For example, diseases that leave the infected individual with lifelong immunity upon recovery are described by the SIR model, whereby individuals are either Susceptible, Infectious or Recovered. This model is also valid for diseases that kill the individual, in which case the R compartment is better understood as Removed. The transition rates between compartments are specific to the disease being modelled and can be inferred from

field-data using statistical techniques [17, 57] but, in general, for a population of size N, the dynamics of SIR type epidemics are described as follows:

$$\dot{S}(t) = -\beta I \frac{S}{N}, \tag{1.1}$$

$$\dot{I}(t) = \beta I \frac{S}{N} - \gamma I, \tag{1.2}$$

$$\dot{R}(t) = \gamma I, \tag{1.3}$$

where βI represents the force of infection, which takes into account both the contact structure of the population and the virulence of the pathogen. In its most general form we write $\beta = pC(N)$, where $C(N)$ is the contact rate and p is the probability of infection per contact [21, 108]. Exactly what is defined as a contact depends upon the particular disease being modelled. For example, an airborne pathogen, such as influenza, has a different mode of transmission to STDs, such as HIV or chlamydia, and also to vector-borne diseases, such as malaria.

Diseases that allow repeat infections are described by the SIS model, in which individuals return to being Susceptible once they have recovered [21, 67]. This model is suitable for some STDs, such as chlamydia or gonorrhoea, and is described by the following ODEs:

$$\dot{S}(t) = -\beta I \frac{S}{N} + \gamma I, \tag{1.4}$$

$$\dot{I}(t) = \beta I \frac{S}{N} - \gamma I. \tag{1.5}$$

Other compartments can be added to describe different stages of infection, such as if the disease has a latent period during which the infected individual is asymptomatic ($SEIR$), or if the disease confers a limited immunity upon recovery but eventually the individual will again become Susceptible ($SIRS$), or if the infected individual enters treatment or contact-tracing programs ($SITS$), but SIR and

SIS type epidemics form the backbone of this thesis as well as the wider literature [21, 67].

1.2.2 Networks and epidemic models

It is clear from Eqs. (1.1 - 1.5) that, even in the case of homogeneous random mixing where each individual can come into contact with every other individual, the rate at which susceptible individuals become infected depends upon the number of infected individuals to whom they are linked. In other words, the spread of a disease from individual to individual depends upon the local structure of the host population. The science of networks has had a massive impact upon the study of epidemics. It dates back to work from the 1980s on the AIDS epidemic [79, 86] and has lately come to dominate the field. Recent papers detail the application of network theory to the study of epidemics [20, 53, 63], and highlight that there are two interrelated areas of study - the dynamics of networks and dynamics on networks. This thesis is primarily concerned with the latter of these two problems as it aims to explore how different network topologies help or hinder the spread of epidemics. Below is a brief overview of the three main approaches available when it comes to modelling epidemics on networks.

Exact master equations

Any given network, whether generated using a theoretical algorithm or constructed from real-world observations, can be described by a simple adjacency matrix which is then used in the construction of exact Kolmogorov/master equations, which describe the probability of the population being in each and every possible configuration.

In the most general sense, for a stochastic system denoted by Γ, where system states are given by $\Gamma^{\alpha}, \quad \alpha \in \{1, 2, \ldots, 2^N\}$ if an SIS dynamic on a network with N nodes is considered, the probabilities for the system being in each state are

Population size	Number of equations
3	8
5	32
10	1024
20	1048576
N	2^N

Table 1.1: Showing how the size of system of master equations, Eq. 1.6, scales with population size.

given by

$$\langle \dot{\Gamma^\alpha} \rangle = \sum_\beta T^{\alpha\beta} \langle \Gamma^\beta \rangle - \sum_\beta T^{\beta\alpha} \langle \Gamma^\alpha \rangle, \tag{1.6}$$

where T is a constant matrix of Poisson rates which also incorporates the network's adjacency matrix, β simply goes over all possible states and $\langle \cdot \rangle$ here denotes the probability of being in a particular state.

The solution of these master equations leads to an exact description of the dynamics of the full system. Indeed, some of the earliest work on epidemics on networks involved the solution of master equations for small, fully-connected networks [7]. However, since the system size of the master equations scales exponentially with population size, even with modern advances in computing power we are unable to numerically integrate these equations for realistic populations, as shown in Table 1.1. In addition, the exact master equation model is compared to other models in Table 1.2.

Stochastic simulation

As an alternative to solving master equations, individual-based stochastic simulations can be performed on the full network. Taking an average of a large number of such simulations remains the most viable way to explore dynamics on large, complex networks. Unfortunately, all information about rare events is lost in the averaging process, whereas if the master equation could be solved, the probability of any possible event could be calculated.

There are two methods of stochastic simulation that are used in this thesis. Firstly, discrete-time simulations can be performed by fixing a time step Δt and, at every time step, allowing every possible event - whether infection or recovery - to occur with a probability calculated from the various disease parameters, the current state of the network and the magnitude of Δt. The state of the system is updated at each time step and, due to testing each possible event within a particular time step, this discrete-time type of simulation is sometimes referred to as a synchronous simulation.

Synchronously updating simulations can be very efficient to implement in terms of coding complexity. However, allowing multiple events to occur simultaneously is not in keeping with the Markovian nature of stochastic models and hence Δt needs to be small enough to avoid this happening. An alternative simulation approach is to use what is known as a Gillespie algorithm [38], whereby the time to next event, T, is an exponentially distributed random variable chosen from an exponential distribution parameterised by R_{total}, where R_{total} is the rate of all possible transitions given the current status of all individuals. It follows that working out R_{total} amounts to summing all infection and recovery rates across the whole network. As the inter-event time is directly related to the total rate, large rates result in small inter-event times. Once the time to next event is determined, a single event out of all possible is chosen at random but proportionally to its rate. Due to the Markovian nature of this type of simulation, it is sometimes referred to as an asynchronous simulation.

Although asynchronous simulations are clearly in closer agreement with the Markovian nature of the master equations, they can sometimes be computationally prohibitive, especially for large networks with complicated dynamics and virulent epidemics, as multiple rates need storing and updating at each time step. As Danon *et al.* note [20], synchronous simulations are a viable alternative, and results converge with those obtained from asynchronous simulations, provided

Δt is small enough to make the mean number of events per time step close to one. During this thesis, both methods of simulation are used at different points and, whenever synchronous simulations have been employed, we always track the number of events per time-step to ensure a suitable Δt has been chosen.

Moment closure approximations

While stochastic simulations allow for a high degree of detail and heterogeneity, they are time consuming and offer no analytic insight into the underlying dynamics. While the master equations offer a full description of the system, they are not feasible for realistic population sizes. However, we can derive equations that describe the dynamics of the expected number of individuals. For SIS dynamics, we can describe the time evolution of the expected number of individuals as follows:

$$[\dot{S}](t) = \gamma[I] - \tau[SI], \tag{1.7}$$

$$[\dot{I}](t) = \tau[SI] - \gamma[I]. \tag{1.8}$$

where $[\cdot]$ represents population level expectations and $\tau = \beta/N$ is the per-contact transmission rate. In Chapter 2 we show that Eqs. (1.7 - 1.8) are exact at the level of individuals, but the system of equations does not form a closed set as clearly the number of individuals depends upon the distribution of (S, I) pairs. Similar equations can be derived to describe the evolution of the number of pairs, however the dynamics of the pairs depends upon the distribution of triples. For example, the expected number of (S, I) pairs is given by:

$$[\dot{SI}](t) = \gamma([II] - [SI]) + \tau([SSI] - [ISI] - [SI]). \tag{1.9}$$

This hierarchical dependence on higher order moments continues until the behaviour of the whole system is recovered. Hence, in order to find a low-order,

solvable set of ODEs, moment closure approximations are needed that approximate higher order moments in terms of the current system variables. For example, to close Eq. (1.8) we can make the assumption of independent mass action, and hence $[SI] \approx n[S][I]/N$, where N is the population size and n is the degree of a node, thus leading to the following closed set of ODEs:

$$[\dot{S}](t) = \gamma[I] - \tau n[S]\frac{[I]}{N}, \tag{1.10}$$

$$[\dot{I}](t) = \tau n[S]\frac{[I]}{N} - \gamma[I]. \tag{1.11}$$

This mean-field approximation loses all information about the network structure and assumes that any individual can connect to any other individual. The consequences of this strong assumption are explored fully in Chapter 3 of this thesis and we investigate under what circumstances this becomes a valid approximation.

An alternative approach is to close at a higher level, for example Eq. (1.9), and approximate triples in terms of pairs and individuals. There is more than one way that triples can be approximated by lower order moments but, in general, we have $[ABC] = f([AB], [AC], [BC], [A], [B], [C])$. This higher order approximation allows some information about the network to be preserved, such as the average degree of the network and the clustering coefficient [61, 103]. Although these pairwise approximations do not make the strong assumption of random mixing, they do assume that the state of an individual's neighbours follows a multinomial distribution, which ignores correlations that naturally develop regarding the distribution of infectious individuals, especially in the early stages of an epidemic. In Chapter 3, we explore how this standard closure performs on networks with different topologies, and also compare its performance with that of an improved pairwise closure that accounts for correlations between infectious individuals. This pairwise approach assumes, in the moment closure approximation, that the network is homogenous, with each node having the same degree.

Model	Assumption	Advantages	Disadvantages
Exact	No assumptions	Full spectrum of behaviour	Unsolvable for networks of realistic size
Heterogeneous pairwise	States of a node's neighbours multinomially distributed	Some network structure preserved; assortative mixing models possible	Analytic results limited; large system of equations
Effective degree	Explicit definition of 'star'-shaped motifs; infection from outside motif proportional to global rate of infection	State of the neighbours of a node explicitly defined	Limited analytic tractability; no facility for clustering
Homogeneous pairwise	States of a node's neighbours multinomially distributed; every node has the same degree	Some network structure preserved; some analytical results possible	Fewer network heterogeneities included
Mean-field	Homogeneous random mixing	Analytical analysis possible	All network heterogeneities excluded from model

Table 1.2: Table highlighting the advantages and disadvantages of a range of approaches for modelling epidemics.

Eames & Keeling [26] generalise this modelling approach to account for networks with heterogenous degree distributions. The system of equations is much larger than for homogenous pairwise models, and analytic results are more limited.

Other methods have been used to approximate epidemics on networks. For example, the effective degree model [83, 85], explored in full in Chapter 4, defines star-like motifs that explicitly track the number and type of neighbours to which an individual is directly linked, which means we know explicitly how many infectious or susceptible individuals are linked to other infectious or susceptible individuals from outside. For example $S_{s,i}$ denotes the expected number of susceptible individuals that have i infectious neighbours and s susceptible neigh-

bours. Hence this class of individuals becomes infectious at rate $\tau i S_{s,i}$. The closure assumption in this model is introduced when accounting for the infection of an individual's susceptible neighbours from outside the basic star-like motif, which is assumed to happen at a rate proportional to the total rate of infection in the system - in other words, random mixing applies outside of the the explicit triples defined by $S_{s,i}$.

A further method of generating low-dimensional ODE approximations of epidemics on networks relies on the use of probability generating functions (PGFs) to describe the degree distribution of a network, and to use these to keep track of the number of susceptibles over time [45, 89, 124]. This novel approach only works for SIR epidemics, as it is unable to account for repeat infections. A recent paper by House & Keeling [53] demonstrates the links between these various epidemic models.

Adding further heterogeneity

Further classes of individuals can also be introduced, to model certain real-world heterogeneities that may be influential. For example, we could include two classes of individuals based on their connectivity - highly-connected individuals and poorly-connected individuals, thus doubling the total number of disease compartments [60]. With this model, the effects of assortative and disassortative mixing can be explored - in other words, what happens if highly-connected individuals only mix with other highly-connected individuals, and vice-versa [72]. These models are designed to account for the intrinsic heterogeneities found in real-world networks.

In addition to these intrinsic properties of the underlying network, external factors, such as individual behaviour, can also be included in the model. For example, we could include classes of awareness where, in this context, awareness implies that an individual is aware of the potential threat of a disease and has

taken action to reduce their chance of becoming infected [35]. This again leads to an increase in the number and complexity of equations in order to account for individuals who are either aware or unaware. Individuals will become aware in response to information about the disease, which could be made available via different routes. This leads to models which consider the interplay between the spread of a disease and the spread of information [74].

As ever, when using mathematics to model real-world situations, a word of warning needs to be sounded. All the various real-world factors that lead to a certain outcome cannot ever be hoped to be captured in even the most complex of models. Assumptions are made, simplifications employed and parameters are inferred. Even highly complex models are vast oversimplifications of the real-world and, as such, cannot accurately predicate the quantitative outcomes of future epidemics. However, simplified, tractable models that consider a few key dynamics allow us to gain a deeper understanding of the importance and effects of the interplay and feedback between these dynamical processes and, as such, can guide and inform any public health measures that may need to be implemented in response to a disease outbreak. Mathematics has a crucial role to play in this exciting and vital multidisciplinary subject area.

1.3 Thesis overview

This thesis is primarily concerned with epidemics on networks. In Chapter 2, we start with a full stochastic description of an SIS type epidemic on an arbitrary contact network, as described by a set of Kolmogorov master equations, and proceed to prove that the system of ODEs that govern the dynamics of individuals and pairs can be described exactly in terms of the number of triples in the system.

In Chapter 3, we look at different methods of closing this system of ODEs by approximating the number of triples in terms of the number of individuals and pairs. We then simulate epidemics on a number of networks generated via

different algorithms and hence displaying different local and global topological structure. We investigate how well the different moment closure approximations perform on each type of network and question their real-world applications and limitations.

In Chapter 4, we derive a model that describes the spread of an SIS-type epidemic on a dynamic contact network, where individuals are able to break and create links with other individuals. We describe the dynamics using an effective degree ODE formalism and show that this system of ODEs agrees well with results from stochastic simulations, both in describing the evolution of the network and the disease. Furthermore, we derive an analytic calculation of the disease threshold and explore the validity of such a measure in the context of a dynamically evolving contact network.

In Chapter 5, we derive a system or ODEs that describes the interacting dynamics of a disease and information relating to the disease. We allow individuals to become responsive in light of received information and, thus, reduce the rate at which they become infected. We consider the effectiveness of different routes of information transmission (such as mouth-to-mouth or mass media campaigns) in slowing or preventing the spread of a disease.

In Chapter 6, we use a range of techniques to model the spread of disease amongst flocks of sheep. The full network model is based on field data that describes the number of contacts per day between the different members of a flock. Data is available for flocks with or without lambs, and is used to parameterise a weighted contact network. We construct a range of network and ODE models that are designed to investigate the effect of link-weight heterogeneity on the spread of disease.

Finally, in Chapter 7 we discuss some open questions related to the work in previous chapters and consider what future research is possible in the field of epidemics on networks.

Chapter 2

From Markovian epidemic models on networks to exact ODEs at the level of individuals and pairs

2.1 Introduction

The spread of directly transmitted diseases within a population depends not only on the nature of the pathogen but also on the way in which infectious individuals come into contact with susceptible individuals. The network of these contacts provides the supporting structure on which the disease transmission process takes place. There is a large body of research examining network epidemic models with the aim of understanding how network properties impact on disease invasion, spread and control [63]. Many different modelling approaches have been proposed, which fall into three broad classes: exact Markovian or state-based models, which are explored in this chapter, individual-based stochastic simulation or micro models [63] and deterministic ODE-based macro models [61, 103, 109, 122]. This classification is not application specific and it simply refers to the scale (e.g. individual level or population level) at which the modelling is

being carried out. The links between state-based, micro and macro models are explored in detail by Gustafsson & Sternard [47].

State-based systems, given by the master equation, or Kolmogorov equation, contain information about all possible states of the system along with the associated rates of transition from one state to another. Solving the resulting set of differential equations provides a full system description with no need for simulation. This approach has typically been used for small networks [68] due to the number of equations increasing exponentially with system size (e.g. SIS type dynamics on a network with N individuals results in $2^N - 1$ equations). With significant increases in computing power, this approach provides a realistic alternative to individual-based stochastic simulation of small populations, although we are unable yet to solve a full state-based set of ODEs for realistic network sizes. For special classes of networks, lumping [21, 55, 113] can lead to significant reductions in system size, and thus the state-based models become a more viable alternative even for large populations. However, for problems involving large networks with complex structure, individual-based simulation remains the most realistic approach.

The advantages offered by individual-based modelling come at the cost of little or no analytical tractability. To overcome this problem, 'moment-closure' type ODE-based models have been developed and formulated, offering faster computational time and more analytical tractability. These differ from classic compartmental-based ODE models in that the evolution equations for the expected number of individuals involves the expected number of pairs and higher-order structures. Many such models have been derived heuristically [53, 61, 103, 109, 122] and the main aim of this chapter is to rigourously demonstrate the direct link between these ODE models and the exact Markovian state-based models.

These systems of ODEs are of a tractable size, however they do not form a

closed set of equations since lower moments depend on higher moments. Much work has been done on deriving moment closure approximations where the expected number of triples is approximated by a combination of the expected number of pairs and individuals [53, 61, 103, 109, 122] and hence closes the system and leads to a set of numerically tractable equations. In chapter 3 we explore several distinct moment closure approximations and investigate how effective they are by comparing their solutions to results generated by individual-based stochastic simulations. Another approach to modelling epidemics on networks through a closed set of ODEs uses a probability generating function formalism [89, 124], although this has so far only been used for SIR type dynamics. A number of papers present reviews and summaries of many of the current approaches to modelling epidemics on networks [20, 53, 63].

In this chapter, we start from an exact continuous time Markov chain formulation of a simple SIS type epidemic on an arbitrary contact network. From this exact stochastic foundation, systems of ODEs for the dynamics of the expected number of singles (e.g. the expected number of susceptible individuals, $[S](t)$) and pairs (e.g. the expected number of (S, I) links, $[SI](t)$) are rigorously derived, hence results that were previously only heuristically justified are proven to be exact before a closure is applied.

2.2 Model

2.2.1 Disease dynamics and the network of contacts

In this chapter epidemics with SIS type dynamics [4] are considered on an arbitrary static contact network. In this section the model formulation used in all subsequent sections is clearly defined. For ease of reference, Table 2.1 summarises all of the notations used. The network has N nodes with links between nodes defined by an adjacency matrix $G = (g_{ij})_{i,j=1,2,\ldots,N} \in \{0, 1\}^{N^2}$ where $g_{ij} = 1$ if node

i and j are connected, and $g_{ij} = 0$ otherwise. Here, we only consider networks with bi-directional edges and without self-loops. This requirement translates to the following two constraints upon G: $G = G^T$ and $g_{ii} = 0$. The dynamics of transmission has two key stages: transmission of the disease and recovery of infectious individuals. Infection starting from an initial index case is transmitted at rate τ across every (S, I) edge. This is followed by the recovery of infectious individuals at rate γ. Upon recovery, infectious individuals become susceptible again. Both infection and recovery are modelled as independent Poisson processes. For example, in a small time interval δt, a susceptible individual with k_I infectious neighbours becomes infected with probability $1 - \exp(-k_I \tau \delta t)$. Similarly, $1 - \exp(-\gamma \delta t)$ represents the recovery probability of a single infectious individual, and this is independent of the status of its neighbours.

2.2.2 Formulation of the disease transmission model

At any point in time, every node can be either susceptible (S) or infected and infectious (I), and hence, the state of the system is given by a vector of length N with all entries either S or I (or zero or one). The state space of system is given by $\mathcal{S} = \{S, I\}^N$ or $\mathcal{S} = \{0, 1\}^N$ and the transmission dynamics on the network can be formulated in terms of a transition matrix between all possible states. In the case of continuous time, this matrix is also known as the infinitesimal generator matrix [16, 18, 69]. Based on the generator matrix, it is straightforward to write down the Kolmogorov differential equations that uniquely determine the probability of the system being in a particular state at a given time [16, 18]. However, in practice even for small network size, this approach becomes unfeasible due to the large number of equations (i.e. $2^N - 1$). As detailed in the introduction, using various techniques, it is possible to reduce the number of states (i.e. number of equations) and derive models that are either equivalent to the original system or are approximations that in the limit of large networks (i.e. $N \to \infty$) become

Table 2.1: Notation for model formulation and parameters

N	Number of nodes in the network.
$G = (g_{ij})_{i,j=1,2,...,N} \in \{0,1\}^{N^2}$	Adjacency matrix with $g_{ij} = 1$ if node i and j are connected, $g_{ij} = 0$ otherwise. The network is bi-directional and has no self loops so that $G = G^T$ and $g_{ii} = 0$ for all i.
τ	Rate of infection per (S, I) edge.
γ	Rate of recovery.
$\mathcal{S} = \{S, I\}^N$	State space of the network, with nodes either susceptible, S, or infected, I, and $\lvert\mathcal{S}\rvert = 2^N$.
$\mathcal{S}^k = \{\mathcal{S}_1^k, \mathcal{S}_2^k, \ldots \mathcal{S}_{c_k}^k\}$	The $c_k = \binom{N}{k}$ states with k infected individuals in all possible configurations, with $k = 0, 1, ..., N$.
$X_j^k(t)$	Probability of being in state $\mathcal{S}_j^k$ at time t, where $k = 0, 1, ...N$ and $j = 1, 2, ..., c_k$.
$A_{i,j}^k$	Rate of transition from $\mathcal{S}_j^{k-1}$ to $\mathcal{S}_i^k$, where $k = 0, 1, ...N$ and $i, j = 1, 2, ..., c_k$. Note that only one individual is changing (i.e. in this case an S node changes to an I through infection).
$C_{i,j}^k$	Rate of transition from $\mathcal{S}_j^{k+1}$ to $\mathcal{S}_i^k$, where $k = 0, 1, ...N$ and $i, j = 1, 2, ..., c_k$. Note that only one individual is changing (i.e. in this case an I node changes to an S through recovery).
$B_{i,j}^k$	Rate of transition out of $\mathcal{S}_j^k$, where $B_{i,j}^k = 0$ if $i \neq j$, with $k = 0, 1, ...N$ and $i, j = 1, 2, ..., c_k$.
$N_{AB}(\mathcal{S}_j^k)$	Number of (A, B) type edges in state $\mathcal{S}_j^k$, where $A, B \in \{S, I\}$, with $k = 0, 1, ...N$ and $j = 1, 2, ..., c_k$.

exact.

2.2.3 Kolmogorov equations in the case of an arbitrary network

The 2^N elements of the state space can be conveniently divided into $N+1$ subsets as follows: (a) $\mathcal{S}^0$ is the subset with one single element, namely the state with all nodes susceptible: $\mathcal{S}^0 = (S, S, \ldots, S)$, (b) $\mathcal{S}^k$ is the subset of all states with k infected nodes (on a network with N nodes, k infected nodes can be arranged in $\binom{N}{k}$ distinct configurations), and (c) $\mathcal{S}^N$ is the subset with one single element, namely the state with all nodes infected: $\mathcal{S}^N = (I, I, \ldots, I)$. The elements of the subset $\mathcal{S}^k$ are denoted by $\mathcal{S}^k_1, \mathcal{S}^k_2, \ldots, \mathcal{S}^k_{c_k}$, where $c_k = \binom{N}{k}$. The status of the l-th node of state $\mathcal{S}^k_j$ will be denoted by $\mathcal{S}^k_j(l)$, thus $\mathcal{S}^k_j(l) = S$ or $\mathcal{S}^k_j(l) = I$. The state of the system can change in two ways:

- *A node becoming infected:* an S node becomes an I node, that is an $\mathcal{S}^k_j \to \mathcal{S}^{k+1}_i$ type transition, where j and i are chosen such that $\exists\ l$ for which $\mathcal{S}^k_j(l) = S$, $\mathcal{S}^{k+1}_i(l) = I$, and $\mathcal{S}^k_j(m) = \mathcal{S}^{k+1}_i(m)$ for $\forall\ m \neq l$. Moreover, $\exists\ r \neq l$ such that $\mathcal{S}^k_j(r) = I$ and $g_{lr} = 1$ (i.e. there is an (S, I) type edge between nodes labelled l and r).

- *The recovery of a node:* an I node becomes an S node, that is an $\mathcal{S}^k_j \to \mathcal{S}^{k-1}_i$ type transition, where j and i are chosen such that $\exists\ l$ for which $\mathcal{S}^k_j(l) = I$, $\mathcal{S}^{k-1}_i(l) = S$, and $\mathcal{S}^k_j(m) = \mathcal{S}^{k-1}_i(m)$ for $\forall\ m \neq l$. This means that that states $\mathcal{S}^k_j$ and $\mathcal{S}^{k-1}_i$ may differ only at one position, this is the l'th position.

The evolution in the state space can be described by a continuous time Markov-process. Let us denote the probability of the system being in state $\mathcal{S}^k_j$ at time t by $X^k_j(t)$. Let

$$X^k(t) = (X^k_1(t), X^k_2(t), \ldots, X^k_{c_k}(t))$$

be a c_k-dimensional vector for $k = 0, 1, \ldots, N$. The above transitions determine the Kolmogorov equations (i.e. a system of linear differential equations) for the probability functions $X_j^k(t)$. In the general case of an arbitrary network, the Kolmogorov equations can be written in terms of a matrix with the following block tridiagonal form

$$\dot{X}^k = A^k X^{k-1} + B^k X^k + C^k X^{k+1}, \qquad k = 0, 1, \ldots, N, \tag{2.1}$$

where A^0 and C^N are zero matrices. Thus Eq. (2.1) can be written in the following form

$$\dot{X} = PX, \tag{2.2}$$

where

$$P = \begin{pmatrix} B^0 & C^0 & 0 & 0 & 0 & 0 \\ A^1 & B^1 & C^1 & 0 & 0 & 0 \\ 0 & A^2 & B^2 & C^2 & 0 & 0 \\ 0 & 0 & A^3 & B^3 & C^3 & 0 \\ 0 & 0 & \cdots & \cdots & \cdots & 0 \\ 0 & 0 & 0 & 0 & A^N & B^N \end{pmatrix},$$

and

$$X = \left(X^0, X^1, X^2, ..., X^N\right)^T.$$

We note that often the transpose of P is used, and then X is a row vector, not a column. However, here we use this formulation since it is more convenient from a dynamical system point of view. The A^k matrices capture the infection while the C^k matrices describe the recovery process. These matrices depend on the structure of the network, and the transmission and recovery rates. The dimension and the entries of these matrices can be obtained using some simple bookkeeping rules.

The entry in the i-th row and j-th column of matrix A^k is denoted by $A^k_{i,j}$. This element gives the rate of transition from $\mathcal{S}^{k-1}_j$ to $\mathcal{S}^k_i$. In the $\mathcal{S}^{k-1}$ class there are c_{k-1} elements, and in the $\mathcal{S}^k$ class there are c_k elements, hence matrix A^k has c_k rows and c_{k-1} columns. The entry $A^k_{i,j}$ is non-zero only in the case when the states $\mathcal{S}^{k-1}_j$ and $\mathcal{S}^k_i$ differ at one position, say at position l and $\mathcal{S}^{k-1}_j(l) = S$, $\mathcal{S}^k_i(l) = I$, and $\mathcal{S}^{k-1}_j(m) = \mathcal{S}^k_i(m)$ for $\forall\ m \neq l$. Moreover, we also require that there $\exists\ r \neq l$ such that $\mathcal{S}^{k-1}_j(r) = I$ and $g_{lr} = 1$ (i.e. there is an (S, I) type edge between nodes labelled l and by r). In this case

$$A^k_{i,j} = \tau \cdot \#\{r \in \{1, 2, \ldots, N\} : \mathcal{S}^{k-1}_j(r) = I, g_{lr} = 1\}, \tag{2.3}$$

where the term multiplying τ simply denotes the number of infectious nodes connected to the susceptible node at position l. In order to better understand the role of the A^k matrix let us consider a state $\mathcal{S}^{k-1}_j$ and choose an index l such that the node at position l is S (i.e. $\mathcal{S}^{k-1}_j(l) = S$). Next, find an index $i \in \{1, 2, \ldots, c_k\}$ such that states $\mathcal{S}^{k-1}_j$ and $\mathcal{S}^k_i$ only differ at position l, that is $\mathcal{S}^k_i(l) = I$ and $\mathcal{S}^{k-1}_j(m) = \mathcal{S}^k_i(m)$ for $\forall\ m \neq l$. Let us denote by q the number of nodes in state $\mathcal{S}^{k-1}_j$ which are I and are connected to node l which is S. Then $A^k_{i,j} = \tau q$. Repeating this for all $l \in \{1, 2, \ldots, N\}$, such that $\mathcal{S}^{k-1}_j(l) = S$, it can be observed that the total number of (S, I) edges in the $\mathcal{S}^{k-1}_j$ state multiplied by τ is equal to the sum of the elements in the j-th column of matrix A^k, that is for $\forall\ j \in \{1, 2, \ldots, c_{k-1}\}$ the following equality holds

$$\sum_{i=1}^{c_k} A^k_{i,j} = \tau N_{SI}(\mathcal{S}^{k-1}_j), \tag{2.4}$$

where $N_{SI}(\mathcal{S}^{k-1}_j)$ denotes the number of (S, I) edges in state $\mathcal{S}^{k-1}_j$.

The entry in the i-th row and j-th column of matrix C^k is denoted by $C^k_{i,j}$. This element gives the rate of transition from $\mathcal{S}^{k+1}_j$ to $\mathcal{S}^k_i$. In the $\mathcal{S}^{k+1}$ class there are c_{k+1} elements, and in the $\mathcal{S}^k$ class there are c_k elements, hence matrix C^k has

c_k rows and c_{k+1} columns. The entry $C^k_{i,j}$ is non-zero only in the case when the states $\mathcal{S}^{k+1}_j$ and $\mathcal{S}^k_i$ differ at one position, say at position l such that $\mathcal{S}^{k+1}_j(l) = I$, $\mathcal{S}^k_i(l) = S$ and $\mathcal{S}^{k+1}_j(m) = \mathcal{S}^k_i(m)$ for $\forall\ m \neq l$. In this case $C^k_{i,j} = \gamma$. In state $\mathcal{S}^{k+1}_j$, $k+1$ nodes of the network are in state I, hence in the j-th column of matrix C^k there are $k+1$ entries that are equal to γ and the remaining entries are zero. Hence, for all $j \in \{1, 2, \ldots, c_{k+1}\}$ the following equality holds

$$\sum_{i=1}^{c_k} C^k_{i,j} = \gamma(k+1). \tag{2.5}$$

The matrix B^k is a diagonal matrix with the number of rows and columns equal to c_k. The B^k matrices account for transitions out of a particular state, either through infection or recovery. The diagonal elements of B^k are determined such that the sum of entries in each column of P sum to zero. This gives the following expression for the entries of B,

$$B^k_{i,i} = -\sum_{j=1}^{c_{k+1}} A^{k+1}_{j,i} - \sum_{j=1}^{c_{k-1}} C^{k-1}_{j,i}. \tag{2.6}$$

The system given by Eq. (2.1) describes the rate of transition from any possible system state to any other possible system state. In other words, all possible system states and transitions are described. However these ODE are impractical to solve or cannot be solved for large N as the system consists of 2^N equations.

2.2.4 Kolmogorov equations in the case of a complete network with $N = 3$

To illustrate and clarify the notations introduced thus far, in this section we derive the full set of master equations for a fully connected network with $N = 3$. We note that the above rules can be conveniently programmed in a code, using a programming language such as *Matlab* for example, that will automatically

generate and provide numerical solution to the full set of differential equations provided N is sufficiently small.

This small network has a state space with 2^3 elements, and following previously introduced notation, this can divided in the following subsets, $X^0 = X_{SSS}$, $X^1 = (X_{SSI}, X_{SIS}, X_{ISS})$, $X^2 = (X_{SII}, X_{ISI}, X_{IIS})$, $X^3 = X_{III}$ with $X = (X^0, X^1, X^2, X^3)$. For $N = 3$, P is given by

$$P = \begin{pmatrix} B^0 & C^0 & 0 & 0 \\ A^1 & B^1 & C^1 & 0 \\ 0 & A^2 & B^2 & C^2 \\ 0 & 0 & A^3 & B^3 \end{pmatrix}.$$

Taking into account the structure of the network (i.e. each node connected to every other node) the entries of matrix P are given by

$$B^0 = \begin{pmatrix} 0 \end{pmatrix}, \qquad C^0 = \begin{pmatrix} \gamma, & \gamma, & \gamma \end{pmatrix},$$

$$A^1 = \begin{pmatrix} 0 \\ 0 \\ 0 \end{pmatrix}, \qquad B^1 = \begin{pmatrix} -2\tau - \gamma & 0 & 0 \\ 0 & -2\tau - \gamma & 0 \\ 0 & 0 & -2\tau - \gamma \end{pmatrix}, \qquad C^1 = \begin{pmatrix} \gamma & \gamma & 0 \\ \gamma & 0 & \gamma \\ 0 & \gamma & \gamma \end{pmatrix},$$

$$A^2 = \begin{pmatrix} \tau & \tau & 0 \\ \tau & 0 & \tau \\ 0 & \tau & \tau \end{pmatrix}, \qquad B^2 = \begin{pmatrix} -2\tau - 2\gamma & 0 & 0 \\ 0 & -2\tau - 2\gamma & 0 \\ 0 & 0 & -2\tau - 2\gamma \end{pmatrix}, \qquad C^2 = \begin{pmatrix} \gamma \\ \gamma \\ \gamma \end{pmatrix},$$

$$A^3 = \begin{pmatrix} 2\tau, & 2\tau, & 2\tau \end{pmatrix}, \qquad B^3 = \begin{pmatrix} -3\gamma \end{pmatrix}.$$

Here, for example, the entries in the first column of matrix A^2, $(\tau,\ \tau,\ 0)$, correspond to the rates of the following transitions, $SSI \to SII$, $SSI \to ISI$ and $SSI \to IIS$. Based on the definition of sub-matrices above, $\dot{X} = PX$ is equiva-

lent to the following system

$$\begin{aligned}
\dot{X}^0 &= B^0X^0 + C^0X^1, \\
\dot{X}^1 &= A^1X^0 + B^1X^1 + C^1X^2, \\
\dot{X}^2 &= A^2X^1 + B^2X^2 + C^2X^3, \\
\dot{X}^3 &= A^3X^2 + B^3X^3.
\end{aligned}$$

In terms of the most intuitive notation, this system is equivalent to

$$\begin{aligned}
\dot{X}_{SSS} &= \gamma(X_{SSI} + X_{SIS} + X_{ISS}), \\
\dot{X}_{SSI} &= \gamma(X_{SII} + X_{ISI}) - (2\tau + \gamma)X_{SSI}, \\
\dot{X}_{SIS} &= \gamma(X_{SII} + X_{IIS}) - (2\tau + \gamma)X_{SIS}, \\
\dot{X}_{ISS} &= \gamma(X_{ISI} + X_{IIS}) - (2\tau + \gamma)X_{ISS}, \\
\dot{X}_{SII} &= \gamma X_{III} + \tau(X_{SSI} + X_{SIS}) - 2(\tau + \gamma)X_{SII}, \\
\dot{X}_{ISI} &= \gamma X_{III} + \tau(X_{SSI} + X_{ISS}) - 2(\tau + \gamma)X_{ISI}, \\
\dot{X}_{IIS} &= \gamma X_{III} + \tau(X_{SIS} + X_{ISS}) - 2(\tau + \gamma)X_{IIS}, \\
\dot{X}_{III} &= -3\gamma X_{III} + 2\tau(X_{SII} + X_{ISI} + X_{IIS}),
\end{aligned}$$

and from either formulation, the transition matrix is

$$P = \begin{pmatrix}
0 & \gamma & \gamma & \gamma & 0 & 0 & 0 & 0 \\
0 & -2\tau - \gamma & 0 & 0 & \gamma & \gamma & 0 & 0 \\
0 & 0 & -2\tau - \gamma & 0 & \gamma & 0 & \gamma & 0 \\
0 & 0 & 0 & -2\tau - \gamma & 0 & \gamma & \gamma & 0 \\
0 & \tau & \tau & 0 & -2\tau - 2\gamma & 0 & 0 & \gamma \\
0 & \tau & 0 & \tau & 0 & -2\tau - 2\gamma & 0 & \gamma \\
0 & 0 & \tau & \tau & 0 & 0 & -2\tau - 2\gamma & \gamma \\
0 & 0 & 0 & 0 & 2\tau & 2\tau & 2\tau & -3\gamma
\end{pmatrix}.$$

2.3 Exact equations at the level of individuals and pairs

The idea of deriving mean-field equations is based on the observation that population level expected values are simply linear combinations of the probability functions in Eq. (2.1). It is not always necessary to determine all probability functions, and in many situations, the expected values of the number, or proportion, of susceptible (S) and infectious (I) nodes or individuals is equally valuable. These expected values at time t are denoted by $[S](t)$ and $[I](t)$ and can be expressed as follows,

$$[I](t) = \sum_{k=0}^{N} k \sum_{j=1}^{c_k} X_j^k(t), \qquad [S](t) = \sum_{k=0}^{N} (N-k) \sum_{j=1}^{c_k} X_j^k(t). \tag{2.7}$$

Hence, based on Eq. (2.1), it is feasible to try to derive a new system of differential equations that will uniquely define $[S]$ and $[I]$. However, we know that the rate at which individuals become infected is proportional to the number of (S, I) pairs in the system, hence $[SI](t)$, the expected value of (S, I) pairs, is expressed as follows:

$$[SI](t) = \sum_{k=0}^{N} \sum_{j=1}^{c_k} N_{SI}(\mathcal{S}_j^k) X_j^k(t). \tag{2.8}$$

However, this means that the newly derived system of equations for $[S]$ and $[I]$ will not be closed since it contains the new variable $[SI]$, and hence and equation for $[SI](t)$ is needed. Similarly the number of pairs in the system depends upon the arrangement of different triples (e.g. an (S, S) pair changes to an (S, I) pair due to infection coming from a third infected node acting from outside the pair, giving rise to a (S, S, I) triple). The precise dependency of lower order moments on higher order moments can be formulated in the following Theorem:

Theorem 2.1. *The expected values of $[S]$, $[I]$, $[SI]$, $[II]$ and $[SS]$ satisfy the following system of differential equations which can be derived directly from the*

Kolmogorov equations, Eq. (2.1)

$$
\begin{aligned}
[\dot{S}] &= \gamma[I] - \tau[SI], && (2.9)\\
[\dot{I}] &= \tau[SI] - \gamma[I], && (2.10)\\
[\dot{SI}] &= \gamma([II] - [SI]) + \tau([SSI] - [ISI] - [SI]), && (2.11)\\
[\dot{II}] &= -2\gamma[II] + 2\tau([ISI] + [SI]), && (2.12)\\
[\dot{SS}] &= 2\gamma[SI] - 2\tau[SSI]. && (2.13)
\end{aligned}
$$

This is a result that is known and has been previously derived based on heuristic arguments [61, 103]. Despite this being a well known system, we provide a proof of this Theorem for two reasons. On one hand, this system is usually not derived from the differential equations of the Markov-process, and on the other hand, the proof illustrates the usefulness of the block tridiagonal form of the transition matrix P.

Proof of Theorem 2.1:

This proof is satisfied by the proof of two lemmas. Firstly, a proof of the dynamics at the level of individuals is given, and this is followed by a separate proof for the equations that govern the dynamics of the pairs.

Lemma 2.2. *The expected values* $[S]$ *and* $[I]$ *satisfy the following system*

$$
\begin{aligned}
[\dot{S}] &= \gamma[I] - \tau[SI],\\
[\dot{I}] &= \tau[SI] - \gamma[I].
\end{aligned}
$$

Proof: Let us introduce the row matrix $S_k = (1\ 1\ \ldots 1)$ with c_k columns. Then

$\sum_{j=1}^{c_k} X_j^k = S_k X^k$ (here X^k is a column vector). Hence from Eq. (2.7) we obtain

$$[I](t) = \sum_{k=0}^{N} k S_k X^k, \qquad [S](t) = \sum_{k=0}^{N} (N-k) S_k X^k. \tag{2.14}$$

Using this notation, Eq. (2.6) takes the following form,

$$B_{i,i}^k = -(S_{k+1} A^{k+1})_i - (S_{k-1} C^{k-1})_i,$$

and using that B^k is a diagonal matrix $B_{i,i}^k = (S_k B^k)_i$ holds, and hence,

$$(S_k B^k)_i = -(S_{k+1} A^{k+1})_i - (S_{k-1} C^{k-1})_i$$

which is true for $\forall\ i = 1, \ldots c_k$. Thus the following equation is obtained

$$S_{k+1} A^{k+1} + S_k B^k + S_{k-1} C^{k-1} = 0, \tag{2.15}$$

and this holds for $\forall\ k = 0, 1, \ldots, N$. We note that, when indices are out of the relevant range (i.e. A^{N+1} and C^{-1}) matrices should be set to zero. Differentiating $[I](t)$ and using Eq. (2.1) we obtain

$$[\dot{I}] = \sum_{k=0}^{N} k S_k \dot{X}^k = \sum_{k=0}^{N} k S_k (A^k X^{k-1} + B^k X^k + C^k X^{k+1})$$

$$= \sum_{k=1}^{N} k S_k A^k X^{k-1} + \sum_{k=0}^{N} k S_k B^k X^k + \sum_{k=0}^{N-1} k S_k C^k X^{k+1}$$

$$= \sum_{k=0}^{N-1} (k+1) S_{k+1} A^{k+1} X^k + \sum_{k=0}^{N} k S_k B^k X^k + \sum_{k=1}^{N} (k-1) S_{k-1} C^{k-1} X^k$$

$$= \sum_{k=0}^{N} \left((k+1) S_{k+1} A^{k+1} + k S_k B^k + (k-1) S_{k-1} C^{k-1} \right) X^k.$$

Now upon using Eq. (2.15), we obtain

$$[\dot{I}] = \sum_{k=0}^{N} \left(S_{k+1} A^{k+1} - S_{k-1} C^{k-1} \right) X^k.$$

The statement for $[I](t)$ follows from the Proposition below. The proof for $[S](t)$ is similar. □

Proposition 2.3. *1.* $S_{k-1} C^{k-1} = \gamma k S_k$

2. $\sum_{k=0}^{N} S_{k-1} C^{k-1} X^k = \gamma [I]$

3. $\sum_{k=0}^{N} S_{k+1} A^{k+1} X^k = \tau [SI]$

PROOF: 1. According to Eq. (2.5), for all $j \in \{1, 2, \ldots, c_k\}$ the following equality holds

$$(S_{k-1} C^{k-1})_j = \sum_{i=1}^{c_{k-1}} C_{i,j}^{k-1} = \gamma k,$$

and this implies that $S_{k-1} C^{k-1} = \gamma k S_k$, since the j-th coordinate of the left and right hand side are equal.

2. The second statement is a direct consequence of the first part of the Proposition and Eq. (2.14).

3. According to Eq. (2.4), for all $j \in \{1, 2, \ldots, c_k\}$ the following equality holds

$$(S_{k+1} A^{k+1})_j = \sum_{i=1}^{c_{k+1}} A_{i,j}^{k+1} = \tau N_{SI}(\mathcal{S}_j^k),$$

with this yielding

$$\sum_{k=0}^{N} S_{k+1} A^{k+1} X^k = \sum_{k=0}^{N} \sum_{j=1}^{c_k} (S_{k+1} A^{k+1})_j X_j^k = \tau \sum_{k=0}^{N} \sum_{j=1}^{c_k} N_{SI}(\mathcal{S}_j^k) X_j^k(t) = \tau [SI].$$

□

We note that the Lemma above holds for any network, and completes the first part of the proof of Theorem 2.1. The remainder rests on the proof of the following:

Lemma 2.4. *The expected values* $[SS]$, $[SI]$ *and* $[II]$ *satisfy the following system*

$$\begin{aligned}
[\dot{SI}] &= \gamma([II]-[SI])+\tau([SSI]-[ISI]-[SI]),\\
[\dot{II}] &= -2\gamma[II]+2\tau([ISI]+[SI]),\\
[\dot{SS}] &= 2\gamma[SI]-2\tau[SSI].
\end{aligned}$$

PROOF: This part of the proof focuses on the derivation of Eq. (2.12), where $[II]$ is the expected number of (I,I) pairs at a given time and is given by

$$[II]=\sum_{k=0}^{N} N_{II}(\mathcal{S}^k)X^k, \tag{2.16}$$

where $N_{AB}(\mathcal{S}^k)$ is a row vector of length c_k and denotes the number of (A,B) pairs in all possible configurations with k infected individuals, i.e.

$$N_{AB}(\mathcal{S}^k)=\left(N_{AB}(\mathcal{S}_1^k),N_{AB}(\mathcal{S}_2^k),\ldots,N_{AB}(\mathcal{S}_{c_k}^k)\right).$$

Similarly, $N_{ABC}(\mathcal{S}^k)$ refers to the number of (A,B,C) triples. By differentiating Eq. (2.16) we obtain that

$$[\dot{II}]=\sum_{k=0}^{N} N_{II}(\mathcal{S}^k)\dot{X^k}=\sum_{k=0}^{N} N_{II}(\mathcal{S}^k)(A^kX^{k-1}+B^kX^k+C^kX^{k+1})$$

$$=\sum_{k=1}^{N} N_{II}(\mathcal{S}^k)A^kX^{k-1}+\sum_{k=0}^{N} N_{II}(\mathcal{S}^k)B^kX^k+\sum_{k=0}^{N-1} N_{II}(\mathcal{S}^k)C^kX^{k+1}$$

$$=\sum_{k=0}^{N}\left(N_{II}(\mathcal{S}^{k+1})A^{k+1}+N_{II}(\mathcal{S}^k)B^k+N_{II}(\mathcal{S}^{k-1})C^{k-1}\right)X^k,$$

where matrices that are out of range (i.e. A^0 and C^N) are zero matrices. The term that involves B^k in the summation above can be written as

$$N_{II}(\mathcal{S}^k)B^k=(N_{II}(\mathcal{S}_1^k)B_{1,1}^k,...,N_{II}(\mathcal{S}_{c_k}^k)B_{c_k,c_k}^k),$$

where $(N_{II}(\mathcal{S}^k)B^k)_j = N_{II}(\mathcal{S}^k_j)B^k_{j,j}$ is the j^{th} component of the $N_{II}(\mathcal{S}^k)B^k$ vector. Matrices B^k are square and diagonal and are defined in terms of A^{k+1} and C^{k-1} as given in Eq. (2.6). This allows us to write the j^{th} component as

$$N_{II}(\mathcal{S}^k_j)B^k_{j,j} = N_{II}(\mathcal{S}^k_j)\left(-\sum_{i=1}^{c_{k+1}} A^{k+1}_{i,j} - \sum_{i=1}^{c_{k-1}} C^{k-1}_{i,j}\right).$$

Using the definition of matrices A and C as given in Eqs. (2.4 & 2.5), the RHS of the expression above can be written as

$$N_{II}(\mathcal{S}^k_j)\left(-\tau N_{SI}(\mathcal{S}^k_j) - k\gamma\right) = -\tau\left(N_{II}(\mathcal{S}^k_j)N_{SI}(\mathcal{S}^k_j)\right) - k\gamma N_{II}(\mathcal{S}^k_j).$$

This per-component identity can be written in vector form to give

$$[\dot{II}] = \sum_{k=0}^{N}\Big(N_{II}(\mathcal{S}^{k+1})A^{k+1} - \tau\left(N_{II}(\mathcal{S}^k) * N_{SI}(\mathcal{S}^k)\right) - \gamma k N_{II}(\mathcal{S}^k) + N_{II}(\mathcal{S}^{k-1})C^{k-1}\Big)X^k \tag{2.17}$$

where the $*$ operator stands for the per component multiplication of two vectors as exemplified below

$$N_{II}(\mathcal{S}^k) * N_{SI}(\mathcal{S}^k) = \left(N_{II}(\mathcal{S}^k_1)N_{SI}(\mathcal{S}^k_1), ..., N_{II}(\mathcal{S}^k_{c_k})N_{SI}(\mathcal{S}^k_{c_k})\right).$$

In Eq. (2.17) the first two terms govern infection and the second two terms govern recovery. These terms can be equated to the appropriate terms in Eq. (2.12). Indeed if Eq. (2.12) is rewritten as

$$[\dot{II}] = -2\gamma\sum_{k=0}^{N} N_{II}(\mathcal{S}^k)X^k + 2\tau\sum_{k=0}^{N} N_{ISI}(\mathcal{S}^k)X^k + 2\tau\sum_{k=0}^{N} N_{SI}(\mathcal{S}^k)X^k,$$

which is just using the same notation as above, then the proof for the equation

governing the dynamics of $[II]$ follows from the identitites below:

$$\sum_{k=0}^{N} \left(-2\gamma N_{II}(\mathcal{S}^k) + \gamma k N_{II}(\mathcal{S}^k) - N_{II}(\mathcal{S}^{k-1})C^{k-1}\right) X^k(t) = 0,$$

$$\sum_{k=0}^{N} \Bigg(2\tau N_{ISI}(\mathcal{S}^k) + 2\tau N_{SI}(\mathcal{S}^k) - N_{II}(\mathcal{S}^{k+1})A^{k+1} + \big(N_{II}(\mathcal{S}^k) * N_{SI}(\mathcal{S}^k)\big) \Bigg) X^k(t) = 0.$$

These have to hold for any $t > 0$ and for all $X^k(t)$. If the coefficients of all terms involving $X^k(t)$ are zero then the identities hold. Upon removing the summation, the above identities become equalities between vectors of the same size. This means that the equality must hold for each of the c_k elements of the vectors. Thus the following Lemma has to be verified to complete the proof of the Theorem.

Lemma 2.5. *For any $k = 0, 1, \ldots, N$ and $j = 1, 2, \ldots, c_k$ the following identities hold,*

$$(k-2)\gamma N_{II}(\mathcal{S}_j^k) = \left(N_{II}(\mathcal{S}^{k-1})C^{k-1}\right)_j, \tag{2.18}$$

$$2\tau N_{ISI}(\mathcal{S}_j^k) + 2\tau N_{SI}(\mathcal{S}_j^k) = \left(N_{II}(\mathcal{S}^{k+1})A^{k+1}\right)_j - \left(N_{II}(\mathcal{S}^k) * N_{SI}(\mathcal{S}^k)\right)_j \tag{2.19}$$

The proof of this Lemma needs the following auxiliary Proposition that will be stated and proved first.

Proposition 2.6. *For any $k = 0, 1, \ldots, N$ and $j = 1, 2, \ldots, c_k$ we have*

$$A\text{:}\ A_{j,i}^k \neq 0 \ \Rightarrow\ C_{i,j}^{k-1} \neq 0, \quad \text{for all } i = 1, 2, \ldots, c_{k-1}, \tag{2.20}$$

$$B\text{:}\ \sum_{i=1}^{c_{k-1}} A_{j,i}^k = \tau N_{II}(\mathcal{S}_j^k), \tag{2.21}$$

$$C\text{:}\ N_{ISI}(\mathcal{S}_j^k) = \frac{1}{\tau^2} \sum_{i=1}^{c_{k+1}} A_{i,j}^{k+1}(A_{i,j}^{k+1} - \tau). \tag{2.22}$$

PROOF: **(A)** In Eq. (2.20), $A^k_{j,i}$ is the rate of moving from the i^{th} arrangement of $\mathcal{S}^{k-1}$ to the j^{th} arrangement of $\mathcal{S}^k$. This means that $\mathcal{S}^{k-1}_i$ and $\mathcal{S}^k_j$ differ only at one position, say l, where $\mathcal{S}^k_j(l) = I$ and $\mathcal{S}^{k-1}_i(l) = S$ and hence the reverse process is also possible, that is a transition from $\mathcal{S}^k_j$ to $\mathcal{S}^{k-1}_i$ captured by $C^k_{i,j}$. Hence, $A^k_{j,i}$ and $C^{k-1}_{i,j}$ are reverse processes leading into and out of the same state through infection and recovery. Therefore, if infection is possible then also recovery can happen and Eq. (2.20) holds.

(B) Eq. (2.21) gives the total rate of entering $\mathcal{S}^k_j$ by infection. This means that for each of the k infected individuals in $\mathcal{S}^k_j$, there is a corresponding state $\mathcal{S}^{k-1}_i$ that differs only at one position, say at position l, where $\mathcal{S}^k_j(l) = I$ and $\mathcal{S}^{k-1}_i(l) = S$. The rate at which such a new infection happens is equal to the number of I neighbours of the S at position l multiplied by the individual transmission rate τ. If there are q such neighbours, giving q (S, I) pairs given that the S is at position l, then once the infection has taken place there will be q new (I, I) pairs. If this is taken into account for all new infections leading to $\mathcal{S}^k_j$, then the sum of these transition rates gives $\tau N_{II}(\mathcal{S}^k_j)$ and Eq. (2.21) holds.

(C) Eq. (2.22) gives the relationship between matrices A that govern the infection process and the number of (I, S, I) triples. If a node l is in state S and has q neighbours that are infected then there are $q(q-1)$ (I, S, I) triples centered around this S. As $A^{k+1}_{i,j}$ captures the infection rate from $\mathcal{S}^k_j$ to $\mathcal{S}^{k+1}_i$, this is equal to τ multiplied by the number of I neighbours connected to the susceptible node S that is being infected at position l. Hence, the number of (I, S, I) triples centered around this node l is given by $\frac{1}{\tau^2} A^{k+1}_{i,j}(A^{k+1}_{i,j} - \tau)$. This allows us to count $N_{ISI}(\mathcal{S}^k_j)$ by summing over all the c_{k+1} possible $\mathcal{S}^k_j$ to $\mathcal{S}^{k+1}_i$ transitions, giving Eq. (2.22).

□

Furthermore, based on the arguments above it is straightforward to derive a relation between the number of (I, I) pairs in a particular state and the number

in a preceding or succeeding state. Namely, the following two identities hold.

Proposition 2.7. *For any $k = 0, 1, \ldots, N$ and $j = 1, 2, \ldots, c_k$ we have*

$$N_{II}(\mathcal{S}_i^{k+1})A_{i,j}^{k+1} = \left(N_{II}(\mathcal{S}_j^k) + \frac{2}{\tau}A_{i,j}^{k+1}\right)A_{i,j}^{k+1}, \quad \forall i = 1, 2, \ldots, c_{k+1}, \tag{2.23}$$

$$N_{II}(\mathcal{S}_i^{k-1})C_{i,j}^{k-1} = \left(N_{II}(\mathcal{S}_j^k) - \frac{2}{\tau}A_{j,i}^{k}\right)C_{i,j}^{k-1}, \quad \forall i = 1, 2, \ldots, c_{k-1}. \tag{2.24}$$

Proof: We prove the first one, the proof of the second is similar. If the states $\mathcal{S}_i^{k+1}$ and $\mathcal{S}_j^k$ differ at more than one position, then $A_{i,j}^{k+1} = 0$, hence the statements trivially holds. In the case when the states $\mathcal{S}_i^{k+1}$ and $\mathcal{S}_j^k$ differ at one position, then there is a position l, such that $\mathcal{S}_i^{k+1}(l) = I$, $\mathcal{S}_j^k(l) = S$, and $\mathcal{S}_i^{k+1}(m) = \mathcal{S}_j^k(m)$ for $\forall\ m \neq l$. Moreover, we also require that there $\exists\ r \neq l$ such that $\mathcal{S}_j^k(r) = I$ and $g_{lr} = 1$ (i.e. there is an(S, I) type edge between nodes labelled l and by r) to ensure that a transition between the two states via infection is possible. In this case one can prove that

$$N_{II}(\mathcal{S}_i^{k+1}) = N_{II}(\mathcal{S}_j^k) + \frac{2}{\tau}A_{i,j}^{k+1}, \quad \text{for all } i = 1, 2, \ldots, c_{k+1}.$$

This identity can be understood by considering the transition from $\mathcal{S}_j^k \to \mathcal{S}_i^{k+1}$ (i.e. a single susceptible node becoming infected). If a single infection has occurred then the increase in the number of (II) pairs can be calculated by examining the number of Is or (SI) links centered around the newly infected node, just before becoming infected. The number of such (SI) pairs is proportional to A_{ij}^{k+1} and is given by $\frac{1}{\tau}A_{ij}^{k+1}$. Since, all the (SI) links, upon infection, become (II) links, and taking into account that (II) pairs must be counted twice, the identity follows immediately. □ These Propositions allow us to prove Lemma 2.5.

PROOF OF LEMMA 2.5: The RHS of (2.18) can be expressed as

$$\left(N_{II}(\mathcal{S}^{k-1})C^{k-1}\right)_j = \sum_{i=1}^{c_{k-1}} N_{II}(\mathcal{S}_i^{k-1})C_{i,j}^{k-1}.$$

Using Eq. (2.24), this can be written as

$$\begin{aligned}\left(N_{II}(\mathcal{S}^{k-1})C^{k-1}\right)_j &= \sum_{i=1}^{c_{k-1}} \left(N_{II}(\mathcal{S}_j^k) - \frac{2}{\tau}A_{j,i}^k\right) C_{i,j}^{k-1} \\ &= N_{II}(\mathcal{S}_j^k)\sum_{i=1}^{c_{k-1}} C_{i,j}^{k-1} - \frac{2}{\tau}\sum_{i=1}^{c_{k-1}} A_{j,i}^k C_{i,j}^{k-1}\end{aligned}$$

From Eq. (2.20) it follows that every non-zero element of A^k multiplies a non-zero element of C^{k-1}. As every non-zero element in a C matrix is γ, each and every non-zero element in A^k is multiplied by γ. Hence using (2.21) and that $\sum_{i=1}^{c_{k-1}} C_{i,j}^{k-1} = k\gamma$ (see Eq. (2.5)), the RHS of Eq. (2.18) can be written as:

$$\left(N_{II}(\mathcal{S}^{k-1})C^{k-1}\right)_j = k\gamma N_{II}(\mathcal{S}_j^k) - 2\gamma N_{II}(\mathcal{S}_j^k) = \gamma(k-2)N_{II}(\mathcal{S}_j^k),$$

which completes the proof of the first part of Lemma 2.5.

In order to prove the identity given in the second part of Lemma 2.5, as given in Eq. (2.19), let us start from the first term in the RHS of Eq. (2.19). Using Eqs. (2.4 & 2.23) it can be written as

$$\begin{aligned}\left(N_{II}(\mathcal{S}^{k+1})A^{k+1}\right)_j &= \sum_{i=1}^{c_{k+1}} N_{II}(\mathcal{S}_i^{k+1})A_{i,j}^{k+1} = \sum_{i=1}^{c_{k+1}} N_{II}(\mathcal{S}_j^k)A_{i,j}^{k+1} + \frac{2}{\tau}\sum_{i=1}^{c_{k+1}}(A_{i,j}^{k+1})^2 \\ &= N_{II}(\mathcal{S}_j^k)\sum_{i=1}^{c_{k+1}} A_{i,j}^{k+1} + \frac{2}{\tau}\sum_{i=1}^{c_{k+1}}(A_{i,j}^{k+1})^2 \\ &= \tau N_{II}(\mathcal{S}_j^k)N_{SI}(\mathcal{S}_j^k) + \frac{2}{\tau}\sum_{i=1}^{c_{k+1}}(A_{i,j}^{k+1})^2 \\ &= \tau\left(N_{II}(\mathcal{S}^k) * N_{SI}(\mathcal{S}^k)\right)_j + \frac{2}{\tau}\sum_{i=1}^{c_{k+1}}(A_{i,j}^{k+1})^2.\end{aligned}$$

This can be rearranged to give the RHS of Eq. (2.19):

$$\left(N_{II}(\mathcal{S}^{k+1})A^{k+1}\right)_j - \left(N_{II}(\mathcal{S}^k) * N_{SI}(\mathcal{S}^k)\right)_j = \frac{2}{\tau}\sum_{i=1}^{c_{k+1}}(A_{i,j}^{k+1})^2. \tag{2.25}$$

However, using Eqs. (2.4 & 2.22), Eq. (2.25) can be rewritten as follows:

$$\begin{aligned}\left(N_{II}(\mathcal{S}^{k+1})A^{k+1}\right)_j &- \left(N_{II}(\mathcal{S}^k) * N_{SI}(\mathcal{S}^k)\right)_j = 2\tau\left(\frac{1}{\tau^2}\sum_{i=1}^{c_{k+1}}(A_{i,j}^{k+1})^2\right)\\ &= 2\tau\left(N_{ISI}(\mathcal{S}_j^k) + \frac{1}{\tau}\sum_{i=1}^{c_{k+1}}A_{i,j}^{k+1}\right)\\ &= 2\tau N_{ISI}(\mathcal{S}_j^k) + 2\sum_{i=1}^{c_{k+1}}A_{i,j}^{k+1} = 2\tau N_{ISI}(\mathcal{S}_j^k) + 2\tau N_{SI}(\mathcal{S}_j^k),\end{aligned}$$

which completes the proof of the Lemma and consequently of Theorem 2.1. □ This proof shows that the system of equations given in Theorem 2.1 are exact for an arbitrary network.

2.4 Discussion

The main result of this chapter is the identification of the direct link between the Markovian formulation and the ODE system that governs the dynamics of pairs. The key to the proof was provided by the special tri-diagonal structure and properties of the transition matrices from the Kolmogorov equations. The resulting system of ODEs is well known, having been derived heuristically before but here the link to the state-based Markovian formulation is emphasized. This macro model is exact at the level of pairs but is not a closed system as the dynamics of the pairs depends upon the number of triples. Again, a set of ODEs that govern the dynamics of the triples can be derived, however they will depend upon the number of four-tuples. This hierarchical dependence will continue until the dynamics of the full system is captured. House at al. [51], following earlier work by Bauch [10], explicitly derived the equations governing the dynamics of

triples:

$$
\begin{aligned}
[S\dot{S}S] &= -\tau(2[S-S-S-I]+[S-\underbrace{S-S}\quad I])+\gamma(2[SSI]+[SIS]),\\
[S\dot{S}I] &= \tau([S-S-S-I]-[I-S-S-I]-[S-\underbrace{S-I}\quad I]-[SSI])\\
&\quad +\gamma([SII]+[ISI]-[SSI]),\\
[S\dot{I}S] &= \tau([S-\underbrace{S-S}\quad I]-2[S-I-S-I]-2[SIS])\\
&\quad +\gamma(2[SII]-[SIS]),\\
[S\dot{I}I] &= \tau([S-I-S-I]+[S-\underbrace{S-I}\quad I]-[I-S-I-I]\\
&\quad +[SIS]+[SSI]-[SII])+\gamma([III]-2[SII]),\\
\dot{[}ISI] &= \tau(2[I-S-S-I]-[I-\underbrace{S-I}\quad I]-2[ISI])\\
&\quad +\gamma([III]-2[ISI]),\\
[I\dot{I}I] &= \tau(2[I-S-I-I]+[I-\underbrace{S-I}\quad I]+2[SII]+2[ISI])-3\gamma[III].
\end{aligned}
\tag{2.26}
$$

Here we have introduced new notation to describe the four-tuples, where $[A-B-C-D]$ describes four nodes in a straight line, but $[A-\underbrace{B-C}\quad D]$ instead describes three nodes A, B and C connected in a straight line but with node D connected only to node B in order to form a 'T' shape motif, as shown in Fig. 2.1. House *et al.* [51] extend these equations to consider how these two four-tuples could become clustered by further connections between the four nodes. For triples, there is only one way a triple can become further connected - by the two end nodes being joined to form a triangle. However, when considering four-tuples there are four distinct closed forms. House *et al.* [51] derive moment closures based around these six distinct four-tuples (two unclosed and four closed) and proceed to solve the equations for the dynamics of triples. They show that there is an improvement in agreement with results from stochastic network simulations when compared with results from the pairwise equations considered in this chapter and the next. However the degree of improvement differs with different network topologies and furthermore the increase in complexity and the resultant

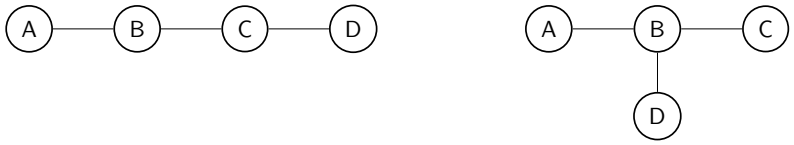

Figure 2.1: The two distinct ways an unclosed four-tuple can be configured.

loss in analytical tractability need to be carefully considered when choosing an appropriate moment at which to close the system. In the next chapter we look at how to close the system at the level of pairs and triples, and look at how well these closures perform on different network topologies. Furthermore, we provide a proof that the system closed at the level of pairs becomes exact in the limit as $N \to \infty$ for a fully connected network.

Chapter 3

On the performance of moment closure approximations

3.1 Overview

In the previous chapter a well known system of ODEs describing the time evolution of SIS type epidemics on an arbitrary static contact network was derived. It was shown that Eqs. (2.9 - 2.10) are exact at the level of the individual and furthermore that including Eqs. (2.11 - 2.13) gives an exact description at the level of pairs, and these equations are shown again here for ease of reference:

$$\begin{aligned}
[\dot{S}] &= \gamma[I] - \tau[SI], && (3.1)\\
[\dot{I}] &= \tau[SI] - \gamma[I], && (3.2)\\
[\dot{SI}] &= \gamma([II] - [SI]) + \tau([SSI] - [ISI] - [SI]), && (3.3)\\
[\dot{II}] &= -2\gamma[II] + 2\tau([ISI] + [SI]), && (3.4)\\
[\dot{SS}] &= 2\gamma[SI] - 2\tau[SSI]. && (3.5)
\end{aligned}$$

This system has an inherent dependence on higher order motifs, and an exact description of the evolution of triples would be dependent on four-tuples. In

order to break this higher order dependence, approximations must be made using the set of system variables. For example, the number of different triples can be approximated in terms of the number of pairs and individuals. In this chapter three different closures are considered. Firstly, the mean-field equations are found by approximating the number of pairs in terms of the number of individuals, and then two pairwise closures are introduced, whereby the number of triples are estimated in terms of the number of pairs and individuals.

The rest of the chapter is concerned with examining the accuracy of these approximations. The simplest mean-field system is rigourously shown to become exact on a complete network in the limit of large N. In addition, the ODEs are solved numerically and these results are compared to realisations from stochastic simulations on a range of different network topologies. It is shown that the ability of the closed sets of ODEs to accurately describe the evolution of an epidemic is fundamentally dependent on the underlying structure of the contact network.

3.2 Moment closure at the level of pairs - the mean-field model

The simplest closing relation is $[SI] \simeq n[S][I]/N$, where n is degree of a node for a homogeneous network, or the mean nodal degree otherwise. This approximation is based on the statistical independence in the state of individuals (in the limit of a fully-connected network, the expected number of $[SI]$ pairs is equivalent to the product of the expected number of $[S]$ and $[I]$). Applying this relation in Eqs. (2.9 - 2.10), we obtain:

$$[\dot{S}] = \gamma[I] - \tau\frac{n}{N}[S][I], \tag{3.6}$$

$$[\dot{I}] = \tau\frac{n}{N}[S][I] - \gamma[I], \tag{3.7}$$

which, as $n \to N$, looks exactly like the well known deterministic mean-field equation:

$$\dot{\tilde{S}} = \gamma \tilde{I} - \tau \tilde{S}\tilde{I}, \tag{3.8}$$

$$\dot{\tilde{I}} = \tau \tilde{S}\tilde{I} - \gamma \tilde{I}. \tag{3.9}$$

Such a closure relation leads to the problem of identifying networks for which the approximation above holds. It is known that for a large, fully connected network this is a good approximation when $\tau = \beta/N$ for some fixed value β, where β is the transmission rate used in classic compartmental models, and as $I, S \to \infty$ in the same way as $N \to \infty$, as first shown by Kurtz [80]. In order to formalize this statement more precisely it is useful to use the scaled variables:

$$\tilde{s} = \tilde{S}/N, \quad \tilde{i} = \tilde{I}/N, \quad [s] = [S]/N, \quad [i] = [I]/N. \tag{3.10}$$

In the new variables, with $\tau = \beta/N$, the system given by Eqs. (3.8 - 3.9) takes the the following form

$$\dot{\tilde{s}} = \gamma \tilde{i} - \beta \tilde{s}\tilde{i}, \tag{3.11}$$

$$\dot{\tilde{i}} = \beta \tilde{s}\tilde{i} - \gamma \tilde{i}. \tag{3.12}$$

It is generally believed that, under appropriate conditions, $\tilde{i}$ is a good approximation of $[i]$. Before formalizing this in a mathematically rigorous way we give details of a key aspect which seems to contradict our previous statement. This observation also justifies the need to formalise rigorously the meaning of $\tilde{i}$ being a good approximation of $[i]$.

It is known, and it can also be easily derived from Eqs. (3.11 - 3.12), that in

the case of $\beta > \gamma$ the following holds

$$\lim_{t\to\infty} \tilde{i}(t) = 1 - \frac{\gamma}{\beta},$$

and in the case when $\beta \leq \gamma$, this limit is zero. However, the corresponding limit for $[i](t)$ is always zero, that is

$$\lim_{t\to\infty} [i](t) = 0,$$

as shown first in [101], as the system is stochastic and there is an absorbing state at $[i] = 0$. Nåsell [90] has shown that in the case of large N, the function $[i]$ has a quasi steady state that is close to the steady state of the ODE system given by Eqs. (3.11 - 3.12), and that the time to extinction scales exponentially with N. Computing $[i](t)$ and $\tilde{i}(t)$ numerically for $N > 30$, the two nearly coincide on a quite long time interval. However, for very large t, $[i](t)$ will tend to zero. Nåsell [90] also investigated the length of the time interval on which $\tilde{i}(t)$ is a good approximation of $[i](t)$.

The next Theorem specifies in rigorous terms the way in which $\tilde{i}(t)$ can be considered a good approximation of $[i](t)$.

Theorem 3.1. *Let G be a fully connected network, and let $\tau = \beta/N$ for some fixed value β. Let X be the solution of $\dot{X} = PX$, the master equation given by Eq. (2.2), and let $[S]$, $[I]$, $[s]$ and $[i]$ be as defined by Eqs. (2.7) & (3.10). Let $(\tilde{s}, \tilde{i})$ be the solutions of the system given by Eqs. (3.11) & (3.12) with the following initial conditions $\tilde{s}(0) = [s](0)$, $\tilde{i}(0) = [i](0)$. Then for any $t \geq 0$ we have*

$$\lim_{N\to\infty} |[s](t) - \tilde{s}(t)| = 0, \qquad \lim_{N\to\infty} |[i](t) - \tilde{i}(t)| = 0.$$

We note that for large t, $\tilde{i}(t)$ remains a valid approximation only if N is suf-

ficiently increased. For finite N, the approximation in the limit of $t \to \infty$ breaks down. While in practical applications $t \to \infty$ is not necessarily an interesting regime, it is worthwhile to formalise precisely and rigorously what is meant by a good approximation.

3.2.1 Proof that the mean-field becomes exact in the limit of a fully connected network and large N

For the proof of Theorem 3.1, it is noted that the full set of $2^N - 1$ Kolmogorov equations, $\dot{X} = PX$, can be significantly reduced in the case of a fully connected network. For a complete network we can introduce $x^k(t)$ as the total probability of states with k infected nodes at time t. This equation lumping exploits the symmetries of complete networks for a fixed number of infected nodes to reduce the system size [113]. Hence for a complete network, the full Kolmogorov equations are given by the following reduced system

$$\dot{x}^k = (k+1)\gamma x^{k+1} + (k-1)(N-k+1)\tau x^{k-1} - (k(N-k)\tau + k\gamma)x^k, \quad (3.13)$$

for $k = 0, 1, \ldots, N$, with $x^{-1} = 0$ and $x^{N+1} = 0$. The scaled expected values of susceptible and infected nodes are

$$[s](t) = \frac{1}{N}\sum_{k=0}^{N}(N-k)x^k(t), \qquad [i](t) = \frac{1}{N}\sum_{k=0}^{N} kx^k(t). \quad (3.14)$$

Our aim here is to investigate the limit of large N and compare these to the solution of the scaled mean-field equations as given by Eqs. (3.11-3.12).

The idea of comparison for large N is to introduce a continuous, time dependent density function $\rho(t, z)$ instead of the discrete distribution $x^k(t)$, with the following formal relation, $z = k/N$. Following this, in Eq. (3.13) we can formally change $\dot{x}^k(t)$ to $\partial_t\rho(t, z)$, $x^k(t)$ to $\rho(t, z)$, $x^{k-1}(t)$ to $\rho(t, z - 1/N)$ and $x^{k+1}(t)$ to

$\rho(t, z + 1/N)$. This leads to the following partial differential equation,

$$\partial_t \rho(t,z) = (Nz+1)\gamma\rho(t,z+1/N) + (Nz-1)(N-Nz+1)\tau\rho(t,z-1/N) -$$

$$(Nz(N-Nz)\tau + Nz\gamma)\rho(t,z).$$

Now using the approximations

$$\rho(t,z+1/N) = \rho(t,z) + \partial_z\rho(t,z)/N, \qquad \rho(t,z-1/N) = \rho(t,z) - \partial_z\rho(t,z)/N,$$

and after some algebra we obtain

$$\partial_t \rho(t,z) = (Nz+1)\gamma\partial_z\rho(t,z)/N + (2Nz-N-1)\tau\rho(t,z) -$$

$$(Nz-1)(N-Nz+1)\tau\partial_z\rho(t,z)/N + \gamma\rho(t,z).$$

Substituting $\tau = \beta/N$, neglecting the $1/N$ and $1/N^2$ terms and writing ρ instead of $\rho(t, z)$, we obtain the following first order partial differential equation for ρ

$$\partial_t\rho = z\gamma\partial_z\rho + (2z-1)\beta\rho - z(1-z)\beta\partial_z\rho + \gamma\rho.$$

Introducing the function $g(z) = \gamma z - \beta z(1-z)$, the equation for ρ becomes

$$\partial_t\rho = \partial_z(g\rho). \tag{3.15}$$

This first order partial differential equation needs an initial condition of the following type

$$\rho(0,z) = \rho_0(z). \tag{3.16}$$

The desired initial condition can be obtained from the initial condition of Eq.

(3.13). This latter initial condition can be written as

$$x^m(0) = 1, \text{ for some } m, \quad x^l(0) = 0, \text{ for } l \neq m, \tag{3.17}$$

that is at the initial instant there are m infected nodes. Since the formal relation between the variables is $z = k/N$, the above initial condition yields

$$\rho_0(z) = 1 \text{ for } \frac{m}{N} < z < \frac{m+1}{N} \text{ and } \rho_0(z) = 0 \text{ otherwise.}$$

Finally, we want to determine the expected value of the infected and susceptible nodes from the first order PDE. Thus we have to find the functions corresponding to $[s](t)$ and $[i](t)$ in Eq. (3.14). Using $z = k/N$ and changing the term $x^k(t)$ to $\rho(t, z)$, we note that the sums in Eq. (3.14) correspond to integrals. Namely, $[i](t)$ corresponds to

$$N \sum_{k=0}^{N} \frac{k}{N} \rho(t, \frac{k}{N}) \frac{1}{N},$$

and this sum is an approximation of the integral

$$N \int_0^1 z\rho(t, z) \mathrm{d}z.$$

Noticing that $\int_0^1 \rho_0(z) \mathrm{d}z = 1/N$, we can introduce $i^*(t)$ as a function corresponding to $[i](t)$ as follows

$$i^*(t) = \frac{\int_0^1 z\rho(t, z) \mathrm{d}z}{\int_0^1 \rho_0(z) \mathrm{d}z}. \tag{3.18}$$

The mean-field equation, Eq. (3.12), can be solved explicitly and the solution is given by

$$\tilde{i}(t) = \frac{B(t) i_0}{\beta - \gamma - A(t) i_0},$$

where $i_0 = \tilde{i}(0)$ is the initial condition and

$$A(t) = \beta - \beta e^{(\beta-\gamma)t}, \qquad B(t) = (\beta - \gamma) e^{(\beta-\gamma)t}.$$

The first order PDE, Eq. (3.15), can also be solved explicitly, and the solution is outlined below.

Intermezzo on the solution of Equation (3.15)

Eq. (3.15) is a first order inhomogeneous linear PDE, with $g(z) = \gamma z - \beta z(1-z)$. Multiplying both sides by $g(z)$ gives

$$\partial_t(g\rho) = g\partial_z(g\rho) \tag{3.19}$$

allowing the introduction of another variable $w(t,z) = g(z)\rho(t,z)$ which leads to the PDE being expressed as

$$\partial_t w - g\partial_z w = 0. \tag{3.20}$$

This PDE, Eq. (3.20), can be solved using the method of characteristics. In parametric form the characteristic equations are given by

$$\frac{\mathrm{d}t}{\mathrm{d}x} = 1, \qquad \frac{\mathrm{d}z}{\mathrm{d}x} = -g \tag{3.21}$$

or alternatively Eqs. (3.21) can be written as the ODE

$$\frac{\mathrm{d}z}{\mathrm{d}t} = -g. \tag{3.22}$$

After substituting for $g(z) = \gamma z - \beta z(1-z)$, Eq. (3.22) can be solved using partial fractions and separation of variables to yield the first integral

$$\frac{1}{\gamma - \beta}\ln\left(\frac{z}{\gamma - \beta + \beta z}\right) + t = C_1. \tag{3.23}$$

This means that the dependent variable, $w(z,t)$, can be written as a function of the first integral Eq. (3.23):

$$w(z,t) = \phi\left(\frac{1}{\gamma-\beta}\ln\left(\frac{z}{\gamma-\beta+\beta z}\right)+t\right). \tag{3.24}$$

In terms of the dependent variable, $\rho(t,z) = w(t,z)/g(z)$, this yields

$$\rho(z,t) = \frac{1}{\gamma-\beta+\beta z}\phi\left(\frac{1}{\gamma-\beta}\ln\left(\frac{z}{\gamma-\beta+\beta z}\right)+t\right). \tag{3.25}$$

Next, the initial condition given in Eq. (3.16) needs to be written in terms of w, which gives

$$w(0,z) = g(z)\rho(0,z) = z(\gamma-\beta+\beta z)\rho_0(z) = \phi\left(\frac{1}{\gamma-\beta}\ln\left(\frac{z}{\gamma-\beta+\beta z}\right)\right). \tag{3.26}$$

A dummy variable u is introduced where

$$u = \frac{1}{\gamma-\beta}\ln\left(\frac{z}{\gamma-\beta+\beta z}\right)$$

which allows us to construct an expression for z, namely

$$z = \frac{(\gamma-\beta)e^{u(\gamma-\beta)}}{1-\beta e^{u(\gamma-\beta)}}. \tag{3.27}$$

Substituting Eq. (3.27) into Eq. (3.26) allows us to define the function $\phi(u)$ explitly

$$\phi(u) = \left[\frac{(\gamma-\beta)e^{u(\gamma-\beta)}}{1-\beta e^{u(\gamma-\beta)}}\left(\gamma-\beta+\beta\frac{(\gamma-\beta)e^{u(\gamma-\beta)}}{1-\beta e^{u(\gamma-\beta)}}\right)\right]\rho_0\left(\frac{(\gamma-\beta)e^{u(\gamma-\beta)}}{1-\beta e^{u(\gamma-\beta)}}\right). \tag{3.28}$$

Now the form of the function ϕ is known, an equation for $\rho(t,z)$ can now be developed as we know that

$$\rho(t,z) = \frac{w(t,z)}{g(z)} = \frac{\phi\left(\frac{1}{\gamma-\beta}\ln\left(\frac{z}{\gamma-\beta+\beta z}\right)+t\right)}{g(z)}. \tag{3.29}$$

After substituting for $\phi\left(\frac{1}{\gamma-\beta}\ln\left(\frac{z}{\gamma-\beta+\beta z}\right)+t\right)$ from Eq. (3.28) and $g(z) = \gamma z - \beta z(1-z)$, some algebra yields an explicit general solution of Eq. (3.15):

$$\rho(t,z) = \rho_0\left(\frac{z(\beta-\gamma)}{\beta z-(\gamma-\beta+\beta z)e^{t(\beta-\gamma)}}\right)\frac{(\beta-\gamma)^2 e^{t(\gamma-\beta)}}{(\beta z-(\gamma-\beta+\beta z)e^{t(\beta-\gamma)})^2}. \tag{3.30}$$

As the objective of this Theorem is to compare Eq. (3.18), the same substitutions, namely

$$A(t) = \beta - \beta exp((\beta-\gamma)t), \qquad B(t) = (\beta-\gamma)exp((\beta-\gamma)t).$$

are made, reducing Eq. (3.30) to

$$\rho(t,z) = \rho_0\left(\frac{z(\beta-\gamma)}{A(t)z+B(t)}\right)\frac{(\beta-\gamma)B(t)}{(A(t)z+B(t))^2}. \tag{3.31}$$

We are now in a position to solve Eq. (3.18) and find an expression for $i^*(t)$. Firstly an expression for $i^*(0)$ is developed

$$i^*(0) = \frac{\int_0^1 z\rho_0(z)\mathrm{d}z}{\int_0^1 \rho_0(z)\mathrm{d}z} = \frac{b_u+b_l}{2}. \tag{3.32}$$

where $b_{l,u}$ are the upper and lower boundaries of the region in which $\rho_0(z) \neq 0$. Note also that $b_u - b_l = 1/N$. Also by solving Eq. (3.31) and noting that a solution only exists if $\rho_0(z) = 1$ then we find that

$$\int_0^1 \rho(t,z)\mathrm{d}z = \int_{z_l}^{z_u}\frac{(\beta-\gamma)B(t)}{(A(t)z+B(t))^2}\mathrm{d}z$$

$$= \frac{(\beta-\gamma)B(t)}{A(t)}\left[\frac{1}{A(t)z_l+B(t)} - \frac{1}{A(t)z_u+B(t)}\right]_{z_l}^{z_u}$$

As $b_{l,u}$ are initial conditions of $\rho_0(z)$, we need to know what $z_{l,u}$ are in terms of $b_{l,u}$. This is found by

$$\frac{(\beta-\gamma)z_{l,u}}{A(t)z_{l,u}+B(t)} = b_{l,u} \qquad \Rightarrow \qquad z_{l,u} = \frac{B(t)b_{l,u}}{(\beta-\gamma)-A(t)b_{l,u}} \tag{3.33}$$

As $\int_0^1 \rho(t,z)\mathrm{d}z = \int_0^1 \rho_0(z)\mathrm{d}z\,\forall t$, substituting the limits given in Eq. (3.33) into our expression for $\int_0^1 \rho(t,z)\mathrm{d}z$, given above, leads us to deduce that

$$\int_0^1 \rho_0(z) = \frac{1}{N}. \tag{3.34}$$

Similarly

$$\int_0^1 z\rho(t,z)\mathrm{d}z = \int_{z_l}^{z_u} z\frac{(\beta-\gamma)B(t)}{\left(A(t)z+B(t)\right)^2}\mathrm{d}z$$

can be solved by using integration by parts and remembering that $i(0) = \frac{b_u+b_l}{2}$ and $b_u - b_l = \frac{1}{N}$ to give

$$\begin{aligned}\int_0^1 z\rho(t,z)\mathrm{d}z &= B(t)(\beta-\gamma)\left(-\frac{1}{NA(t)(\beta-\gamma)}\right. \\ &\quad \left. +\frac{1}{A^2}\ln\left(1+\frac{2A(t)}{2N((\beta-\gamma)-A(t)i_0)-A(t)}\right)\right).\end{aligned} \tag{3.35}$$

By substituting Eqs. (3.34 & 3.35) into Eq. (3.18) yields a final expression for $i^*(t)$:

$$i^*(t) = \frac{B(t)}{A(t)}\left[\frac{N(\beta-\gamma)}{A(t)}\ln\left(1+\frac{2A(t)}{2N(\beta-\gamma-A(t)i_0)-A(t)}\right)-1\right].$$

End of Intermezzo

Having these explicit formulas for $i^*(t)$ and $\tilde{i}(t)$, it is easy to see that i^* is not a solution of the mean-field equation, Eq. (3.12), but it can be proved that as $N \to \infty$ it tends to the solution of Eq. (3.12). Namely, we have the following

Lemma.

Lemma 3.2. *Let ρ be the solution of the system given by Eq. (3.15) with initial condition given by Eq. (3.16). Let $i^*(t)$ be defined by Eq. (3.18). Let $\tilde{i}(t)$ be the solution of the scaled mean-field equation given by Eq. (3.12) with initial condition $\tilde{i}(0) = m/N$. Then for any $t \geq 0$ we have*

$$\lim_{N\to\infty} |\tilde{i}(t) - i^*(t)| = 0.$$

This Lemma can be proved by using the explicit formulas for $i^*(t)$ and $\tilde{i}(t)$. As $N \to \infty$

$$\begin{aligned} i^*(t) &\approx \frac{B(t)}{A(t)} \left[\frac{N(\beta-\gamma)}{A(t)} \frac{2A(t)}{2N(\beta-\gamma-A(t)i_0)} - 1 \right] \\ &\approx \frac{B(t)}{A(t)} \left[\frac{\beta-\gamma}{\beta-\gamma-A(t)i_0)} - 1 \right] \\ &\approx \frac{B(t)}{A(t)} \left[\frac{\beta-\gamma-(\beta-\gamma-A(t)i_0)}{\beta-\gamma-A(t)i_0)} \right] \\ &\approx \frac{Bi_0}{\beta-\gamma-A(t)i_0} \\ &= \tilde{i}(t) \end{aligned}$$

Now the proof of the Theorem can be concluded as follows. We want to prove that the scaled expected value $[i](t)$ tends to the solution $\tilde{i}(t)$ of the scaled mean-field equation as $N \to \infty$. In order to prove this, we introduced a first order PDE that can be considered the limit of Eq. (3.13) as $N \to \infty$. Using this PDE, we defined the function $i^*(t)$ that corresponds to $[i](t)$. According to Lemma 3.2, $i^*(t)$ is close to $\tilde{i}(t)$ for large N. Hence, we only have to show finally that $[i](t)$ is close to $i^*(t)$. Thus the proof of Theorem 3.1 will be complete if the following Lemma is verified.

Lemma 3.3. *Let x^k be the solution of Eq. (3.13) satisfying the initial condition*

given by Eq. (3.17), and let ρ be the solution of Eq. (3.15) with initial condition given by Eq. (3.16). Let $[i](t)$ and $i^*(t)$ be defined by Eq. (3.14) and by Eq. (3.18). Then for any $t \geq 0$ we have

$$\lim_{N\to\infty} |[i](t) - i^*(t)| = 0.$$

□ The proof of the Lemma is based on the fact that the lumped system, Eq. (3.13), can be considered as the discretisation of the first order PDE, Eq. (3.15), in the variable z. It is known even for more general PDEs, see e.g. Chapters 3 and 4 in [54], that the solution of the discretised system tends to that of the PDE as the step size of the discretisation goes to zero, that is in our case N tends to infinity.

3.3 Moment closure at the level of triples (pairwise models)

The exact system of Equations (2.9 - 2.13) that has been derived from the Kolmogorov equation, as shown again at the start of this Chapter, is now closed at the level of triples by finding approximate closures that describe them in terms of pair and individual counts.

We assume here that every individual has the same neighbourhood size n (in the case of networks with heterogeneous degree distribution we obtain an approximation by taking n to be the real-valued mean degree, which is not rigorously interpretable) and also define a clustering coefficient ϕ

$$n = \sum_j G_{ij}, \forall i \ , \qquad \phi = \frac{\mathrm{Tr}(G^3)}{\|G^2\| - \mathrm{Tr}(G^2)} \in [0,1] \ .$$

We will use these two real parameters n, ϕ in the formulation of different closure approximations. In the absence of clustering ($\phi = 0$) both approximations we will consider agree that

$$[ABC] \approx n(n-1)p_{A|B}p_{C|B} \text{ , where } \quad p_{A|B} := \frac{[AB]}{n[B]} \text{ .} \tag{3.36}$$

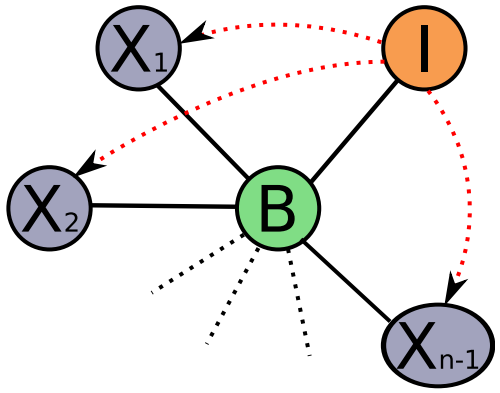

Figure 3.1: Motivation for improved pairwise closure. Triples of type [ABI] are counted by consideration of the neighbourhood around a typical [BI] pair. The states $X_1, \ldots, X_{n-1}$ are chosen in order, with the presence or absence of potential transitive links (red dotted lines) decided simultaneously as outlined in Eq. (3.38) of the main text.

This closure implicitly assumes that the disease states of individuals around a node in state B are given by independent trials, and so neighbourhood types are multinomially distributed [19]. However, this assumption breaks down as correlations will develop between the status of neighbouring nodes, as new infections are bound to be the neighbours of their infectors. This will especially become an issue for SIS type dynamics as, for example, if the middle node of an $[III]$ triple recovers, it is likely to quickly become infected again, leading to more $[II]$ pairs and $[III]$ triples than would be expected if the infected nodes were distributed at random. This effect is further exacerbated when the disease spreads on networks with heterogeneous degree distributions [23]. Furthermore, for the case of clustering, understanding the implicit assumptions behind different closure methods is much harder. Here, we present a new motivation of existing moment closure

techniques, similar to the classic statistical approach to clustering of Klotz [78] who developed a method of statistical inference for non-independent Bernoulli trials, whereby there is assumed to be a statistical dependence between the state of a given node and the state of that node's neighbourhood. This new explanation makes it much easier to see which kinds of network structure are assumed during moment closure, and how different closures are related to each other.

Our starting point is the correlation matrix between different adjacent dynamical states, which is equal to unity for homogeneous random mixing

$$\mathcal{C}_{A,B} := \frac{N}{n}\frac{[AB]}{[A][B]} \ . \tag{3.37}$$

Figure 3.1 shows the construction used in our closure derivation. We start by noting that only triples of type $[ABI]$ need to be closed, and that this can be done in terms of the neighbourhood around each $[BI]$ pair. We consider each of the other $n-1$ neighbours of a B in such a $[BI]$ pair in turn. For each such neighbour X_i, we decide with probability ϕ whether it is connected to the I in the $[BI]$ pair or not. We then pick its dynamical state, taking into account the correlations between the proposed state and I if they are connected. Making use of equation (3.37), the fact that X_i state probabilities have to sum to unity, and provided the identity $\sum_a [aB] = n[B]$ is conserved by the dynamics (as it was shown to in [52]), our explicit consistent local assumption is that

$$\Pr(X_i = A) = \begin{cases} p_{A|B} \text{ with probability } (1-\phi) \ , \\ p_{A|B}\mathcal{C}_{A,I} / \left(\sum_a p_{a|B}\mathcal{C}_{a,I}\right) \text{ with probability } \phi \ . \end{cases} \tag{3.38}$$

Averaging over all neighbourhoods around $[BI]$ pairs gives the expected number

(a) Unclustering rewiring

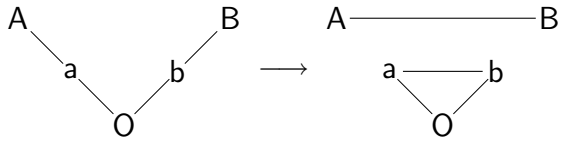

(b) Big-V rewiring

Figure 3.2: Rewiring methods. (a) shows the unclustering rewiring, which will evolve a network towards an unclustered configuration-model network of the same degree distribution. (b) shows the big-V rewiring, which generates clustering of the type expected to agree with moment closure approximations.

of relevant triples in the network as

$$\begin{aligned}[ABI] &\approx (n-1)[BI]\left((1-\phi)p_{A|B} + \phi\frac{p_{A|B}\mathcal{C}_{A,I}}{\sum_a p_{a|B}\mathcal{C}_{a,I}}\right) \\ &\approx (n-1)\left((1-\phi)\frac{1}{n}\frac{[BI][BA]}{[B]} + \phi\frac{[BA][IA]/[A]}{\sum_a ([Ba][Ia]/[a])}\right) \ .\end{aligned} \tag{3.39}$$

This is the improved pairwise approximation (IPA) proposed in [52], which was originally motivated by its satisfaction of two practical desiderata: the conservation of pair number and consistent behaviour of $[III]$-type triples. These properties can now be seen to follow from the consistent probabilistic neighbourhood-based description of the improved closure above.

The standard clustered pairwise closure presented in [61, 103] can be recovered by making the assumption $\left(\sum_a p_{a|B}\mathcal{C}_{a,I}\right) \approx 1$ so that

$$[ABI] \approx \frac{n-1}{n}\frac{[AB][BI]}{[B]}\left((1-\phi) + \phi\frac{N}{n}\frac{[AI]}{[A][I]}\right) \ . \tag{3.40}$$

This closure, referred to as the original pairwise approximation (OPA), has the

benefit of significantly reducing the complexity (and hence numerical effort in integration) of the closed set of equations, but since the approximation used is logically inconsistent there is the possibility of serious pathologies creeping into numerical results. This possibility partly motivates our comparison below of both closures against a more comprehensive set of clustered networks than has previously been considered.

In both the standard and improved closures, the now-explicit assumption made about clustering is that each transitive link exists with independent probability ϕ, and so we would expect networks where transitive links are themselves clustered together into cliques as in [8] or unclustered as in [127] where no triangles overlap not to give good dynamical agreement with the proposed closures.

3.4 The performance of different moment closures versus stochastic simulation

The pairwise models aim to capture the local or small scale network properties such as n, the average node degree, and ϕ, the clustering coefficient by using different moment closures. However, there are many known large-scale network properties that have been observed in real-world networks [128]. As shown by Green & Kiss [41], it is possible to produce theoretical networks that capture a range of these observed real-world features, and hence can produce networks that differ vastly in large scale properties even though the local properties are identical. In this section, we explore how much of the underlying network structure is captured by n and ϕ alone on networks generated by different algorithms by examining how well the pairwise models based on the closures given in Eqs. (3.40 & 3.39) agree with results from stochastic simulation.

The network generating algorithms used here are deliberately chosen such that some agree well with the pairwise ODEs whilst other agree poorly, despite having

the same values of n and ϕ. This is done in order to demonstrate the limited ability of these local metrics to accurately describe the full network structure. For each network generating algorithm 100 distinct networks were produced. Thereafter, 5 realisations of an epidemic were performed on each, leading to the mean number of individuals, pairs and triples being averaged over 500 realisations for each family of network. For all simulations, we set $\gamma = 1$ and $\tau = 0.5$ to ensure that an epidemic will break out. Each network has $N = 10,000$ nodes, and simulations were synchronously updated. Initially 5 nodes are chosen at random to be infected. In fact, apart from the networks themselves, the only differences between the simulations are the parameters n and ϕ, with $n \in \{5, 10\}$ and $\phi \in \{0, 0.4\}$.

The first networks explored were generated using the spatial algorithm [105] whereby nodes are distributed uniformly at random across a $\sqrt{N} \times \sqrt{N}$ square with toroidal boundary conditions. The probability p_{ij} of two nodes i and j being connected is dependent on the distance d_{ij} between them and is determined by a normal-like connectivity kernel such that $p_{ij} = p_0 e^{-d_{ij}^2/2D^2}$, where p_0 and D are parameters to be adjusted to obtain the required values of n and ϕ. A second set of networks were generated by first removing any existing clustering, and then re-wiring the spatial networks using big-V rewiring [41, 53], as shown in Fig. 3.2. This preserves the clustering coefficient and node degree but removes other forms of structure.

A third set of networks were generated using the group-based algorithm [92] which is based on a bipartite network. The N nodes are assigned to groups and the connections within groups are explained in detail by Green & Kiss: "Multiple group membership by nodes leads to between group linkages. For each of g groups, ν nodes are chosen at random (without replacement), with nodes thus enjoying a mean of $\mu = gN/\nu$ groups, binomially distributed. For every pair of nodes that are members of the same group, an edge is added with probability $p = \frac{n}{\mu(\nu-1)}$.

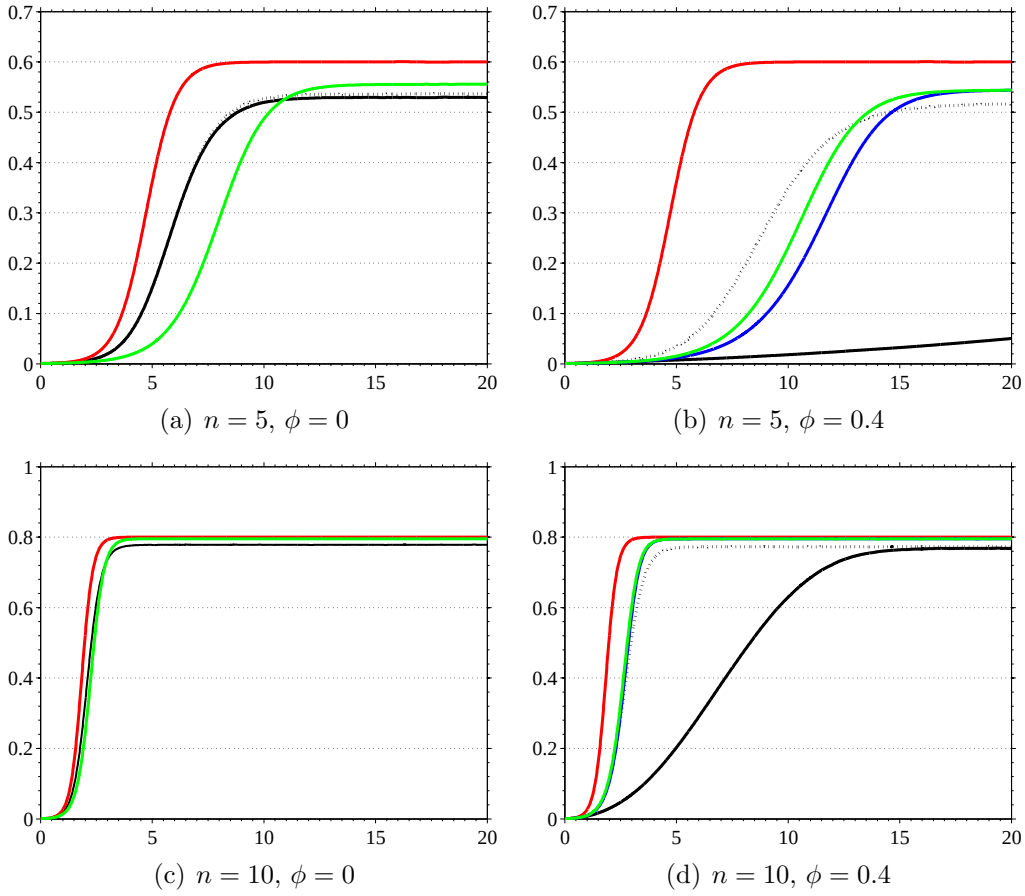

Figure 3.3: Infection prevalence time series for networks generated using the spatial algorithm along with results given by moment closure equations. In all plots $N = 10,000$, $\tau = 0.5$ and $\gamma = 1$ with varying n and ϕ. The solid black line is for simulation results from the spatial algorithm and the black dashed line is for simulation results from the same spatial algorithm but with the networks reclustered using big-V rewiring. The red line is the mean-field approximation, the blue line is the ordinary pairwise approximation (OPA) and the green line is for the improved pairwise approximation (IPA). In the cases where $\phi = 0$ the OPA and IPA coincide.

The resulting networks have clustering coefficient $\phi = \frac{p}{1+\mu(\nu-1)/(\nu-2)}$" [41]. Thus the desired values of n and ϕ can be obtained by varying the number of groups per node, μ, subject to the constraint that $p \leq 1$. A fourth set of networks comes from applying big-V rewiring to the group-based algorithm.

A fifth set comes from an iterative algorithm proposed by Eames [25], which is a two step process. Firstly n_1 triples are generated by connecting three unique, randomly chosen nodes. Secondly n_2 triangles are generated by selecting a node

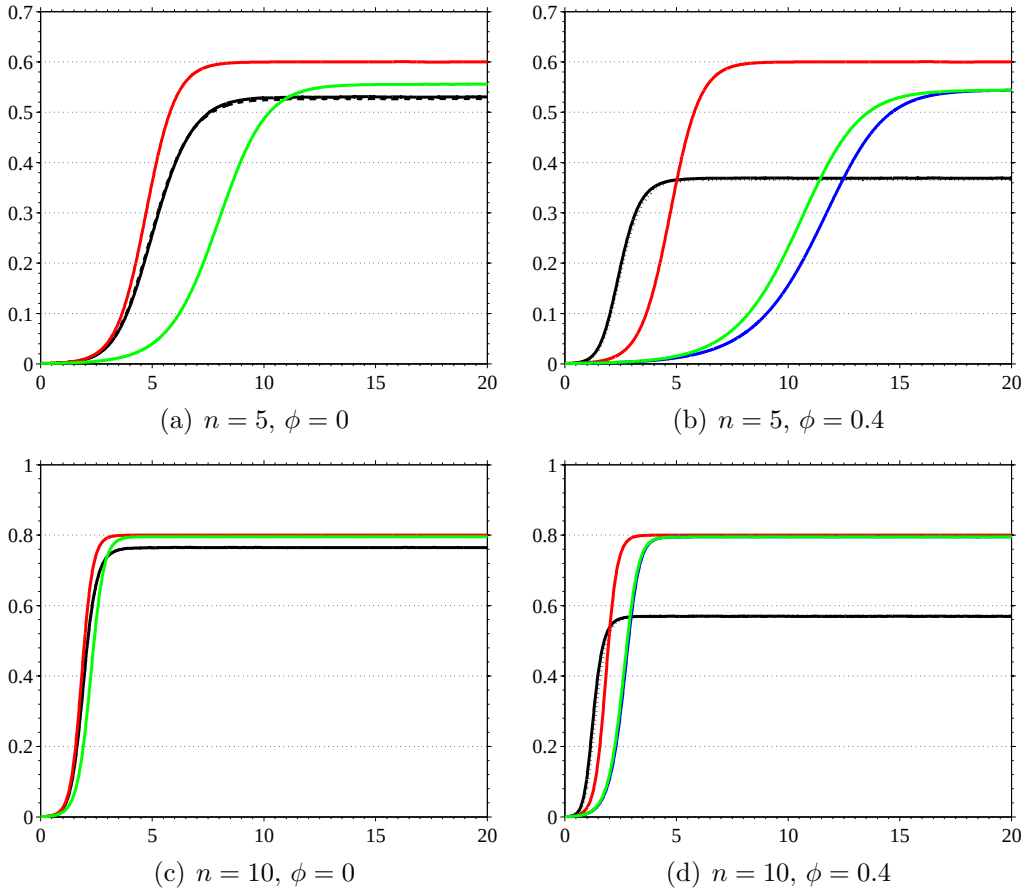

(a) $n = 5$, $\phi = 0$ (b) $n = 5$, $\phi = 0.4$

(c) $n = 10$, $\phi = 0$ (d) $n = 10$, $\phi = 0.4$

Figure 3.4: Infection prevalence time series for networks generated using the group-based algorithm along with the results given by moment closure equations. In all plots $N = 10,000$, $\tau = 0.5$ and $\gamma = 1$ with varying n and ϕ. The solid black line is for simulation results from the group-based algorithm and the black dashed line is for simulation results from the same group-based algorithm but with the networks reclustered using big-V rewiring. The red line is the mean-field approximation, the blue line is the ordinary pairwise approximation (OPA) and the green line is for the improved pairwise approximation (IPA). In the cases where $\phi = 0$ the OPA and IPA coincide.

at random that has at least two neighbours, of which two neighbours are then chosen at random to themselves be connected. The parameters n_1 and n_2 are varied to obtain the required values of n and ϕ. A final set is generated by unclustering the networks generated by the iterative algorithm. Further details of all these algorithms can be found in [41]. The rewirings used are shown in Figure 3.2, where (a) shows the unclustering rewiring and (b) shows the big-V rewiring.

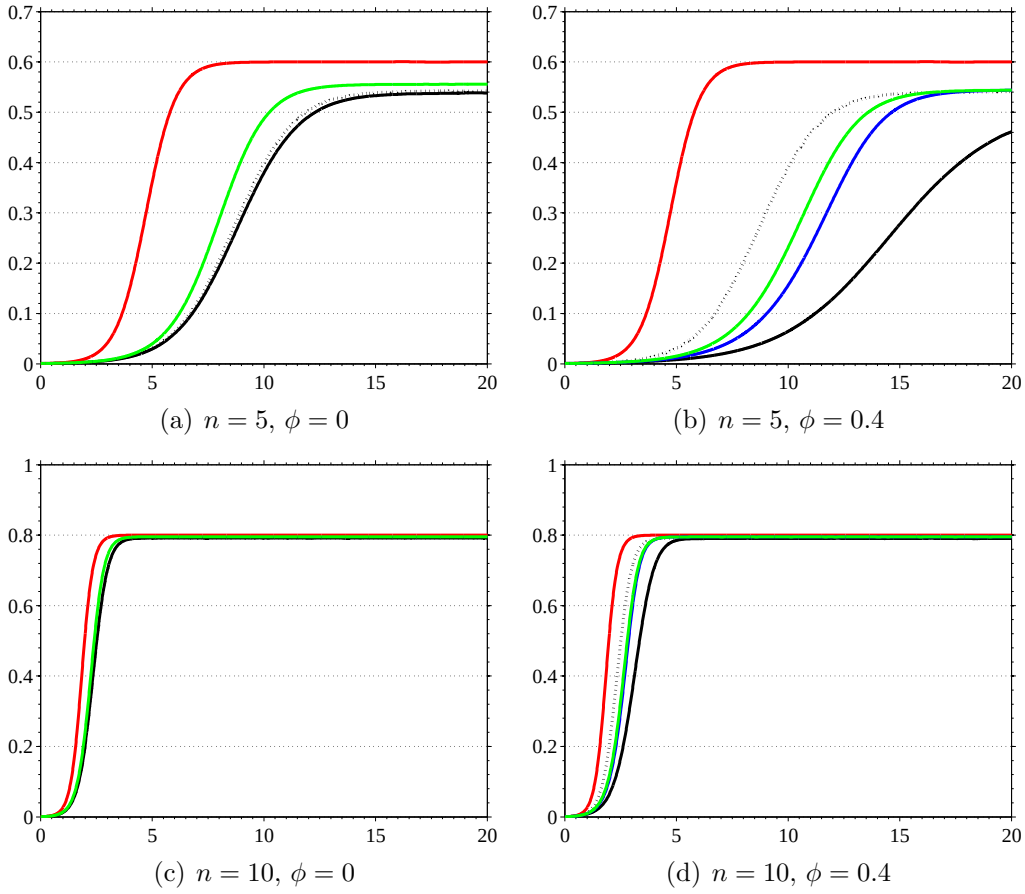

(a) $n = 5$, $\phi = 0$ (b) $n = 5$, $\phi = 0.4$

(c) $n = 10$, $\phi = 0$ (d) $n = 10$, $\phi = 0.4$

Figure 3.5: Prevalence time series for networks generated using the iterative algorithm along with the results given by moment closure equations. In all plots $N = 10,000$, $\tau = 0.5$ and $\gamma = 1$ with varying n and ϕ. The solid black line is for simulation results from the iterative algorithm and the black dashed line is for simulation results from the same iterative algorithm but with the networks unclusterd. The red line is the mean-field approximation, the blue line is the ordinary pairwise approximation (OPA) and the green line is for the improved pairwise approximation (IPA). In the cases where $\phi = 0$ the OPA and IPA coincide.

The different combinations of n and ϕ values leads to four versions of each network type. For each of these, the prevalence of infection over time is compared with the approximations from the two pairwise closures as well as the mean-field model. Figure 3.3 shows results for both the spatial networks and their reclustered counterparts, Figure 3.4 show results for both the group-based networks and their reclustered versions and Figure 3.5 shows results for the iterative networks and their unclustered versions. Both of the pair approximations agree best with

simulation results at equilibrium when $n = 10$ and $\phi = 0$ regardless of the network and this is in line with previous findings [61, 113]. In this case, even the mean-field approximation provides a good fit even though $n << N$. The figures show that reducing n or increasing ϕ reduce the goodness of fit between the moment closure approximations and the simulation results for all networks, although the amount they differ depends on the network generating algorithm.

The networks that show the worst fit for the moment closures are the group-based networks when n is low and ϕ is high, as seen in Figure 3.4(b). Here the epidemic picks up much quicker than predicted even by the mean-field approximation but the final epidemic size is much smaller. This is a result of the algorithm producing high degree heterogeneity with many nodes remaining unconnected for higher values of ϕ, as shown by Green & Kiss [41]. Indeed for all four combinations of n and ϕ there is negligible difference between the results on the standard group-based networks and those on their reclustered counterparts. For these group-based networks ϕ has a more important role than n in determining whether or not the pairwise approximations are in good agreement with simulations. Another interesting feature of the group-based networks is the limited impact of the big-V rewiring on the underlying structure, as this simply rearranges the local links within the existing groups and will not change the way the two groups are linked together.

The somewhat simpler and more straightforward iterative algorithm shown in Figure 3.5 shows good qualitative agreement between the simulations and ODEs, with the ODEs overpredicting the initial growth in all cases but with agreement becoming good for increasing n. Unclustering these networks returns simulation results that are similar to those seen in the cases where $\phi = 0$ and this provides a good check for the effectiveness of the unclustering algorithm.

The most interesting case is for networks generated by the spatial algorithm as shown in Figure 3.3. Here the ODEs overpredict final epidemic size in all cases,

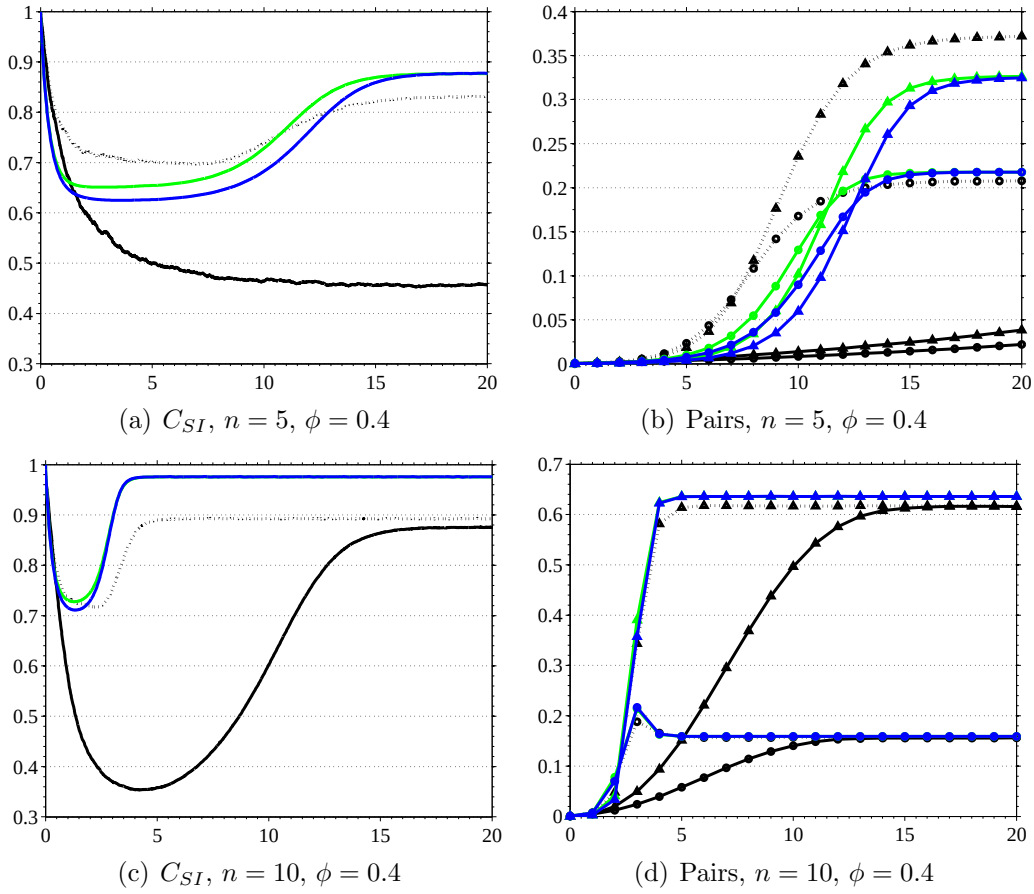

(a) C_{SI}, $n = 5$, $\phi = 0.4$

(b) Pairs, $n = 5$, $\phi = 0.4$

(c) C_{SI}, $n = 10$, $\phi = 0.4$

(d) Pairs, $n = 10$, $\phi = 0.4$

Figure 3.6: Figures 3.6(a) & 3.6(c) show time series for the correlation C_{SI} as defined in Eq. (3.37). Figures 3.6(b) & 3.6(d) show time series for proportion of pairs that are (S, I) (circles) and (I, I) (triangles). In all plots $N = 10,000$, $\tau = 0.5$ and $\gamma = 1$. The solid black line is for simulation results from the spatial algorithm and the black dashed line is for simulation results from the same spatial algorithm but with the networks reclustered using big-V rewiring. The blue line is the ordinary pairwise approximation (OPA) and the green line is for the improved pairwise approximation (IPA).

but not by a significant amount. For the cases with $\phi > 0$ the initial growth of the epidemic is much slower than predicted by the ODEs, especially when $n = 5$. This type of network, however, responds very well to being reclustered using big-V rewiring. The difference in agreement for the standard networks and their reclustered counterparts when $\phi > 0$ is very large, showing that there is much underlying network structure generated by the spatial algorithm that is not captured by n and ϕ. There are remarkable differences between the results from these two networks, as seen in Figures 3.3(b) and 3.3(d), and these show

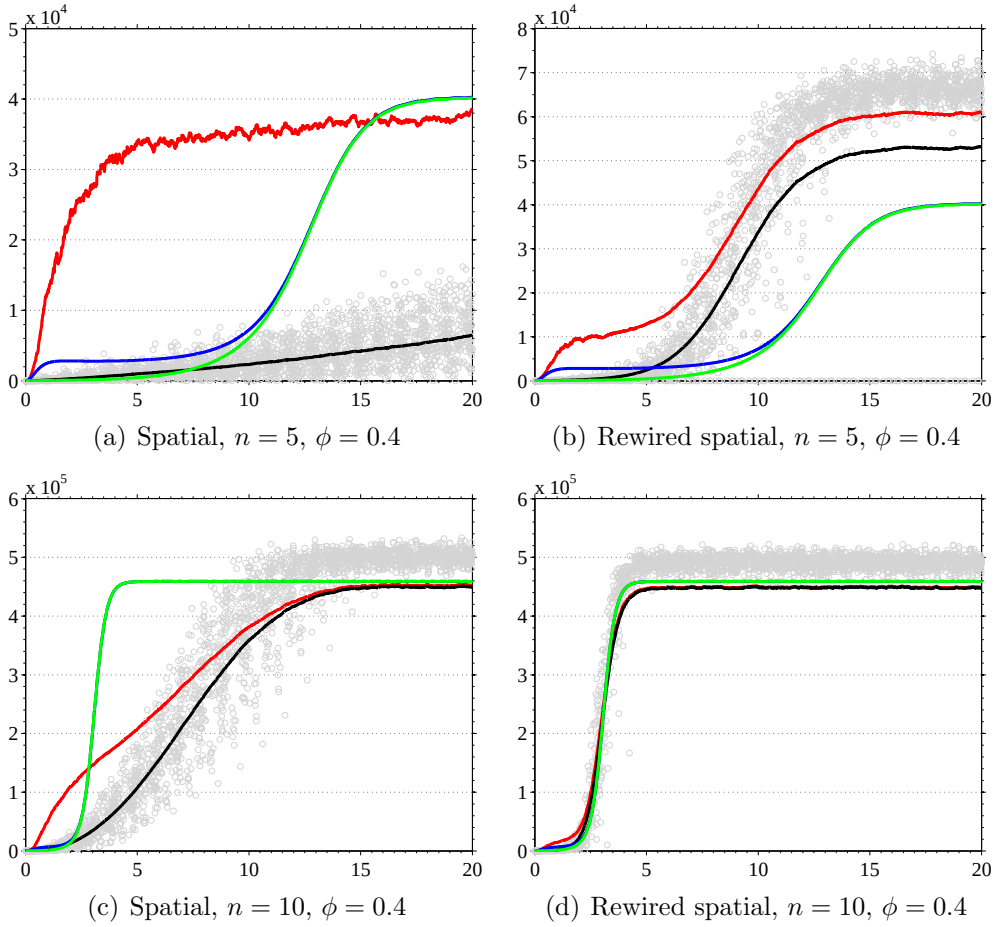

(a) Spatial, $n = 5$, $\phi = 0.4$

(b) Rewired spatial, $n = 5$, $\phi = 0.4$

(c) Spatial, $n = 10$, $\phi = 0.4$

(d) Rewired spatial, $n = 10$, $\phi = 0.4$

Figure 3.7: Showing $[III]$ triples counted in different ways for $n = 5, 10$ and $\phi = 0.4$ on spatial networks and their big-V rewired counterparts. The grey cloud shows actual counts of $(I - I - I)$ triple from individual stochastic realisations. The blue and green line show [III] calculated using the OPA given by Eq. (3.40) and the IPA given by Eq. (3.39) respectively with both using pair and individual values from solving the macro ODE system (Eqs. (2.9 - 2.13)). The red and black lines show the OPA and IPA respectively, but with values for individuals and pairs as averages from the stochastic simulation.

the importance of large scale spatial structure in determining how an epidemic can invade. The goodness of agreement is directly linked to the capability of the pairwise models to correctly describe the pair dynamics. This is captured in Figure 3.6 that shows the correlations, C_{SI}, and the normalised expected number of $[II]$ and $[SI]$ pairs. It can be seen that the rewired networks display much better agreement in both the growth of pairs and C_{SI} when comparing pairwise approximations to simulation results. This shows that the big-V rewiring has

successfully removed higher level structure, and in this case, the pairwise closures correctly capture the evolution of correlations and pairs.

The performance of pairwise models does not depend solely on the structure of the network but also on the dynamics (e.g. SIS, SIR, $SITS$, where T stands for tracing triggering individuals) that unfold on the network. For example, House & Keeling [52], show that for contact tracing models, the OPA does not account correctly for the evolution of triangles with three infected individuals and this can lead to skewed outcomes and they went on to address this via the IPA. In Figure 3.7 we show that for simple SIS dynamics the IPA captures the initial growth of $[III]$ triples much better than the OPA. This difference is emphasised when the values of the pairs and singles that constitute the two different closures are taken directly from the simulation. Figure 3.7(a) shows this difference most dramatically, with the OPA predicting a much more rapid early growth of these $[III]$ triples, whereas the IPA describes their actual evolution with a much higher degree of accuracy. However, the failure of the OPA to correctly capture the evolution of $[III]$ triples does not translate to a significant difference in the time evolution of the prevalence (see Figure 3.3) but as House & Keeling [52] point out, the evolution of these triples becomes important when more complicated dynamics, e.g. $SITS$, are playing out on the networks. The evolution of all other triples is much better approximated by both the OPA and IPA and moreover, as noted before, the big-V rewiring successfully removes higher level network structure and leads to an overall better agreement between all approaches. Thus, these observations highlight the importance of considering both network structure and the particular dynamics when deriving macro-ODE models.

3.5 Discussion

In this chapter we have used three different moment closures approximations and rigourously proven that they become exact in the limit of large fully connected

networks. Also, we have compared results from these ODEs to those from the micro-modelling process of individual-based simulations. The results reveal that moment closures heavily rely on exploiting local network structure and for networks where higher order structure is present the agreement breaks down. We have shown that using a special rewiring technique, that removes higher-order or large-scale structure while keeping local properties unchanged, improves the agreement between micro and macro models significantly for certain types of network but has little effect on certain others.

Our analysis shows that large-scale network structure plays a crucial role when deriving moment closure approximations. Existing closures often rely on local network properties alone and perform poorly in accounting for larger scale features. However, much progress has been made in accounting for properties such as node degree and degree distribution heterogeneity [26, 71], preferential mixing [24, 72], clustering [27] and even directed or weighted edges [112]. While most of these models rely on some form of pairwise closure, there is scope for better understanding and justification of the approximations used, as well as working towards a unifying framework for such approximation models.

This chapter shows that it is worthwhile to consider alternative custom-made closures for different networks, and to do this, it may be necessary to incorporate non-local network properties especially when local network metrics such as n and ϕ fail to capture the key network features. For example, Green & Kiss [41] use network measures other than n and ϕ to investigate the correlation between simulation results and non-local network metrics. An alternative approach may rely on higher order motifs, such as quadruples [51], and accounting for these could lead to improved approximation models. One of the key challenges for generating valid and accurate moment closure approximations is to account for the dependence of the state of a node on the state of neighbouring nodes, and the correlations that arise as a result. Indeed these dependencies will act on a larger

scale than simply a node's immediate neighbours, so the challenge of finding appropriate closures may be very difficult. Such approaches, at least in the initial stages of development, will rely on generating theoretical toy networks that can be used to assess the goodness of the approximations. If these novel approximations will only yield satisfactory results for specific networks, their practical benefits will be small but could form the building blocks to develop models that are valid for larger or more realistic sets of networks. It is clear that only by understanding the fundamental structures that underpin any network can moment closure techniques be confidently used to model dynamical processes on networks.

Chapter 4

Dynamic contact networks - an epidemic model with random link activation and deletion

4.1 Introduction

In this chapter we present a model describing SIS type epidemics spreading on a dynamic contact network with random link activation and deletion, where link activation can be locally constrained. We use and adapt an improved effective degree compartmental modelling framework recently proposed by Lindquist *et al.* [83] and separately by Marceau *et al.* [85]. The resulting set of ODEs is solved numerically and results are compared to those obtained using individual-based stochastic network simulation. We show that the ODEs display excellent agreement with simulation for the evolution of both the disease and the network, and are able to accurately capture the epidemic threshold for a wide range of parameters. We also present an analytical R_0 calculation for the dynamic network model and show that, depending on the relative timescales of the network evolution and disease transmission, two limiting cases are recovered: (i) the static network case

when network evolution is slow and (ii) homogeneous random mixing when the network evolution is rapid. We also use our threshold calculation to highlight the dangers of relying on local stability analysis when predicting epidemic outbreaks on evolving networks.

4.2 Background

The rise in the popularity and relevance of networks as a tool for modelling complex systems is well illustrated by the ever increasing body of research concerned with the spread of diseases within host populations exhibiting non-trivial contact structures [1, 93]. Networks offer an intuitive and relatively simple modelling framework which enables us to relax the strong implicit assumptions of more classical ODE based approaches and to account for complexities in the contact structure of the host population [9, 26, 44, 91, 114]. This approach has shown that epidemic thresholds not only depend upon the infectiousness of the pathogen, or even simply the mean number of contacts per individual, but also upon the exact structure of the host population [5, 120]. In addition to its inherent theoretical value, this paradigm has immediate practical benefits, as the primary role of public health services is to put measures in place to bring diseases below their epidemic threshold. These measures depend heavily upon disrupting the transmission of a disease through vaccination and also more directly through the closure of public services, or even quarantine and curfews in extreme cases. Hence the knowledge of how the structure of the host population is contributing to the spread of a disease would help to increase the efficacy of any intervention [88].

Despite advances in both rigorous and non-rigorous analysis of networks, a key assumption in many network models is that contacts are fixed for the duration of an epidemic and that the disease propagates with a constant intensity across links. This will not be true for many diseases, especially those with long infectious periods, or diseases that become endemic. Indeed human contact patterns are

well described by short repeated events, with individuals having a number of contacts best described by some appropriate time dependent random variable [104]. Furthermore, individuals and the communities they belong to are likely to change their contact behaviour as a result of natural evolution and endogenous or exogenous perturbations such as a disease outbreak [82].

Recently a number of studies have attempted to relax this assumption by allowing the networks to evolve over time by either varying contacts independently of the status of individuals [125, 126] or by explicitly coupling contact activation and deletion to the disease status of individuals [44, 85, 123]. Thus, in the latter case, the dynamics of the disease is coupled with the dynamics of the network itself, with both acting as a feedback mechanism for the other [43, 123, 129]. Many of these studies have built macro ODE-based models that describe the coevolution of networks and the diseases that spread along them [44, 85, 111, 123]. All these studies confirm that dynamic networks and the coupling between the two dynamics lead to a richer spectrum of behaviour than is found for epidemics on static networks.

A crucial feature of allowing the co-evolution of disease and network is the interplay and feedback between both dynamics, however this interdependence is difficult to measure empirically. The models developed so far mainly use rewiring rules that intuitively make sense given that individuals would have knowledge of the disease states of the rest of the population. However in this chapter we move away from these assumptions and we propose a dynamic network model that is based on random link activation-deletion, which would be more relevant for asymptomatic diseases, such as chlamydia [84]. Furthermore our dynamic network model is refined by introducing a local constraint on link activation to account for the difference in the magnitude of the number of contacts of a node relative to system size. This dynamic network coupled with the simple SIS disease dynamics leads to the full model that will be analysed and discussed. We

study this system and explore to what extent a macro ODE-based compartmental model proposed for static networks is flexible enough to be adapted to a dynamic network case. Specifically, we focus on the SIS effective degree model as described in detail by Lindquist *et al.* [83] and also proposed by Marceau *et al.* [85] independently. Gleeson [39] later uses this same modelling framework and demonstrates that the effective degree formulation can be used to model other binary-state dynamics such as Glauber spin dynamics and shows that the ODE model can be used to carry out linear stability type analysis.

Whereas both Lindquist *et al.* [83] and Gleeson [39] confine themselves to modelling on static contact networks, Marceau *et al.* [85] uses this same improved effective degree formalism to explore SIS disease dynamics on adaptive networks. In this model the number of links in the network is fixed but the susceptible individuals can replace links to infectious neighbours with links to other randomly chosen susceptible individuals, as originally proposed by Gross *et al.* [45]. Our proposed model also uses SIS type epidemics on dynamic networks, but, unlike in Marceau *et al.* [85], our model allows for the random activation and deletion of links over time. As such not only the network topology will evolve and change over time, but also the number of links. This modified dynamic effective degree model is also governed by a closed set of ODEs, which is then solved and compared to results from individual based simulations and its ability to accurately predict the epidemic threshold over a range of parameters is investigated. We also derive an analytical R_0 calculation that describes the stability of the disease-free equilibrium and we discuss the limitations of such a calculation in the light of having a dynamically active and evolving contact network.

4.3 The model

Linquist *et al.* [83], who work in the mathematical biology community, and Marceau *et al.* [85] and Gleeson [39], who both work in the physics community,

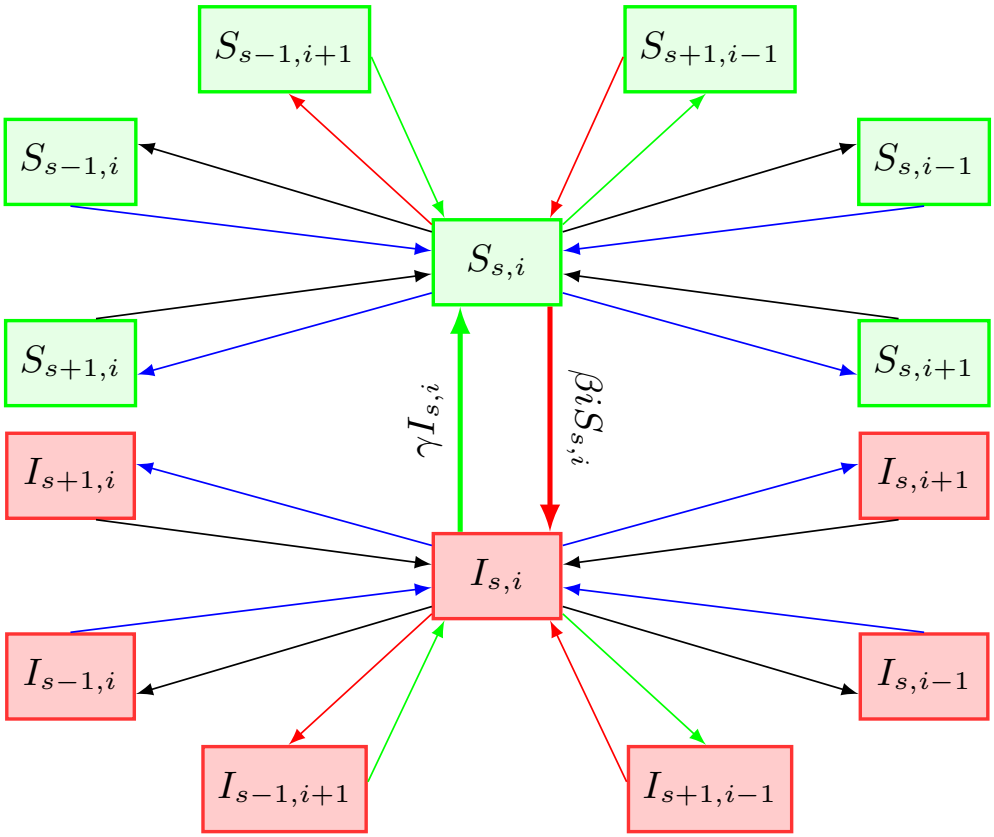

Figure 4.1: Flow chart showing transitions in the dynamic SIS effective degree model. The directed red (gray), green (light gray), blue (dark gray) and black lines represent changes in state of an individual via infection, recovery, link creation and link deletion respectively. The thick lines represent changes to the individual, and thin lines represent changes to that individual's immediate neighbourhood. In relation to nodes of type $X_{si}, X \in \{S, I\}$, infection of neighbours occurs at rate sG_X, recovery of neighbours at rate γi, creation of a susceptible (infectious) link at rate $\alpha(M-(s+i))P_{S(I)}$ and deletion of a susceptible (infectious) link at rate $\omega s(i)$, where:
$G_S = \beta\frac{\sum_{k=1}^{M}\sum_{j+l=k} jlS_{jl}}{\sum_{k=1}^{M}\sum_{j+l=k} jS_{jl}}$, $G_I = \beta\frac{\sum_{k=1}^{M}\sum_{j+l=k} l^2S_{jl}}{\sum_{k=1}^{M}\sum_{j+l=k} jI_{jl}}$, $P_X = \frac{\sum_{k=0}^{M}\sum_{j+l=k}(M-(j+l))X_{jl}}{\sum_{k=0}^{M}\sum_{j+l=k}(M-(j+l))(S_{jl}+I_{jl})}$.

use different notation to describe the same modelling framework. However, in both cases the resulting models not only categorize the disease state of each individual as susceptible (S) or infected (I) but also describes the state of their immediate neighbourhood. This is achieved by keeping track of the number of susceptible and infected neighbours that belongs to a given node.

Marceau at al. [85] build upon the work on adaptive networks by Gross *et al.* [45] to construct a model that not only describes individuals infecting

their neighbours and recovering, but also allows susceptible individuals to replace links to infectious neighbours with links to individuals chosen randomly from the susceptible population. This re-wiring process ensures that even while the topologies of local neighbourhoods are evolving over time, the number of links in the whole population remains constant. This process is captured by introducing $S_{kl}(t)$ and $I_{kl}(t)$ as the number of nodes of total degree k and infectious degree $l \leq k$ at time t. Population level counts of individuals, pairs and triples can be easily obtained by using the explicit information about the state of each neighbourhood, and summing over all possible values of k and l. For example:

$$S = \sum_{kl} S_{kl}, \qquad S_I = I_S = \sum_{kl} (k-l) I_{kl}, \qquad S_{SI} = \sum_{kl} (k-l) l S_{kl}, \tag{4.1}$$

which give us the number of susceptibles, (SI) pairs and (SSI) triples respectively. The full dynamics are given by a system of ODEs which is $\mathcal{O}(k_{max}^2)$, with k_{max} being the degree of the most highly connected node or nodes, as follows:

$$\begin{aligned}
\dot{S_{kl}} &= \alpha I_{kl} - \beta l S_{kl} + \alpha[(l+1)S_{k(l+1)} - l S_{kl}] + \beta \frac{S_{SI}}{S_S}[(k-l+1)S_{k(l-i)} \\
&\quad -(k-l)S_{kl}] + \gamma[(l+1)S_{k(l+1)} - l S_{kl}] + \gamma \frac{S_I}{S}[S_{(k-1)l} - S_{kl}], \\
\dot{I_{kl}} &= -\alpha I_{kl} + \beta l S_{kl} + \alpha[(l+1)I_{k(l+1)} - l I_{kl}] + \beta \left(1 + \frac{S_{II}}{S_I}\right)[(k-l+1)I_{k(l-i)} \\
&\quad -(k-l)I_{kl}] + \gamma[(k-l+1)I_{(k+1)l} - (k-l)I_{kl}] + \gamma \frac{S_I}{S}[S_{(k-1)l} - S_{kl}],
\end{aligned}$$

where in this case Marceau [85] has used α to be the per-node recovery rate, β the per-link infection rate and γ the per-link rate at which (S, I) pairs are rewired to become (S, S) pairs. This is at odds with notation used thus far in this Thesis, where γ has been used as the rate of recovery. In addition, terms such as S, S_I, S_{SI} and so on, are calculated following Eqs. (4.1).

Gleeson [39] used this same modelling formalism, but for generalised binary-

state dynamics on a static network:

$$\begin{aligned}
\dot{s_{k,m}} &= -F_{k,m}s_{k,m} + R_{k,m}i_{k,m} - \beta^s(k-m)s_{k,m} \\
&\quad +\beta^s(k-m+1)s_{k,m-1} - \gamma^s m s_{k,m} + \gamma^s(m+1)s_{k,m+1}, \\
\dot{i_{k,m}} &= F_{k,m}s_{k,m} - R_{k,m}i_{k,m} - \beta^i(k-m)i_{k,m} \\
&\quad +\beta^i(k-m+1)i_{k,m-1} - \gamma^i m i_{k,m} + \gamma^i(m+1)i_{k,m+1},
\end{aligned}$$

where here F and R are general functions that describe the infection or recovery of a node, and β^x and γ^x, $x \in \{s, i\}$ describe the infection or recovery of an individuals neighbours. These rates are derived fully in Gleeson [39], as well as the closures implicit in approximating the rate of infection of a susceptible neighbour.

For the model we present in this chapter, however, we use the notation proposed by Lindquist *et al.* [83] to describe the same binary-state dynamics on a static network as did Glesson [39], however Lindquist at al. [83] have written their model specifically for SIS type epidemics.

In Linquist *et al.* [83] for example, S_{si} represents the number of susceptible individuals that have s susceptible and i infected neighbours. This gives rise to more states and equations than would be seen in a standard pairwise model, where equations are given at the population level for all types of singles and pairs [63]. For example if a S_{si} type node became infected via one of its i infectious neighbours, this individual would move to state I_{si} as only the status of the node itself is changing. However, if one of the i infected neighbours of an S_{si} type node recovered then the node would enter the $S_{s+1,i-1}$ class, whereas infection of one of the s neighbouring susceptible nodes moves the S_{si} type node into the $S_{s-1,i+1}$ class.

Lindquist *et al.* [83] defined γ to be the per node recovery rate, β the per link infection rate and M the maximum nodal degree of a network with N nodes.

They then derived the following system of $\sum_{k=1}^{M} 2(k+1) = M(M+3)$ equations:

$$\begin{aligned}
\dot{S_{si}} &= -\beta i S_{si} + \gamma I_{si} + \gamma[(i+1)S_{s-1,i+1} - iS_{si}] \qquad (4.2)\\
&\quad +\beta \frac{\sum_{k=1}^{M}\sum_{j+l=k} jlS_{jl}}{\sum_{k=1}^{M}\sum_{j+l=k} jS_{jl}}[(s+1)S_{s+1,i-1} - sS_{si}],\\
\dot{I_{si}} &= \beta i S_{si} - \gamma I_{si} + \gamma[(i+1)I_{s-1,i+1} - iI_{si}]] \qquad (4.3)\\
&\quad +\beta \frac{\sum_{k=1}^{M}\sum_{j+l=k} l^2 S_{jl}}{\sum_{k=1}^{M}\sum_{j+l=k} jI_{jl}}[(s+1)I_{s+1,i-1} - sI_{si}],
\end{aligned}$$

for $\{(s,i) : s,i \geq 0, 1 \leq k = s+i \leq M\}$. This is the SIS effective degree model for a *static* contact network.

In order to adapt this model to describe SIS dynamics on a *dynamic* contact network, we introduce two new parameters: ω, the per link deletion rate and α, the per non-link, or more precisely the per *potential* link creation rate. These rates could also be made to be link-type dependent, i.e. ω_{SI} would be the per SI link deletion rate. For the dynamic network cae, the system size will increase slightly from $M(M+3)$ to $\sum_{k=0}^{M} 2(k+1) = (M+1)(M+2)$ equations, to account for nodes of the type $X_{0,0}$ where $X \in \{S, I\}$. In the static case, these nodes were dynamically unimportant as they could neither infect nor become infected by other nodes. However in the dynamic model, they could connect to other nodes in the system and so enter states $X_{1,0}$ or $X_{0,1}$ depending on the state of the node with which they have just formed a new link.

When adding the terms that govern link creation and deletion to Eqs. (4.2) and (4.3) it is far simpler to construct the terms that govern deletion of existing links than those for the creation of new links. Links to nodes of type X_{si} where $X \in \{S, I\}$ are cut at a rate proportional to their degree, so individuals will leave X_{si} through link deletion at a rate $\omega(s+i)$ and will either enter the $X_{s-1,i}$ or $X_{s,i-1}$ classes depending on the state of the nodes to which they were previously connected. Similarly individuals can enter state X_{si} if they were in states $X_{s,i+1}$ or $X_{s+1,i}$ and a link to an infected or susceptible node was deleted, respectively.

When creating new links to nodes of type X_{si}, there are $M-(s+i)$ stubs remaining, so nodes will transition out of this state at a rate $\alpha(M-(s+i))$ and will either enter the $X_{s+1,i}$ or $X_{s,i+1}$ classes depending on the state of the node to which they have just connected. The rate at which nodes enter the X_{si} class from either $X_{s-1,i}$ or $X_{s,i-1}$ depends not only on the number of stubs still available in the node in question, but also on the probability that the newly created link attaches to a node of state S or I, respectively. So nodes enter X_{si} from $X_{s-1,i}$ at the rate $\alpha P_S(M-(s-1+i))$, and nodes enter X_{si} from $X_{s,i-1}$ at rate $\alpha P_I(M-(s+i-1))$, where $P_X = \frac{\sum_{k=0}^{M}\sum_{j+l=k}(M-(j+l))X_{jl}}{\sum_{k=0}^{M}\sum_{j+l=k}(M-(j+l))(S_{jl}+I_{jl})}, X \in \{S,I\}$ is the probability of picking an available stub belonging to nodes of type X where $X \in \{S,I\}$. The full set of transitions captured by this model is shown in Fig. 4.1.

The addition of these terms to Eqs. (4.2) and (4.3) transforms the SIS effective degree model for a static network into one that captures the spread of SIS type diseases on a dynamic contact network and is described by the following system of $(M+1)(M+2)$ equations:

$$\begin{aligned}
\dot{S_{si}} &= -\beta i S_{si} + \gamma I_{si} + \gamma[(i+1)S_{s-1,i+1} - iS_{si}] \\
&\quad +\beta\frac{\sum_{k=0}^{M}\sum_{j+l=k} jlS_{jl}}{\sum_{k=0}^{M}\sum_{j+l=k} jS_{jl}}[(s+1)S_{s+1,i-1} - sS_{si}] \\
&\quad -\omega[(s+i)S_{si} - (i+1)S_{s,i+1} - (s+1)S_{s+1,i}] \\
&\quad -\alpha(M-(s+i))S_{si} + \alpha(M-(s-1+i))P_S S_{s-1,i}, \\
&\quad +\alpha(M-(s+i-1))P_I S_{s,i-1}
\end{aligned} \tag{4.4}$$

$$\begin{aligned}
\dot{I_{si}} &= \beta i S_{si} - \gamma I_{si} + \gamma[(i+1)I_{s-1,i+1} - iI_{si}] \\
&\quad +\beta\frac{\sum_{k=1}^{M}\sum_{j+l=k} l^2 S_{jl}}{\sum_{k=1}^{M}\sum_{j+l=k} jI_{jl}}[(s+1)I_{s+1,i-1} - sI_{si}] \\
&\quad -\omega[(s+i)I_{si} - (i+1)I_{s,i+1} - (s+1)I_{s+1,i}] \\
&\quad -\alpha(M-(s+i))I_{si} + \alpha(M-(s-1+i))P_S I_{s-1,i} \\
&\quad +\alpha(M-(s+i-1))P_I I_{s,i-1},
\end{aligned} \tag{4.5}$$

for $\{(s,i) : s,i \geq 0, 0 \leq k = s+i \leq M\}$. This system is the *dynamic* SIS effective degree model.

The total number of links in the system at time t, $\Lambda(t)$, and potential links, $\Phi(t)$ can easily be calculated from the effective degree formulation as

$$\begin{aligned}
\Lambda(t) &= \sum_{k=0}^{M} \sum_{j+l=k} (j+l)(S_{jl} + I_{jl}), \\
\Phi(t) &= \sum_{k=0}^{M} \sum_{j+l=k} (M - (j+l)) (S_{jl} + I_{jl}) \\
&= MN - \Lambda(t),
\end{aligned}$$

with the mean nodal degree given by $\langle k(t) \rangle = \frac{\Lambda(t)}{N}$. At the equilibrium, $\alpha\Phi = \omega\Lambda$ which gives us the mean nodal degree at equilibrium to be:

$$\langle k \rangle^* = \frac{\alpha}{\alpha + \omega} M. \tag{4.6}$$

Note that Eq. (4.6) does not depend on the system size, N, but rather on the maximum nodal degree, M. This is important because in the static model, M is simply given by the node or nodes with the highest degree whilst in the dynamic case, however, M can be considered as a carrying capacity, whereby no node can have more than M links. This subtle but important difference means that in the dynamic case, M itself can be regarded as a parameter which controls the potential level of network saturation, and hence the network is locally constrained.

4.4 Calculating the disease threshold

For the static case, Lindquist *et al.* [83] used the next generation matrix approach [21] to calculate the disease threshold to be

$$\mathcal{R}_0 = \rho(FV^{-1}) = \frac{\beta}{\sum_{k=1}^{M} k S_{k,0}} \sum_{k=1}^{M} v_k^T V_k^{-1} u_k. \tag{4.7}$$

In this approach, Eqs. (4.4) and (4.5) are linearized at the disease-free equilibrium (DFE) and the Jacobian at the DFE is written as $F - V$. In this formulation, F accounts for transitions from disease-free states to disease states (in the static case only the transition from $S_{s,0}$ to $S_{s-1,1}$ needs to be considered) and V accounts for transitions between , and out of, different disease states. The spectral radius, ρ, the leading eigenvalue of FV^{-1}, gives R_0 and describes the stability of the DFE. If $R_0 < 1$ the DFE is stable and no epidemic will occur, but if $R_0 > 1$ the DFE is unstable and the infectious agent can spread through the population.

We can calculate F in the dynamic case by noting that the same $S_{s,0}$ to $S_{s-1,1}$ type transitions can still occur, but in addition nodes can enter the disease states by linking to an infected node, namely $S_{s,0}$ to $S_{s,1}$ transitions. If we introduce a subscript s to denote the static version of the next generation matrix, so the static version of F is called F_s and so on, we have

$$F_s = \frac{\beta}{\sum_{k=0}^{M} kS_{k,0}} \begin{bmatrix} u_{s_0} \\ u_{s_1} \\ \vdots \\ u_{s_M} \end{bmatrix} \begin{bmatrix} v_{s_0}^T & v_{s_1}^T & \dots & v_{s_M}^T \end{bmatrix}, \tag{4.8}$$

where u_{s_k} and v_{s_k} are $(2k+1)$ x 1 vectors. The u_{s_k} vectors have $kS_{k,0}$ as their first entry and zeros elsewhere and the v_{s_k} vectors have their first $(k-1)$ entries equal to $(k-1), 2(k-2), \dots, s(k-s), \dots, (k-1)$ and zeros elsewhere. This is almost identical to the F matrix constructed by Lindquist *et al.*, but is augmented by u_{s_0} and v_{s_0} to account for the new disease state, $I_{0,0}$, and the summation starts at $k = 0$ rather than $k = 1$.

We now introduce a new subscript d to describe the new transitions that are only possible in the dynamic model. Hence a new F matrix, F_d, is created, which

has exactly the same dimensions as F_s, and is given by

$$F_d = \frac{\alpha}{\sum_{k=0}^{M}(M-k)S_{k,0}} \begin{bmatrix} u_{d_0} \\ u_{d_1} \\ \vdots \\ u_{d_M} \end{bmatrix} \begin{bmatrix} v_{d_0}^T & v_{d_1}^T & \dots & v_{d_M}^T \end{bmatrix}. \tag{4.9}$$

Here, u_{d_k} is again a $(2k+1)$ x 1 vector with the first entry equal to $(M-(k-1))S_{k-1,0}$ and all other entries equal to zero. In the case where $k=0$, $u_{d_0}=(0)$. In addition, v_{d_k} is the same size as u_{d_k} and the first k entries are equal to zero, with the remaining $k+1$ entries equal to $M-k$. The final F matrix that captures all the possible transitions in the dynamic effective degree model is found by taking a linear sum of the two, namely $F = F_s + F_d$.

As with the static case, the V matrix is constructed through careful book-keeping, which can be done through iterative routines. In the static case, as the nodes have fixed degree, V_s is a block diagonal matrix with $V_s = V_{s_1} \oplus V_{s_2} \oplus ... \oplus V_{s_M}$, as described by Lindquist *et al.* [83]. For the dynamic model, V_d will be a block tri-diagonal matrix, as state transitions can now also occur by nodes gaining or losing a link. In addition, the extra disease state $I_{0,0}$ needs to be considered, and V will now also depend upon α and ω as well as β and γ. Once $F = F_s + F_d$ and $V = V_d$ are constructed, the leading eigenvalue or R_0 is computed numerically.

Intermezzo - Recipe for constructing the V matrix

Below is a descriptive account of how to construct the V matrix required in the R_0 calculation described above. Unless the reader intends to reproduce the results in this chapter, the reader can safely leave this Intermezzo and move onto the next section without any loss of clarity.

For a given M, the leading block diagonal on V will be a concatenation of $M+1$ sub-matrices, V_k for $k = 0 : M$. Each has dimensions $2k+1$ and contain all

the transitions included in V for the static case and, in addition, it will include new dynamic terms on the leading diagonal that govern transitions out of a state by link creation or deletion.

In order to keep track of the various transitions that can occur within and out of disease states, it is important to have a structured lexicographical approach to ordering the different states. Noting that states of the form $S_{k,0}$ are not disease states, the ordering of states for each $k = 0 : M$ is $(S_{k-1,1}, S_{k-2,2}, ..., S_{0,k}, I_{k,0}, I_{k-1,1}, ..., I_{0,k})$.

Each sub-matrix V_k can be constructed from four further parts that can be thought of as containing, from top left clockwise, $S_k \to S_k$, $I_k \to S_k$, $I_k \to I_k$ and $S_k \to I_k$ type transitions respectively. It should be noted that for the case where $k = 0$, there are no susceptible states as $S_{0,0}$ is not a disease state.

The leading diagonal of the V_k contains the rate of transitions out of a particular state. These entries are all positive and contain β, γ, α and ω. The link creation and deletion terms are the same for both $S \to S$ and $I \to I$ transitions and hence each entry on the leading diagonal of the V_k has a contribution $(M - k)\alpha + k\omega$. The recovery rates are proportional to the infectious degree of a state and hence contributes $j\gamma$, with $j = 1 : k$ for $S \to S$ and $j = 1 : k + 1$ for $I \to I$. When considering infection rates, it should be noted that at the DFE only within pair infections are possible, and we are assuming an entirely susceptible population. Hence the infections rates are proportional to the infectious degree for $S \to S$ and contribute $j\beta$ for $j = 1 : k$, and are proportional to the susceptible degree for $I \to I$ and contribute $k - (j - 1)$ for $j = 1 : k + 1$. These are all the ways transitions out of a particular state can occur. All other transitions described below are for transitions into a state and are therefore all negative.

To finish constructing the $S \to S$ and $I \to I$ parts of the V_k, entering a state via infection and recovery of a neighbour must be considered. The upper off-diagonals govern recovery and the lower off-diagonals infection. The recovery

rates for $S \to S$ are $-(j+1)\gamma$ for $j = 1 : k-1$ and for $I \to I$ they are $-j\gamma$ for $j = 1 : k$. The infection rates are all zero for $S \to S$ as at the DFE there are no further infectious neighbours of a particular node's own susceptible neighbours. For $I \to I$, only within pair infection is possible for the same reason, and hence the infection rate is proportional to the node's infectious degree and is given by $-(k-j+1)\beta$ for $j = 1 : k$.

Now all possible $S \to S$ and $I \to I$ transitions have been accounted for, the $S \to I$ and $I \to S$ sections of the V_k sub-matrices need to be constructed. Clearly transitions of this type can only occur by the infection and recovery respectively of the node itself. At the DFE, $S \to I$ transitions are proportional to a node's infectious degree so on the diagonal starting from position $(2, 1)$ the rates are $-j\beta$ for $j = 1 : k$. On the other hand for $I \to S$ transitions, as recovery is neighbourhood independent the rates are all simply $-\gamma$ on the diagonal starting at position $(1, 2)$.

Once each of the four components of the individual V_k are joined, and then each of the V_k concatenated, the entire leading block diagonal of V has been constructed. The upper and lower block diagonals govern transitions into states via changes in the network structure rather than changes in the disease states of individuals.

The upper block diagonal deals with link deletion and hence a change in degree of $k \to k-1$. It is constructed by a concatenation of M sub-matrices, called V_{ω_k}, with dimensions $(2(k-1)+1)$x$(2k+1)$. Once again these sub-matrices can be split into four parts, but as the disease state of the node cannot change only $S \to S$ and $I \to I$ will be non-zero. Each state $X_{a,b}$, where $X \in S, I$ and $a + b = k - 1$, can be entered in two ways, from $X_{a+1,b}$ or $X_{a,b+1}$, where $a+b+1 = k$. For $S \to S$, these are described by two diagonals, firstly capturing deletion of a susceptible link and starting from position $(1, 1)$ with entries $-(k-j)\omega$ for $j = 1 : k-1$ and secondly capturing deletion of an infectious link and starting from position

$(1,2)$ with entries $-(j+1)\omega$ for $j = 1 : k-1$. Similarly $I \to I$ has two non-zero diagonals, starting at $(1,1)$ with entries $-(k-j+1)\omega$ for $j = 1 : k$.

The lower block diagonal deals with link creation and hence a change in degree of $k \to k+1$. It is constructed by a concatenation of M sub-matrices, called V_{α_k}, with dimensions $(2k+1)$x$(2(k+1)+1)$. Once again only $S \to S$ and $I \to I$ need be considered. At the DFE only $X_{a,b} \to X_{a+1,b}$ type transitions need to be accounted for, and furthermore the are always $M-k$ stubs available. For both $S \to S$ and $I \to I$, there is one non-zero diagonal starting at position $(1,1)$ with entries always $-(M-k)\alpha$.

This completes the construction of V, and hence $R_0 = \rho(FV^{-1})$ can be rapidly calculated for SIS type epidemics on a dynamic contact network with random link creation and deletion.

End of Intermezzo

4.5 Results

As shown in Fig. 4.2, the ODEs given by Eqs. (4.4) and (4.5) closely capture the time evolution of an epidemic as predicted by stochastic simulations. The only parameter that is varied in Fig. 4.2 is M, and it is interesting to note the effect it has on the evolution of the disease. As per Eq. (4.6), the mean nodal degree at equilibrium is dependent on M, and hence, given the same initial network configuration and values of α and ω, the network either loses or gains links as the system evolves. Thus varying the carrying capacity alone leads to different outcomes depending on whether the network can reach a level of connectedness that allows an epidemic to spread and become established. Allowing M to become an active model parameter that is able to control the outcome of an epidemic has potentially interesting real world implications. The number of contacts per person is a natural, countable property unlike the other model parameters, such

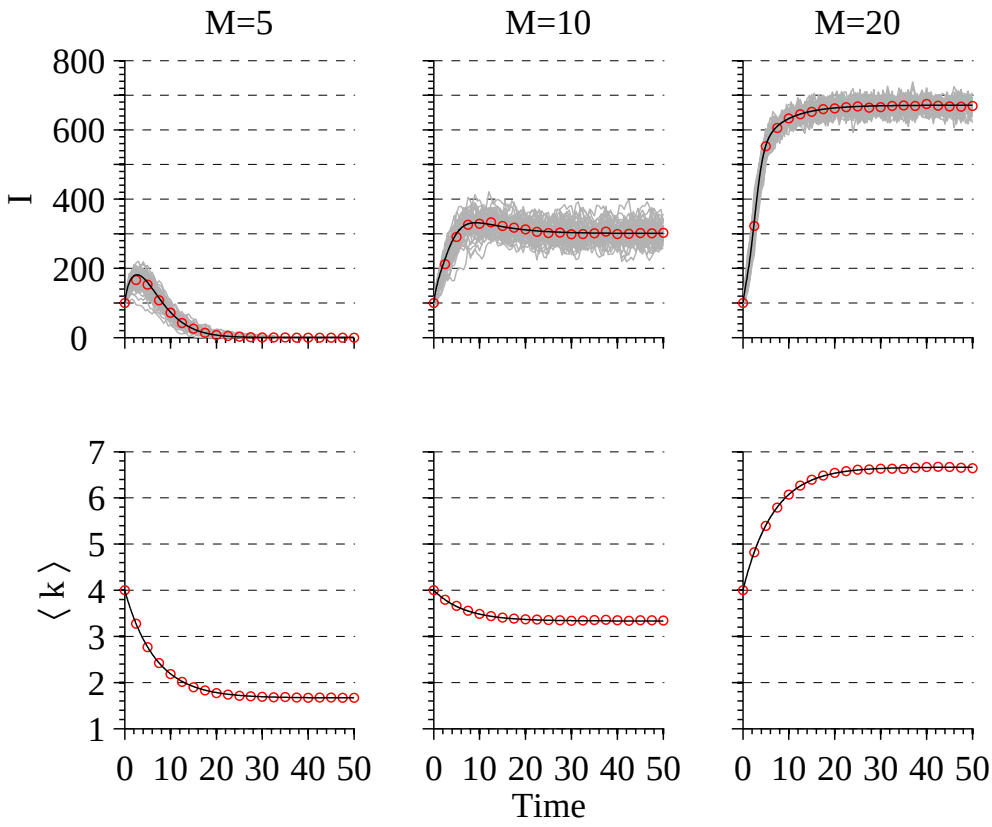

Figure 4.2: Time evolution of $I(t) = \sum_{k=0}^{M} \sum_{j+l=k} I_{jl}(t)$ and $\langle k \rangle(t) = \frac{\Lambda(t)}{N}$ for three different values of M. Results from the ODE are given by solid lines and those from simulation by points. In all cases $N = 1000$, $I_0 = 100$, $\alpha = 0.05$, $\omega = 0.1$, $\beta = 0.5$ and $\gamma = 1$. The initial network is a regular random network with $k = 4$. In each case, mean values from the stochastic simulations were found by averaging over 100 repetitions, with the individual realisations plotted in grey.

as ω, which are more difficult to infer. Therefore local constraints that limit the maximum number of contacts per person could be potentially used as a metric when promoting safe behaviour at a population level in the event of an outbreak or other public health crisis.

In Fig. 4.3, for a given value of α, M and β, the epidemic threshold has been calculated from the ODEs in terms of ω and compared to that predicted by simulations. The agreement is excellent and this is strong evidence that the dynamic effective degree model accurately captures the evolution of an epidemic on a network with random link creation and deletion. When considering the (β, ω) parameter space used for the threshold plot in Fig. 4.3, there are three

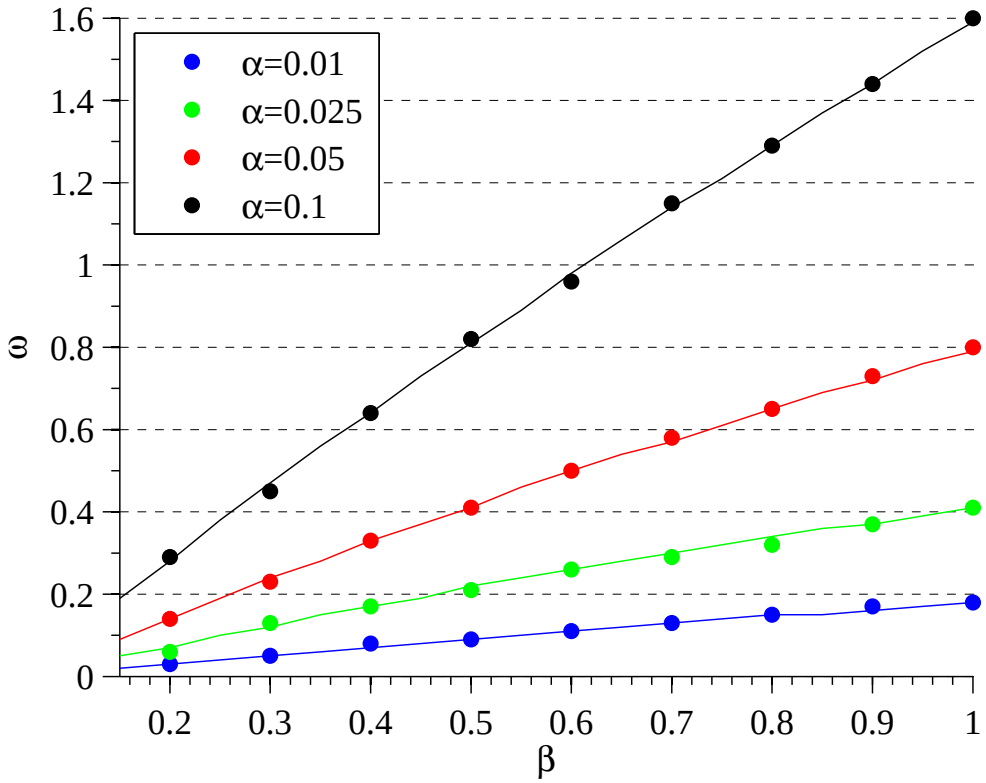

Figure 4.3: Epidemic threshold plot in the (β, ω) parameter space for four distinct values of α. Above the lines/points represents parameter space that leaves the system at the DFE, and below the lines/points represents parameter space in which the disease invades the population. Results from the ODE are given by solid lines and those from simulation by solid points. In each case, $N = 1000$, $I_0 = 10$, $M = 20$ and $\gamma = 1$. The initial network is a regular random network with $k = 4$.

distinct regions that are worth noting. Firstly, given an initial starting network, it is possible to calculate the threshold value of β in the static network case. For the regular random network with $k = 4$ used here, that value is $\beta^* \approx 0.36$. For values of $\beta < 0.36$, the relative time scales of disease and network evolution are crucial in determining whether or not an epidemic will occur. In this situation, the network needs to quickly evolve to become more densely connected in order for there to be an outbreak. The second area of interest is when the disease is highly infectious and as a result requires a high value of ω to drive the epidemic below threshold. Indeed, if the disease parameters β and γ are fixed then the

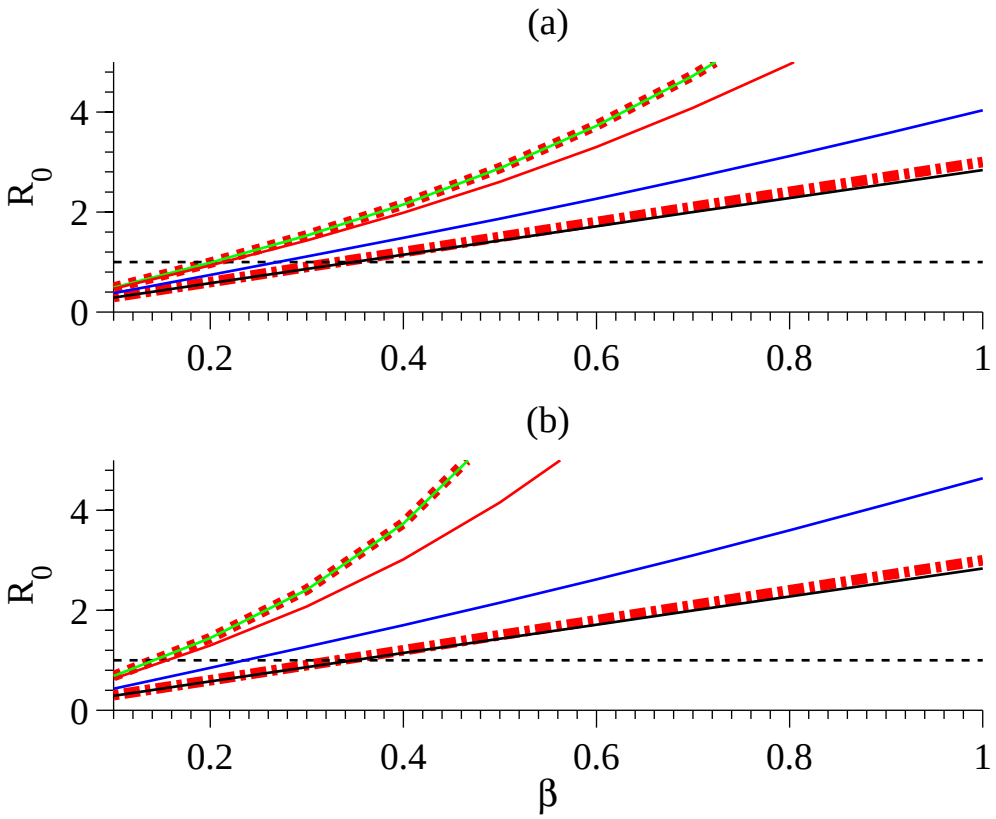

Figure 4.4: R_0 for a range of values of β and α, with fixed parameters $\gamma = 1$, $M = 20$ and $\langle k \rangle^* = 3$ for (thin solid lines, in order from top to bottom) $\alpha = 10^{-4}$ (green), $\alpha = 10^{-2}$ (red), $\alpha = 10^{-1}$ (blue) and $\alpha = 10$ (black). In (a) the initial network is a regular random network with $k = 6$ and in (b) the initial degree distribution is negative binomial with $\langle k \rangle = 6$ and $\sigma^2 = 12$. In each case, $\omega = \alpha \frac{M - \langle k \rangle^*}{\langle k \rangle^*}$. The thick short-dashed red line is the theoretical value of R_0 for a static network, and the thick red dash-dotted line is the mean field limit $R_0 = \frac{\beta}{\gamma} \langle k \rangle^*$.

only way of affecting the outcome of an epidemic is through changing the network structure, i.e. reducing the number of links or the variance. Hence, for a fixed α and M, a value of β can be chosen large enough so that the minimum value of ω needed to reduce the connectivity of the network sufficiently to stop an outbreak (see Fig. 4.3), gives $\langle k \rangle^* < 2$ as can be calculated from Eq. (4.6). If a network has $\langle k \rangle^* < 2$ then it becomes fragmented, with many nodes becoming unconnected. In these situations, the value ω needed to prevent an epidemic virtually destroys the network. In terms of real world implications, a large value of ω could correspond to a situation of strict quarantine and curfew whereby links between individuals

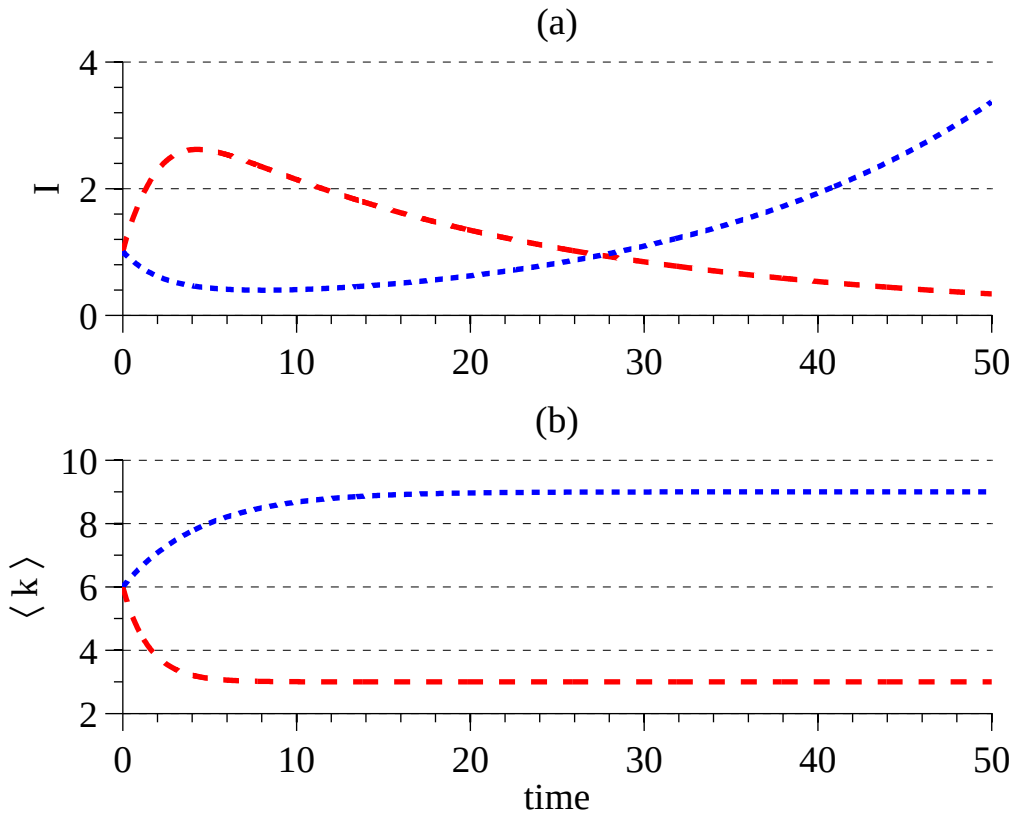

Figure 4.5: Time evolution of I and $\langle k \rangle$ with $\gamma = 1$, $M = 20$, $\alpha = 0.1$, $\omega = \alpha \frac{M - \langle k \rangle^*}{\langle k \rangle^*}$ and an initial regular random network with $k = 6$. The two cases illustrated above correspond to: $\langle k \rangle^* = 3$ and $\beta = 0.35$, giving $R_0 \approx 1.29$ (red long-dashed line) and $\langle k \rangle^* = 9$ and $\beta = 0.125$, giving $R_0 \approx 0.77$ (blue short-dashed line).

are kept to a minimum. In between these two cases lies a region within which an epidemic would take hold naturally, given the initial network, but which can be prevented by a value of ω that leaves the network well connected.

In Fig. 4.4, we show analytical values of R_0 for a range of values of β and α. It is worth noting that two limiting cases are recovered when the timescale of the network dynamics is fast and slow relative to the timescale of the disease dynamics. The thick short-dashed red line shows R_0 calculated for a static network, as proposed by Lindquist *et al.* [83] and given in Eq. (4.7), and this is exactly followed by results from our dynamic R_0 calculation when the network dynamics are set to be much slower than the disease dynamics. The other extreme is shown

by the thick dash-dotted red line, and is the value of R_0 that results form the classic mean-field calculation $R_0 = \frac{\langle k \rangle \beta}{\gamma}$. The time evolution of $\langle k \rangle$ is given by $\dot{\langle k \rangle} = \alpha(M - \langle k \rangle) - \omega \langle k \rangle$ but, when the network dynamics is fast, the equilibrium network distribution, and hence $\langle k \rangle^*$, is approached much quicker than the epidemic timescale and hence a value of $\langle k \rangle = \langle k \rangle^*$ as given by Eq. (4.6) can be used. This limit is closely matched by results from our dynamic R_0 calculation when the network dynamics are rapid compared to disease transmission as shown in Fig. 4.4.

Although Fig. 4.4 demonstrates the accuracy of our analytical R_0 calculation, Fig. 4.5 highlights two example cases where the long term epidemic outcomes are the opposite of what is predicted by R_0. In the cases $R_0 < 1$ (blue short-dashed curve) and $R_0 > 1$ (red long-dashed curve) the system settles to an endemic and to a disease free equilibrium respectively, due to the different ways the networks evolve. Given that R_0 is based on a local stability analysis, it can only incorporate the immediate next-generation effects of random link activation and deletion, and cannot account for long term changes to the network structure. It is well established in the literature (see, for example [21, 119]) that R_0 is of limited value when used as a predictor, and even for static networks needs to be used with care. Our results add weight to this argument, and we show that when dealing with diseases spreading through dynamic contact networks the use of R_0 as any kind of predictor on long term disease evolution should be met with some degree of caution.

4.6 Discussion

In summary, this chapter has proposed an effective degree model for epidemics on dynamic networks with random link activation and deletion, where activation is locally constrained. We have shown that this model agrees extremely well with results obtained from stochastic simulations, and as such can reliably be

used for the analytical and semi-analytical study of coupled disease and network dynamics. We have shown how a local constraint limiting the number of contacts per individual can be used to control and prevent the outbreak of an epidemic in this dynamic model. We have also proposed a next-generation based calculation of R_0, but also demonstrated the limited value of threshold stability analysis in predicting the evolution of a disease in a dynamic contact network. In future work, this model can be adapted and extended to account for individuals cutting and creating links with knowledge of the state of others in the population, i.e., link-type dependent network dynamics. This two-way feedback will lead to more sophisticated network properties such as degree correlations, high clustering or even network fragmentation. This is in contrast with the model proposed in this Chapter, in which the network remains Poisson-like due to the random, state-independent link activation and deletion. In such cases ODE models need to be used with care, making sure that the agreement with simulations remains valid. Besides modelling epidemics, this framework could also be used to study the spread of information, beliefs and new ideas within populations, and as such could have implications across a wide range of disciplines beyond the mathematical biology and physics communities.

Chapter 5

Epidemic control through behavioural change: the effect of information on disease spread

5.1 Introduction

When confronted by a disease outbreak, human beings will, consciously or subconsciously, become more aware of the potential new risks they face. Indeed, individual behavioural change forms a key part of any public health campaign. From leaflets found in a local clinic all the way up to national and global multimedia campaigns, efforts are put into effect with the goal of changing people's behaviour in the presence of an infectious disease thus reducing the overall impact of an epidemic [30, 36, 121].

When disease spread through relatively well defined contact networks, as in the case of sexually transmitted diseases (STDs), contact tracing data collected at clinics can be used to identify individuals with a prominent structural role in the network who can then be approached or screened preferentially. Similar approaches can be taken when considering the dissemination of information. Well-

connected individuals can be approached and seeded with information in the hope that they will diffuse this through their social network [82, 121].

Besides centrally organised campaigns, research suggest that people's decisions on whether to adopt a change in behaviour are influenced by others in their personal network of contacts [77, 121]. This peer-to-peer effect has been observed and utilized in electronic marketing [40, 81, 100] and when modelling the diffusion of innovations [73, 87]. In addition to information flowing along our social network of contacts, it is possible to pick up information from 'random' encounters, such as overhearing a conversation on a bus. These sort of random encounters lend themselves to being modelled as mean-field type transmissions [25].

Besides mass-media, peer-to-peer and random contacts, a fourth route to awareness is via direct, personal experience: once an infected individual becomes symptomatic, they are inevitably aware of the disease and are likely to seek medical advice.

A major motivation for the incorporation of behavioral change models in infectious disease studies was the AIDS epidemic from the early 1980s and onwards. The main driver for this was the realisation that the growth of STDs, including AIDS/HIV, could be understood as a consequence of lifestyles choices and subjective risk perception motivated by individual attitudes and beliefs [13, 15]. This field of work is still very prominent, and is of particular interest when considering the explosive nature of the AIDS epidemic in Africa [42, 59, 106]. In this situation, where money and resources are scarce, control via public awareness and behaviour modification offers a potentially very effective and cost efficient method of control.

In the past few years, a number of compartmental models have been proposed that incorporate various aspects of the spread of a disease and human behavioral response to the growing epidemic. Broadly speaking, most of the research can be classified into one of two categories. In the first class are models that deal

with vaccine-preventable diseases [11, 12, 22, 98]. In this case, a natural question is whether (and to what extent) individuals' attitudes to vaccination can affect the dynamics of the disease. In cases of voluntarily vaccination, without further incentives, as vaccination coverage increases the risk of infection decreases due to herd immunity. At the same time any real or imaginary risks from the vaccine itself remain in effect. This effect may motivate individuals to act in self-interest and avoid vaccination even if the risks of the vaccine are very small. Consequently disease eradication may become very difficult [98].

The second class of models deal with behavioral change in response to an epidemic outbreak [29, 34, 35, 74, 75, 102]. Our model belongs in the latter class. Here individuals may alter the course of an epidemic by taking disease specific risk-reducing measures such as washing hands or using condoms. In modeling terms, this is usually represented as subdivisions of a population into classes differentiated by degrees of risk exposure, a body of work reviewed in [36].

In this Chapter, we propose a model that allows individuals of any disease state to belong to either an 'responsive' or 'non-responsive' sub-state, with responsive individuals having a lower risk of infection due to changes in their behaviour. We allow for multiple sources of information generation and transmission, explore the relative effectiveness of each of these and consider the implications for effective public health decision making.

5.2 Model

Following on from Kiss *et al.* [74], the population is divided into five different classes that specify the individual's status with respect to disease and information. These are: susceptible non-responsive (S_{nr}), susceptible responsive (S_r), infected non-responsive (I_{nr}), infected responsive (I_r) and in treatment (T). The term *responsiveness* emphasizes that the willingness to act or respond to the available information is key in trying to avoid infection or halting further spread.

transition	rate	contact	type
$I_{nr} + S_{nr} \to 2I_{nr}$	τ	G_d	infection
$I_{nr} + S_r \to I_{nr} + I_r$	$\sigma_s\tau$	G_d	infection
$I_r + S_{nr} \to I_r + I_{nr}$	$\sigma_i\tau$	G_d	infection
$I_r + S_r \to 2I_r$	$\sigma_s\sigma_i\tau$	G_d	infection
$I_{nr} \to T$	γ	independent	infection
$I_r \to T$	$\sigma_r\gamma$	independent	infection
$T \to S_{nr}$	rp	independent	infection
$T \to S_r$	$r(1-p)$	independent	infection
$X_r + Y_{nr} \to X_r + Y_r$	α_X	G_i	information
$X_{nr} \to X_r$	$\delta_X G_X([I_{nr}],[I_r])$	independent	information
$I_{nr} \to I_r$	ω	independent	information
$X_r \to X_{nr}$	d_X	independent	information

Table 5.1: All transitions allowed by the coupled infection/information system, where $X, Y \in \{S, I\}$ with individuals in treatment acting as members of the responsive classes (i.e. $X_r \in \{S_r, I_r, T\}$). Individuals in the treatment class return to being susceptible non-responsive and responsive at rate pr and $r(1-p)$ with $0 \leq p \leq 1$, respectively. The reduced susceptibility, infectivity and faster recovery, as a result of acting on information, is captured by the discount factors $\sigma_s, \sigma_i \in (0, 1]$ and $\sigma_r > 1$. The function $G_X([I_{nr}],[I_r])$ maps the prevalence of infection to the unit interval and is subsequently multiplied by the constant rate δ_X. This form models the saturating effect of media on individual behavioral response.

The important ingredients of the model relate to the *generation* and *transmission* of information as well as the *benefits of possessing and responding* to information. In the current model, information or responsiveness about the disease is generated in three ways: **(a)** $I_{nr} \to I_r$ as a result of symptoms, **(b)** $I_x \to T$, where $x \in \{nr, r\}$, as a result of being diagnosed and moving to the treatment class and **(c)** $X_{nr} \to X_r$, where $X \in \{S, I\}$ either as a result of global information transmission, or from local neighbourhood contact with other 'aware' individuals. While information dissemination locally represents the simple interaction of individuals where they can engage in discussions about an ongoing outbreak or diseases in general, global information transmission is used to model the effect of mass-media campaigns which act as a single-source of information with its strength and duration often linked to the prevalence of infection in the population. This is not an exhaustive list of mechanisms that could account for information generation. For

example, a mean-field form of transmission across randomly generated links could be introduced to model the effect of random encounters or overhearing strangers' conversations. Many of these different mechanisms of information generation and transmission can be easily linked to various ways in which information is disseminated in real-life.

It is natural to also incorporate the possibility for loss of responsiveness, consequently every X_r individual will transition to the X_{nr} class at a constant rate d_X, where $X \in \{S, I\}$. Note that this form is general enough that it could also model an individual's inability or refusal to act on information. Alternatively, as suggested in [74], the rate of information loss can be encoded as a decreasing function of the prevalence, a form that we do not explore here. The principal benefits of being informed and responding to the information can translate into reduced susceptibility, reduced infectivity and/or faster recovery if infected. The full suite of possible transitions are given in Table 5.1, and the model proposed by Kiss *et al.* [74] is described by the following system of ODEs:

$$\begin{aligned}
[\dot{S_{nr}}] &= -\beta^d([I_{nr}] + \sigma_i[I_r])[S_{nr}]/N - \beta^i([S_r] + [I_r] + [T])[S_{nr}]/N \\
&\quad -G_s([I_{nr}], [I_r])[S_{nr}] + d_s[S_r] + pr[T], \qquad (5.1) \\
[\dot{S_r}] &= -\beta^d\sigma_s([I_{nr}] + \sigma_i[I_r])[S_r]/N + \beta^i([S_r] + [I_r] + [T])[S_{nr}]/N \\
&\quad +G_s([I_{nr}], [I_r])[S_{nr}] - d_s[S_r] + (1-p)r[T], \qquad (5.2) \\
[\dot{I_{nr}}] &= \beta^d([I_{nr}] + \sigma_i[I_r])[S_{nr}]/N - \beta^i([S_r] + [I_r] + [T])[I_{nr}]/N \\
&\quad -G_i([I_{nr}], [I_r])[I_{nr}] + d_i[S_r] - \gamma[I_{nr}], \qquad (5.3) \\
[\dot{I_r}] &= \beta^d\sigma_s([I_{nr}] + \sigma_i[I_r])[S_r]/N + \beta^i([S_r] + [I_r] + [T])[I_{nr}]/N \\
&\quad -G_i([I_{nr}], [I_r])[I_{nr}] - d_i[S_r] - \gamma\sigma_r[I_{nr}], \qquad (5.4) \\
[\dot{T}] &= \gamma[I_{nr}] + \gamma\sigma_r[I_r] - r[T], \qquad (5.5)
\end{aligned}$$

where here β^x, $x \in \{d, i\}$ is the number of infectious contacts an individual has per unit time, and the superscripts d and i represent contacts that transmit disease

or information, respectively.

This model incorporates multiple ways that information can be generated and transmitted, and Kiss *et al.* show that there are three potential long-term model outcomes: **(a)** a trivial disease-free steady state, with the whole population in the S_{nr} class, **(b)** a non-trivial disease-free steady state, where a finite proportion of the population are in the S_r class, and **(c)** an endemic state, where individuals can be infected, aware or both. The model described by Kiss *et al.* is constructed using a random mixing assumption, as can be seen in the term $\beta^d[I_{nr}][S_{nr}]/N$, for example, and hence contact between individuals is random and no information about local network structures is included in the model. In this chapter, we take the system of ODEs given in Eqs. (5.1 - 5.5) and extend it to a pairwise model that retains information about the state of pairs of individuals, thus relaxing the assumption of random mixing somewhat. This allows us to not only consider the effect of various routes of information generation on the size of a potential epidemic, but also to investigate the effects of information on the network structure, and to examine, for example, how responsive individuals are distributed amongst the population.

5.2.1 Full system of ODEs

Extending Eqs. (5.1 - 5.5) and taking account of the full suite of transitions given in Table 5.1, gives the following pairwise model:

$$\begin{aligned}
[\dot{S_{nr}}] &= -\tau[S_{nr}I_{nr}] - \tau\sigma_i[S_{nr}I_r] + pr[T] - \lambda_C\alpha_s([S_{nr}S_r] + [S_{nr}I_r] + [S_{nr}T]) \\
&- \lambda_G G_s([I_{nr}],[I_r])[S_{nr}] + d_s[S_r], \qquad (5.6)
\end{aligned}$$

$$\begin{aligned}
[\dot{S_r}] &= -\tau\sigma_s[S_rI_{nr}] - \tau\sigma_i\sigma_s[S_rI_r] + (1-p)r[T] + \lambda_C\alpha_s([S_{nr}S_r] + [S_{nr}I_r] + [S_{nr}T]) \\
&+ \lambda_G G_s([I_{nr}],[I_r])[S_{nr}] - d_s[S_r], \qquad (5.7)
\end{aligned}$$

$$
\begin{aligned}
[\dot{I_{nr}}] &= +\tau[S_{nr}I_{nr}] + \tau\sigma_i[S_{nr}I_r] - \gamma[I_{nr}] - \lambda_C\alpha_i([I_{nr}S_r] + [I_{nr}I_r] + [I_{nr}T]) \qquad (5.8)\\
&- \lambda_G G_i([I_{nr}],[I_r])[I_{nr}] + d_i[I_r] - \omega[I_{nr}],
\end{aligned}
$$

$$
\begin{aligned}
[\dot{I_r}] &= +\tau\sigma_s[S_rI_{nr}] + \tau\sigma_i\sigma_s[S_rI_r] - \gamma\sigma_r[I_r] + \lambda_C\alpha_i([I_{nr}S_r] + [I_{nr}I_r] + [I_{nr}T])\\
&+ \lambda_G G_i([I_{nr}],[I_r])[I_{nr}] - d_i[I_r] + \omega[I_{nr}], \qquad (5.9)
\end{aligned}
$$

$$
[\dot{T}] = +\gamma[I_{nr}] + \gamma\sigma_r[I_r] - r[T], \qquad (5.10)
$$

$$
\begin{aligned}
[S_{nr}\dot{S_{nr}}] &= -2\tau[S_{nr}S_{nr}I_{nr}] - 2\tau\sigma_i[S_{nr}S_{nr}I_r] + 2pr[S_{nr}T] + 2d_s[S_{nr}S_r] \qquad (5.11)\\
&- 2\lambda_C\alpha_s([S_{nr}S_{nr}S_r] + [S_{nr}S_{nr}I_r] + [S_{nr}S_{nr}T]) - 2\lambda_G G_s([I_{nr}],[I_r])[S_{nr}S_{nr}],
\end{aligned}
$$

$$
\begin{aligned}
[S_{nr}\dot{S_r}] &= -\tau\sigma_s[S_{nr}S_rI_{nr}] - \tau\sigma_i\sigma_s[S_{nr}S_rI_r] - \tau[I_{nr}S_{nr}S_r] - \tau\sigma_i[I_rS_{nr}S_r]\\
&+ pr[TS_r] + (1-p)r[S_{nr}T] + \lambda_C\alpha_s([S_{nr}S_{nr}S_r] + [S_{nr}S_{nr}I_r] + [S_{nr}S_{nr}T])\\
&+ \lambda_G G_s([I_{nr}],[I_r])[S_{nr}S_{nr}] - \lambda_C\alpha_s([S_rS_{nr}S_r] + [I_rS_{nr}S_r] + [TS_{nr}S_r])\\
&- -\lambda_G G_s([I_{nr}],[I_r])[S_{nr}S_r] - d_s[S_{nr}S_r] + d_s[S_rS_r] - \lambda_C\alpha_s[S_{nr}S_r], \qquad (5.12)
\end{aligned}
$$

$$
\begin{aligned}
[S_r\dot{S_r}] &= -2\tau\sigma_s[S_rS_rI_{nr}] - 2\tau\sigma_s\sigma_i[S_rS_rI_r] + 2(1-p)r[S_rT]\\
&+ 2\lambda_C\alpha_s([S_rS_{nr}S_r] + [I_rS_{nr}S_r] + [TS_{nr}S_r])\\
&+ 2\lambda_G G_s([I_{nr}],[I_r])[S_{nr}S_r] - 2d_s[S_rS_r] + 2\lambda_C\alpha_s[S_{nr}S_r], \qquad (5.13)
\end{aligned}
$$

$$
\begin{aligned}
[S_{nr}\dot{I_{nr}}] &= +\tau[S_{nr}S_{nr}I_{nr}] + \tau\sigma_i[S_{nr}S_{nr}I_r] - \tau[I_{nr}S_{nr}I_{nr}] - \tau\sigma_i[I_rS_{nr}I_{nr}] - \tau[S_{nr}I_{nr}]\\
&- \lambda_C\alpha_s([S_rS_{nr}I_{nr}] + [I_rS_{nr}I_{nr}] + [TS_{nr}I_{nr}]) - \lambda_G G_s([I_{nr}],[I_r])[S_{nr}I_{nr}]\\
&- \lambda_C\alpha_i([S_{nr}I_{nr}S_r] + [S_{nr}I_{nr}I_r] + [S_{nr}I_{nr}T]) - \lambda_G G_i([I_{nr}],[I_r])[S_{nr}I_{nr}]\\
&- \gamma[S_{nr}I_{nr}] + rp[TI_{nr}] + d_i[S_{nr}I_r] + d_s[S_rI_{nr}] - \omega[S_{nr}I_{nr}], \qquad (5.14)
\end{aligned}
$$

$$
\begin{aligned}
[S_{nr}\dot{I_r}] &= +\tau\sigma_s[S_{nr}S_rI_{nr}] + \tau\sigma_i\sigma_s[S_{nr}S_rI_r] - \tau[I_{nr}S_{nr}I_r] - \tau\sigma_i[I_rS_{nr}I_r] - \tau\sigma_i[S_{nr}I_r]\\
&+ \lambda_C\alpha_i([S_{nr}I_{nr}S_r] + [S_{nr}I_{nr}I_r] + [S_{nr}I_{nr}T]) + \lambda_G G_i([I_{nr}],[I_r])[S_{nr}I_{nr}]
\end{aligned}
$$

$$
\begin{aligned}
&- \lambda_C\alpha_s([S_rS_{nr}I_r]+[I_rS_{nr}I_r]+[TS_{nr}I_r])-\lambda_G G_s([I_{nr}],[I_r])[S_{nr}I_{nr}] \qquad (5.15)\\
&- \gamma\sigma_r[S_{nr}I_r]-d_i[S_{nr}I_r]+d_s[S_rI_r]-\lambda_C\alpha_s[S_{nr}I_r]+pr[TI_r]+\omega[S_{nr}I_{nr}],
\end{aligned}
$$

$$
\begin{aligned}
[S_r\dot{I}_{nr}] &= +\tau[S_rS_{nr}I_{nr}]+\tau\sigma_i[S_rS_{nr}I_r]-\tau\sigma_s[I_{nr}S_rI_{nr}]-\tau\sigma_i\sigma_s[I_rS_rI_{nr}]-\tau\sigma_s[S_rI_{nr}]\\
&+ \lambda_C\alpha_s([S_rS_{nr}I_{nr}]+[I_rS_{nr}I_{nr}]+[TS_{nr}I_{nr}])+\lambda_G G_s([I_{nr}],[I_r])[S_{nr}I_{nr}]\\
&- \lambda_C\alpha_i([S_rI_{nr}S_r]+[S_rI_{nr}I_r]+[S_rI_{nr}T])-\lambda_G G_i([I_{nr}],[I_r])[S_rI_{nr}] \qquad (5.16)\\
&- \gamma[S_rI_{nr}]+(1-p)r[TI_{nr}]-d_s[S_rI_{nr}]+d_i[S_rI_r]-\lambda_C\alpha_i[S_rI_{nr}]-\omega[S_rI_{nr}],
\end{aligned}
$$

$$
\begin{aligned}
[S_r\dot{I}_r] &= +\tau\sigma_s[S_rS_rI_{nr}]+\tau\sigma_i\sigma_s[S_rS_rI_r]-\tau\sigma_s[I_{nr}S_rI_r]-\tau\sigma_i\sigma_s[I_rS_rI_r]-\tau\sigma_i\sigma_s[S_rI_r]\\
&+ \lambda_C\alpha_s([S_rS_{nr}I_r]+[I_rS_{nr}I_r]+[TS_{nr}I_r])+\lambda_G G_s([I_{nr}],[I_r])[S_{nr}I_r]\\
&+ \lambda_C\alpha_i([S_rI_{nr}S_r]+[S_rI_{nr}I_r]+[S_rI_{nr}T])+\lambda_G G_i([I_{nr}],[I_r])[S_rI_{nr}]\\
&- \gamma\sigma_r[S_rI_r]+(1-p)r[TI_r]-d_s[S_rI_r]-d_i[S_rI_r]\\
&+ \lambda_C\alpha_s[S_{nr}I_r]+\lambda_C\alpha_i[S_rI_{nr}]+\omega[S_rI_{nr}], \qquad (5.17)
\end{aligned}
$$

$$
\begin{aligned}
[I_{nr}\dot{I}_{nr}] &= +2\tau[I_{nr}S_{nr}I_{nr}]+2\tau\sigma_i[I_{nr}S_{nr}I_r]+2\tau[S_{nr}I_{nr}]-2\gamma[I_{nr}I_{nr}]\\
&- 2\lambda_C\alpha_i([I_{nr}I_{nr}S_r]+[I_{nr}I_{nr}I_r]+[I_{nr}I_{nr}T])\\
&- 2\lambda_G G_i([I_{nr}],[I_r])[I_{nr}I_{nr}]+2d_i[I_{nr}I_r]-2\omega[I_{nr}I_{nr}], \qquad (5.18)
\end{aligned}
$$

$$
\begin{aligned}
[I_{nr}\dot{I}_r] &= +\tau[I_{nr}S_{nr}I_r]+\tau\sigma_i[I_rS_{nr}I_r]+\tau\sigma_s[I_{nr}S_rI_{nr}]+\tau\sigma_i\sigma_s[I_{nr}S_rI_r]\\
&+ \tau\sigma_i[S_{nr}I_r]+\tau\sigma_s[I_{nr}S_r]-(\gamma+\gamma\sigma_r)[I_{nr}I_r]\\
&+ \lambda_C\alpha_i([I_{nr}I_{nr}S_r]+[I_{nr}I_{nr}I_r]+[I_{nr}I_{nr}T])+\lambda_G G_i([I_{nr}],[I_r])[I_{nr}I_{nr}])\\
&- \lambda_C\alpha_i([S_rI_{nr}I_r]+[I_rI_{nr}I_r]+[TI_{nr}I_r])-\lambda_G G_i([I_{nr}],[I_r])[I_{nr}I_r]\\
&- d_i[I_{nr}I_r]+d_i[I_rI_r]-\lambda_C\alpha_i[I_{nr}I_r]+\omega[I_{nr}I_{nr}]-\omega[I_{nr}I_r], \qquad (5.19)
\end{aligned}
$$

$$
\begin{aligned}
[I_r\dot{I}_r] &= +2\tau\sigma_s[I_{nr}S_rI_{nr}]+2\tau\sigma_i\sigma_s[I_rS_rI_r]+2\tau\sigma_i\sigma_s[S_rI_r]\\
&+ 2\lambda_C\alpha_i([S_rI_{nr}I_r]+[I_rI_{nr}I_r]+[TI_{nr}I_r])+2\lambda_G G_i([I_{nr}],[I_r])[I_{nr}I_r]\\
&- 2\gamma\sigma_r[I_rI_r]+2\lambda_C\alpha_i[I_rI_{nr}]-2d_i[I_rI_r]+2\omega[I_{nr}I_r], \qquad (5.20)
\end{aligned}
$$

$$
\begin{aligned}
\dot{[S_{nr}T]} &= -\tau[I_{nr}S_{nr}T] - \tau\sigma_i[I_rS_{nr}T] - \lambda_C\alpha_s([S_rS_{nr}T] + [I_rS_{nr}T] + [TS_{nr}T]) \\
&- \lambda_G G_s([I_{nr}],[I_r])[S_{nr}T] + \gamma[S_{nr}I_{nr}] + \gamma\sigma_r[S_{nr}I_r] \\
&+ d_s[S_rT] + pr[TT] - r[S_{nr}T] - \lambda_C\alpha_s[S_{nr}T], \qquad (5.21)
\end{aligned}
$$

$$
\begin{aligned}
\dot{[S_rT]} &= -\tau\sigma_s[I_{nr}S_rT] - \tau\sigma_i\sigma_s[I_rS_rT] + \lambda_C\alpha_s([S_rS_{nr}T] + [I_rS_{nr}T] + [TS_{nr}T]) \\
&+ \lambda_G G_s([I_{nr}],[I_r])[S_{nr}T] + \gamma[S_rI_{nr}] + \gamma\sigma_r[S_rI_r] \\
&- d_s[S_rT] - r[S_rT] + r(1-p)[TT] + \lambda_C\alpha_s[S_{nr}T], \qquad (5.22)
\end{aligned}
$$

$$
\begin{aligned}
\dot{[I_{nr}T]} &= +\tau[I_{nr}S_{nr}T] + \tau\sigma_i[I_rS_{nr}T] - \lambda_C\alpha_i([S_rI_{nr}T] + [I_rI_{nr}T] + [TI_{nr}T]) \\
&- \lambda_G G_i([I_{nr}],[I_r])[I_{nr}T] + \gamma[I_{nr}I_{nr}] + \gamma\sigma_r[I_{nr}I_r] + d_i[I_rT] \\
&- r[I_{nr}T] - \gamma[I_{nr}T] - \lambda_C\alpha_i[I_{nr}T] - \omega[I_{nr}T], \qquad (5.23)
\end{aligned}
$$

$$
\begin{aligned}
\dot{[I_rT]} &= +\tau\sigma_s[I_{nr}S_rT] + \tau\sigma_i\sigma_s[I_rS_rT] + \lambda_C\alpha_i([S_rI_{nr}T] + [I_rI_{nr}T] + [TI_{nr}T]) \\
&+ \lambda_G G_i([I_{nr}],[I_r])[I_{nr}T] + \gamma[I_rI_{nr}] + \gamma\sigma_r[I_rI_r] - \gamma\sigma_r[I_rT] \\
&- r[I_rT] + \lambda_C\alpha_i[I_{nr}T] - d_i[I_rT] + \omega[I_{nr}T], \qquad (5.24)
\end{aligned}
$$

$$
\dot{[TT]} = 2\gamma[I_{nr}T] + 2\gamma\sigma_r[I_rT] - 2r[TT], \qquad (5.25)
$$

where $N = S_{nr} + S_r + I_{nr} + I_r + T$ is the population size, $\tau = \beta^d/N$ is the rate of disease transmission across a (S, I) link and $\alpha = \beta^i/N$ is the rate of information transmission across a (X_{nr}, X_r) link. The routes of responsiveness transmission can be switched on and off or can be combined using λ_C and λ_G which are set to 0 or 1 accordingly. For our purposes we set

$$
G_s([I_{nr}],[I_r]) = G_i([I_{nr}],[I_r]) = \frac{\delta([I_{nr}]+[I_r])^n}{K + ([I_{nr}]+[I_r])^n}. \qquad (5.26)
$$

In this chapter, $n = 1$ unless otherwise stated. To integrate the equations numerically, we use the classic closure proposed in [61]. This amounts to approximating all triples in terms of singles and pairs, with the general closure relation given by

$$[ABC] = \frac{\langle k \rangle - 1}{\langle k \rangle} \frac{[AB][BC]}{[B]}$$

where $\langle k \rangle$ is the mean degree of a node, and the closure assumes that the states of an individual's neighbouring nodes follow a multinomial distribution. This approximation, discussed in detail in Chapter 3, closes the system and numerical integration can be performed. Parameter values are based on those used in [74] but with units changed from weeks to years. For simplicity we assume that $\alpha_s = \alpha_i = \alpha$, $d_s = d_i = d$ and $\delta_s = \delta_i = \delta$. The present model, in some sense, can be seen as a generalization of the model in [34] but with a few important remarks. The model by Funk [34] is different in that information is only generated via self-diagnosis from infected individuals and this can lead to a qualitatively different behaviour when compared to the present case where information is also generated via treatment. The model by Funk [34] uses a general pairwise approach but it does not include the global prevalence-based transmission of information. In light of the above, the model proposed here shares some common features with some of the existing models but incorporate new ways in which information can be generated and transmitted.

5.3 Results

Pairwise ODE models [61] provide a good compromise between simple compartmental and full simulation models and allows us to capture more of the local nature of contacts and to depart from the very limiting homogeneous random mixing assumption. For example, this is important when modelling contact tracing [26, 52] where control relies on being able to answer the 'who infected whom'

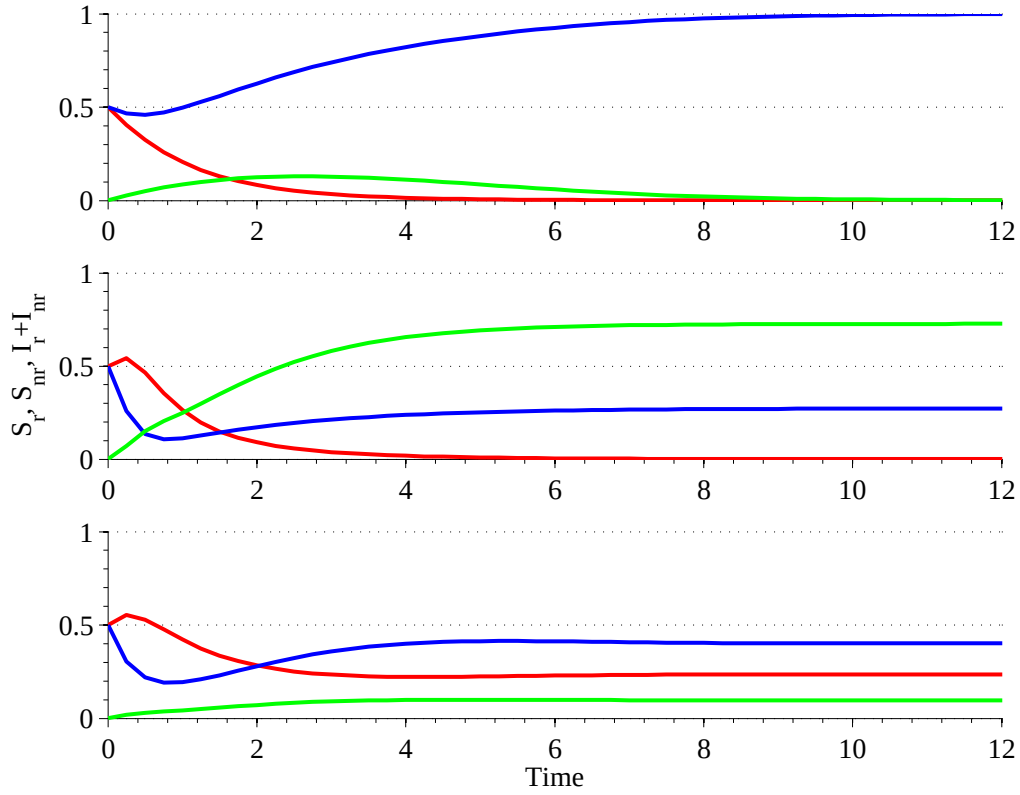

Figure 5.1: The three distinct outcomes of the pairwise information model: the trivial disease-free steady state with $\tau = 0.1\gamma$ and $\alpha_s = \alpha_i = 0.1d_s$ (top panel), the non-trivial disease-free steady state with $\tau = 0.1\gamma$ and $\alpha_s = \alpha_i = d_s$ (middle panel) and the endemic state with $\tau = \gamma$ and $\alpha_s = \alpha_i = 0.1d_s$ (bottom panel). The plots show S_{nr} in blue, S_r in green and $I_{nr} + I_r$ in red. Other parameters are: $N = 1000$, $\langle k \rangle = 4$, $\gamma = 1$, $\sigma_r = 2$, $\sigma_i = \sigma_s = 0.5$, $d_i = d_s = \sigma_r\gamma$, $r = 1$, $p = 0.9$, $K = 10$, $n = 1$, $\delta = 0.1d_i$ and $\omega = 0$.

type questions. In this case, the situation is similar in that the local nature of individual to individual transmission of information can lead to clusters of responsive individuals that are difficult to capture via simple compartmental models. The pairwise model given by Eqs. (5.6 - 5.25), which can be numerically integrated, allows us to explore not only how the levels of infection and awareness in the population evolve over time, but also to investigate the local correlations between individuals in different states.

The system exhibits three qualitatively different long-term behaviors: **(a)** neither disease nor responsiveness can spread - the trivial disease-free steady state, **(b)** only responsiveness spreads and a state of endemic-responsiveness is

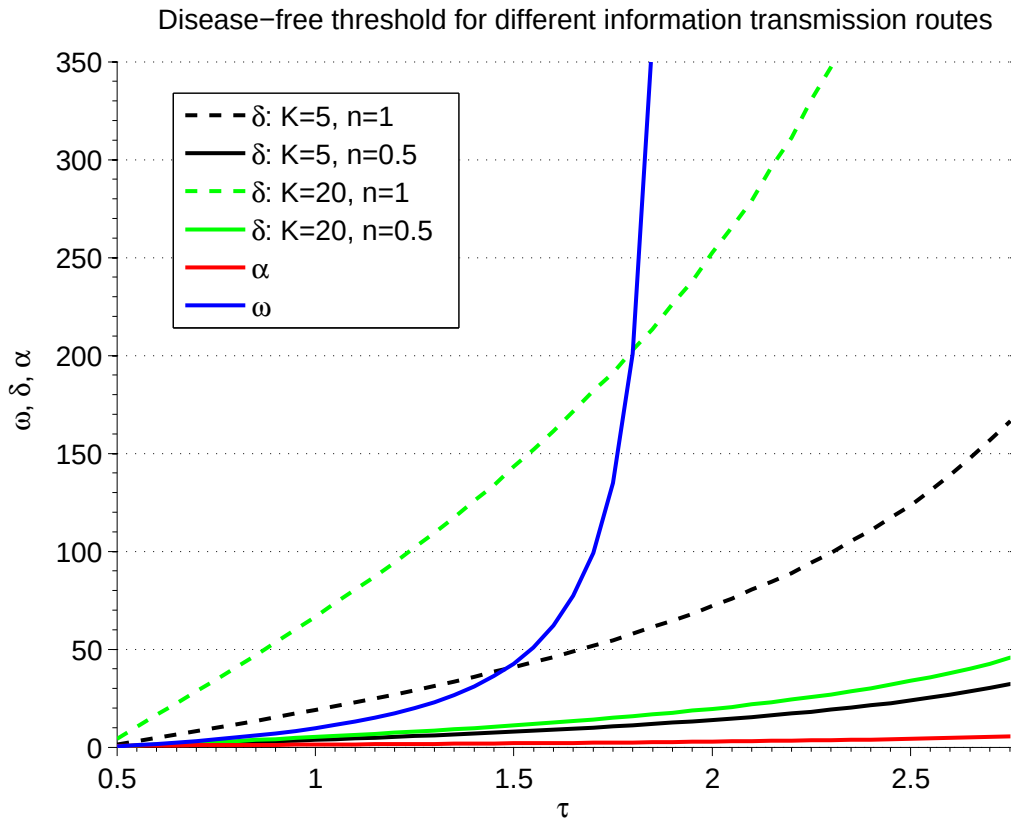

Figure 5.2: The critical information transmission rates that bring $I^{eq} < 1/N$ as a function of τ. The red line corresponds to α, the blue to ω and the black and green to δ, with black representing $K = 5$, green $K = 20$, dashed show where $n = 1$ and solid where $n = 0.5$. Other parameters are: $N = 1000$, $\langle k \rangle = 6$, $\gamma = 1$, $\sigma_r = 2$, $\sigma_i = \sigma_s = 0.5$, $d_i = d_s = \sigma_r \gamma$, $r = 1$, $p = 0.9$.

reached - the non-trivial disease-free steady state - and **(c)** both responsiveness and infection are endemic. The three distinct outcomes are shown in Fig 5.1. The model is highly complex, with many states, transitions and parameters. We will focus our investigation on comparing the effectiveness of the different routes of information generation and transmission, in addition to exploring how resistant a recently recovered population is to reinfection.

The analysis begins by comparing information sources with respect to their capacity to bring the prevalence to a desired low level, when each is acting in isolation. Information can achieve this by shifting a large fraction of the population into the responsive class. Such informed individuals will then experience

decreases in their infectivity and susceptibility as well as a faster recovery. The minimum rate at which a source of information can bring the prevalence to a desired low level will be referred to as the *critical information transmission rate*. We choose a prevalence level greater than zero, specifically $I^{eq} = 1/N$, because as the prevalence approaches zero precise identification of the critical information rates becomes numerically challenging. Starting with a small initial information generation or transmission rate, for a range of infection rates τ with fixed recovery parameters, the system is seeded with a small number of I_{nr} and S_r individuals. The system of pair approximation equations, Eqs. (5.6 - 5.25) is then numerically integrated to identify the smallest or critical rate that will lead to the desired prevalence level I^{eq}. Next, the relative capacities of α, ω and δ to deliver a state of low infection prevalence for different values of τ are considered. We let $p = 0.9$, which approaches a worse case scenario limit whereby no information is generated by the individuals themselves through past experience. This parameter choice allows us to examine the effects of α, ω and δ in relative isolation.

As shown in Fig. 5.2, contact-based transmission of information is by far the most efficient way to generate a responsive population, a result well known in the diffusion of innovations literature [87]. In this case every receiver of information (I_{nr} or S_{nr}) immediately also becomes a transmitter of information, in contrast to global transmission of information from a single source.

We model the transition to the responsive class due to media exposure at a rate given by the Holling-type response function given in Eq. (5.26). The effectiveness of global information (acting on I_{nr} or S_{nr}) is strongly tied to the K parameter which controls the growth of $G()$ such that when the prevalence is low the function grows like $\frac{1}{K}(I_{nr} + I_r)^n$. It is helpful to think of K as a measure of population inertia in responding to information. Populations with high values of K are resistant to behavioral change which can therefore act as an indicator for the quality of global information campaigns. For example, high values of K

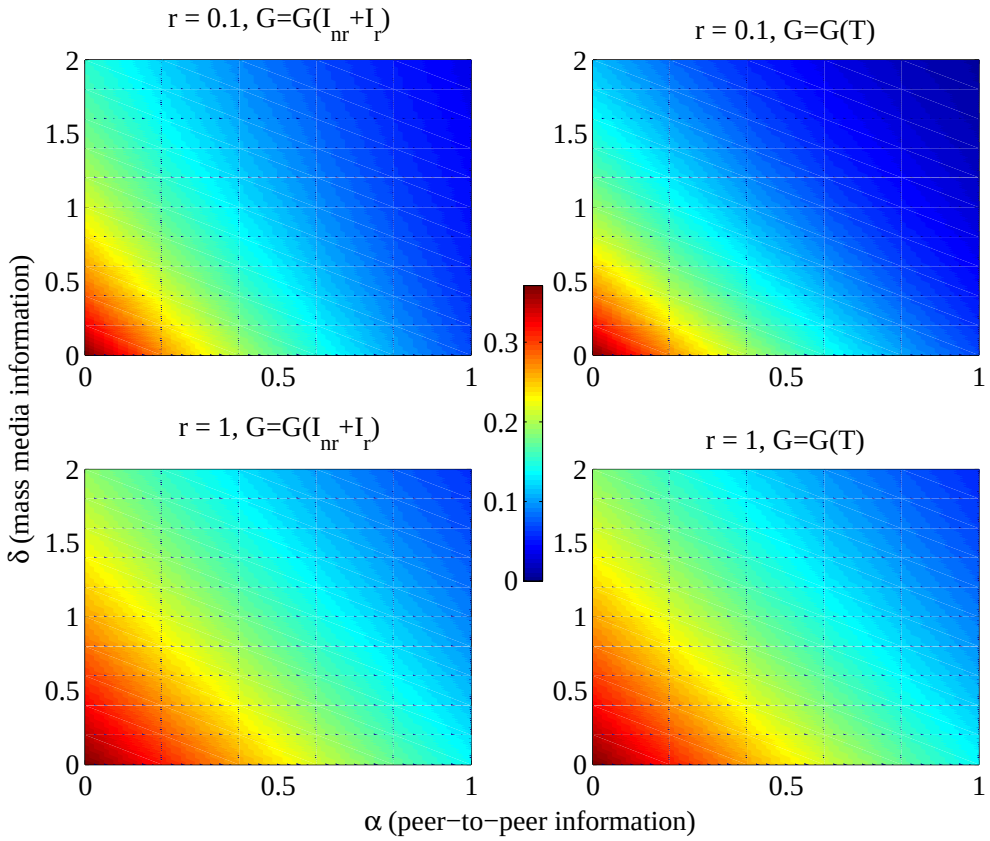

Figure 5.3: Combined effects of globally generated information, δ, versus peer generated information, α, with the different colours representing different proportions of the population that are infected at equilibrium. Four distinct global scenarios are shown as combinations of fast and slow treatments ($r = 1$ and $r = 0.1$) and global information being generating based on the number in treatment ($G = G(T)$) or the number of infected ($G = G(I_{nr} + I_r)$). Parameters are: $N = 1000$, $\langle k \rangle = 6$, $\tau = 2.5$, $\gamma = 1$, $\sigma_r = 2$, $\sigma_i = \sigma_s = 0.5$, $d_i = d_s = \sigma_r \gamma$, $p = 0.5$, $\delta = 1$, $n = 1$, $K = 10$, $\omega = 1$.

will simply lead to observing vanishingly small benefits from global information campaigns.

The critical rates for self-diagnosis, ω, are at best similar to those for global information, especially for diseases with low transmissibility, as shown in Fig. 5.2. As is the case for global information, self-diagnosis will only function once infected individuals are present and the situation is somehow even less fortunate given that ω can only act on I_{nr}, and hence awareness can only follow infection, and cannot build up a sub-population of S_r type individuals to slow or prevent

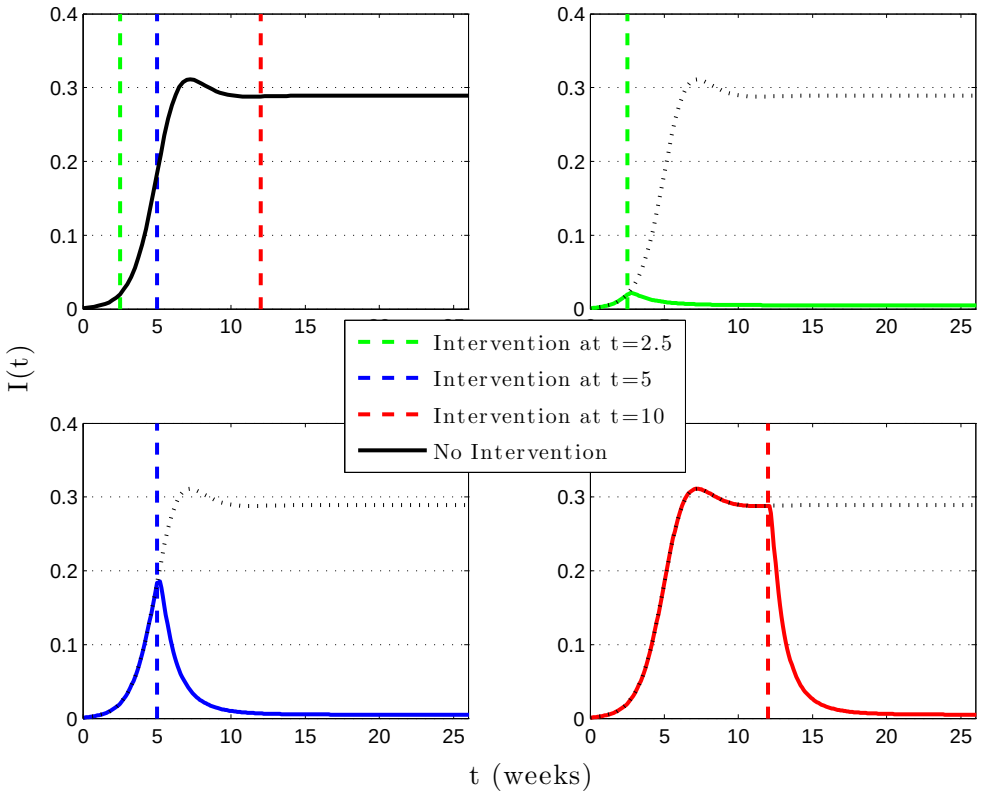

Figure 5.4: Intervention via global information transmission, $G([I_{nr}] + [I_r])$, and three different stages of an outbreak, compared to no intervention. In each intervention plot, the course of the epidemic without any intervention is shown as a black dashed line. Parameters are: $N = 1000$, $k = 6$, $\gamma = 1$, $\sigma_r = 2$, $\sigma_i = \sigma_s = 0.5$, $d_i = d_s = \sigma_r\gamma$, $r = 1$, $p = 0.9$, $\delta = 1$, $n = 1$, $K = 10$, $\omega = 0$.

the onwards spread of the epidemic. The self-diagnosis rate can be thought of as a model for the probability of a particular infection being symptomatic. Thus for diseases with mild symptoms or those that are asymptomatic, the need for peer-to-peer communication and low population inertia is even more pressing. Finally self-diagnosis can, in cases where the population has very high behaviorial inertia, be more effective than certain methods of global information dissemination. This can be seen by comparing the appropriate curves in Fig. 5.2, but is only true for low values of τ, and compared to weak global media campaigns. It is also worth noting that as τ increases it is less and less likely that any route information generation and/or transmission can prevent an epidemic. More precisely at large but finite values of τ, the rates of information generation and/or transmission

needed to halt the spread will tend to unfeasible large values.

Results suggest that global information is never a more efficient way to lower infection prevalence than contact-based transmission. The global information transmission rate takes its maximum value as $K \to 0$, for large δ and high prevalence of infection, at which point $G \simeq \delta$. For any value of δ we have found that there is a contact-based rate α ($\alpha < \delta$) that will lower the prevalence at least by the same amount, as shown in Fig. 5.3. However, we also note that peer-to-peer information transmission requires information generating sources, for example people in treatment. With self diagnosis and global information transmission this is not the case, but, on the other hand, they do rely on infection being present. In reality no single information source will act in isolation. Media campaigns encourage discussion which can bring forth behavioral change. Infected individuals are likely to learn from experience and further communicate this to their family and friends. Our model is able to accommodate such scenarios as we show in Fig. 5.3 for various combinations of α and δ.

One challenge for central administrative bodies who are responsible for national or global awareness campaigns is to estimate the number of infected individuals, in order to pitch the messages so as to raise enough concern as to be effective but without causing unnecessary panic. In our proposed model, we have $G([I_{nr}], [I_r])$, but in reality data will in the first instance be derived from health care records, which will be related to the number of people in or seeking treatment. In Fig. 5.3 we compare $G([T])$ with $G([I_{nr}] + [I_r])$ for two different rates of treatment for diagnosis rates of $\gamma = 1$ for non-responsive individuals and $\gamma\sigma_r = 2$ for responsive individuals. In the instance where the rate of treatment is slow compared to the rate of diagnosis, $r = 0.1$, we find that $G([T])$, i.e. a media campaign based on numbers in treatment, lead to a smaller epidemic than $G([I_{nr}], [I_r])$, whereas when the treatment rate is of the same order, $r = 1$, both measures of prevalence lead to similar results. It is clear that each disease needs

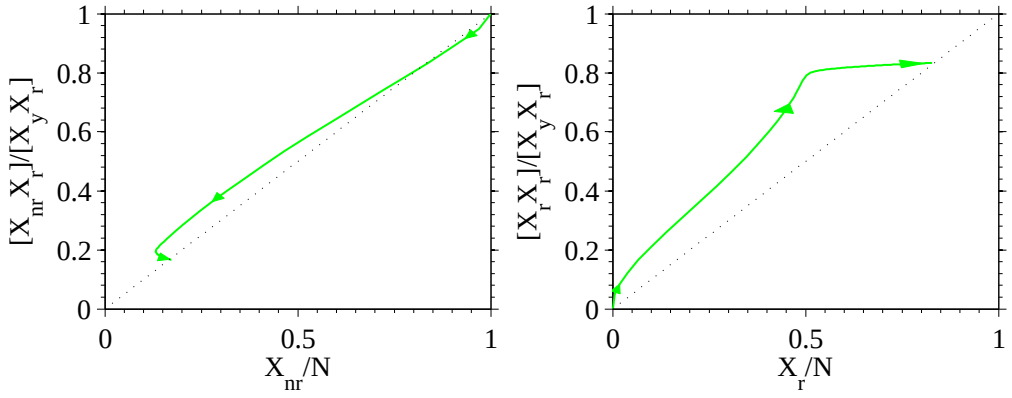

Figure 5.5: Correlation plots showing the probability that the neighbour of a responsive individual is (i) non-responsive (first panel) or (ii) responsive (second panel), plotted against the probability of picking either a (i) non-responsive (first panel) or (ii) responsive (second panel) individual at random. Information is spread via peer-to-peer transmission with $\alpha_i = \alpha_s = \sigma_r\gamma$, with the population being at a disease-free equilibrium. Other parameters are: $\tau = 0.5$ $N = 1000$, $k = 6$, $\gamma = 1$, $\sigma_r = 2$, $\sigma_i = \sigma_s = 0.5$, $d_i = d_s = \sigma_r\gamma$, $r = 1$, $p = 0.5$, $\delta = 1$, $n = 1$, $K = 10$.

to be taken on its own merits, and careful analysis of the rates of transition in and out of treatment needs to be considered in order to effectively estimate the actual number of infected individuals from the number in treatment.

A second challenge is to know *when* to act. In Fig. 5.4 we have investigated the effect of a global awareness campaign initiated at different stages of the development of the epidemic. As can clearly be seen in Fig. 5.4, early intervention has a significant effect on the levels of infection experienced, as would be expected, and it is reassuring that such a complex model agrees with intuitively simple real-world arguments. However, a full national or global awareness campaign is expensive and could cause panic, so the ability to recognise potentially serious epidemics in their early stages is crucial for effective public health care, a problem highlighted in the recent FMD outbreak in the UK [31].

Contact based transmission of information is by far the single most efficient transmission mechanism, as shown in Fig. 5.2, as it constantly builds new sources of information. Responsive individuals are then able to halt the spread of an

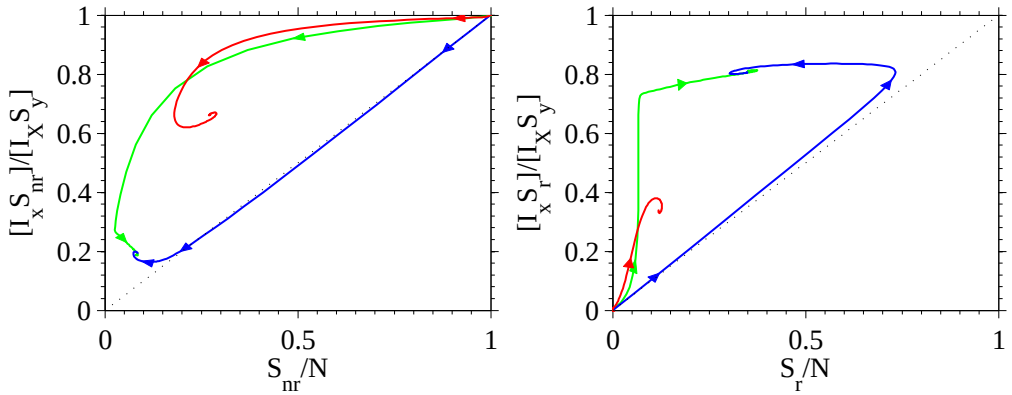

Figure 5.6: Correlation plots showing the probability that in an $(S_x - I_y)$ pair, with $x, y \in \{nr, r\}$, the susceptible individual is (i) non-responsive (first panel) and (ii) responsive (second panel). These are plotted against the probability of picking either (i) a non-responsive susceptible individual (first panel) and (ii) a responsive susceptible (second panel) at random. Three different sources of information are shown: Self-diagnosis with $\omega = 50$ (red), peer-to-peer information transmission with $\alpha_i = \alpha_s = \sigma_r\gamma$ (green) and global information transmission with $K = 10$, $n = 1$, $\delta = d_s$ (blue). The population is in an endemic state with $\tau = 2.5$ and $I^* \approx 0.2$ for each of the three information routes. Other parameters are: $N = 1000$, $k = 6$, $\gamma = 1$, $\sigma_r = 2$, $\sigma_i = \sigma_s = 0.5$, $d_i = d_s = \sigma_r\gamma$, $r = 1$, $p = 0.5$, $\delta = 1$, $n = 1$, $K = 10$.

epidemic by forming clusters that can resist infection invasions, as can be seen in Fig. 5.5. If no peer-to-peer routes of information transmission are in place, and the self-diagnosis rate or a global prevalence based media campaign are alone used to control an epidemic, then once the system reaches a disease-free equilibrium, all individuals are non-responsive with no memory of the disease. However, control via α leads to an endemic level of awareness once the disease has died, and thus the population is left resistant to reinfection in the future. This can be seen in Fig. 5.5, which also reveals that in the non-trivial disease free state, the distribution of S_r type individuals in the population is at random. From Fig 5.5, we can see that the probability that a S_r individual has a S_{nr} neighbour, given it is part of a S_xS_r pair, is the same as the probability of picking a S_{nr} type individual at random from the whole population, and hence the random mixing assumption

holds at the non-trivial disease-free equilibrium:

$$\frac{[X_{nr}X_r]}{[X_yX_r]} \approx \frac{X_r\langle k\rangle\frac{X_{nr}}{N}}{X_r\langle k\rangle} = \frac{X_{nr}}{N}.$$

However, in the case where both disease and information are endemic, as shown in Fig. 5.6, responsive and non-responsive individuals are non-randomly mixed, and correlations arise. Indeed, both global and peer-to-peer transmissions lead to a much higher proportion of $(S_x - I_x)$ type links having a S_r type individual as part of them than is found from simply allowing information to be generated via self-diagnosis. This high correlation of responsive susceptible individuals with infected individuals will have a significant effect on the efficacy of different forms of intervention, leading to a greater awareness of potential risks of infection.

5.4 Discussion

Incorporating behavioural change into epidemiological models is a challenging task with many unknowns when modelling the transmission of information and responsiveness of people. These are complex processes with many heterogeneities at the individual level in how information is acquired, processed, acted upon and transmitted further. In this chapter, we derived and analysed a pairwise model that captures multiple ways of generating and transmitting information. This pairwise model was used to assess the efficacy of different sources of information generation and routes of information transmission in bringing prevalence to as a low level as possible. Contact based transmission of information was found to be the most efficient as it creates multiple secondary sources of information and out-competes processes such as the global transmission of information. The analysis, in line with previous findings [35], also shows that information cannot always stop an epidemic but can significantly reduce its impact via lowering the prevalence of infection.

The particular types of information generation and transmission will heavily depend on disease characteristics and these will impact on model outcome and on establishing what the most influential factors are in controlling epidemics via information transmission. In addition, a balance needs to be found between the epidemiological impacts of different control strategies and their economic costs [76].

It is rarely the case that diseases invade populations that are fully naive. A number of responsive individuals are always present due to past epidemics or simply due to awareness being a trait that arises independently of past epidemics through genetic, social, cultural or economic reasons. In either case, the number of responsive individuals and their precise distribution will have an important impact on whether newly seeded infections can invade.

A number of simplifying assumptions on human behaviour are built into our model. There are only two levels of information awareness and transitions between them are instantaneous. In the real world an individual's exposure to the risk of infection is certainly not limited to two categories. People are also likely to react to information around them via imitative behaviour with individuals having different propensity for changing their behaviour. Furthermore the decision to act on information may depend on the source of information - or the combination of sources of information - the order of arrival of information, or any segmentation of the population as discussed in the introduction. Indeed, cognitive and social aspects of a host population, as well as a network of contacts (particularly in the case of STDs), are interacting and altering the epidemiological profile of an infectious pathogen.

Also, these information and disease transmission mechanisms could be applied to full network simulations to include more detailed heterogeneities. This approach would also allow us to research the effect of allowing information and infection to travel on two overlapping networks, as, for example, a phone call to

a friend could result in a transmission of awareness but certainly not of infection.

These are early days for behaviorial epidemiology and in the future it is likely that knowledge generated in other fields, for example cognitive and evolutionary psychology, communications theory, market research, game theory and anthropology should be examined for integration into epidemiological modelling.

Chapter 6

Modelling disease transmission in domestic sheep flocks: from weighted network to multi-group ODE models

6.1 Overview

In the previous chapters of this Thesis, we have derived and analysed various models the help understand how disease spread in host populations. We have focused on how networks can be used to capture real-world heterogeneities in the structure of populations and we have proceeded to investigate how well different ODE models can capture the structure of these networks.

In this chapter, we use some of the network and ODE modelling tools and techniques studied in previous chapters to focus on a real-world epidemiological problem - modelling how diseases spread within domestic sheep flocks. Successful control of livestock diseases requires an understanding of how the pathogens spread both amongst animals and between premises. While a number of studies

have considered the problem of how a disease spreads from one farm to another (see for example [31, 62, 64]), how the disease spreads within a flock is poorly understood.

A key difference between work in previous chapters and work in this chapter is the type of disease being modelled. Up until this point we have considered SIS type epidemics, which have particular relevance to human health, such as some STDs. In this chapter, two disease that pose a real threat to sheep are considered - foot-and-mouth disease, a viral disease with a fast recovery rate, and brucellosis, a bacterial disease with a slow recovery rate. Both of these disease are SIR type epidemics, whereby the infected individual enters the Removed class upon recovery, instead of returning to the Susceptible class and hence becomes dynamically unimportant with respect to disease transmission.

In this chapter the quantitative results from observational studies of contact within domestic sheep flocks [110] are applied to range of epidemiological models, both network and ODE based models, and the subsequent dynamics and real-world implications are explored.

We start with a full network simulation model, similar to those used in previous chapters, but here we are able to construct a weighted network from the field-data, whereby each link is not represented simply by 0 or 1, as was the case in previous chapters, but by values that represent the relative strengths of different links.

The field-data has been collected at three distinct times of the year, firstly just after ewes have given birth, secondly when their lambs are nearly weaned and thirdly when the lambs have left the flock. These three different types of flock composition each have their own full weighted network, and hence seasonal variation to the susceptibility of a flock to an outbreak can be investigated.

We show that the observed heterogeneity of contacts amongst members of a flock is best captured by full weighted network simulations, although simple

compartmental models describe the key features of an outbreak but, as expected, often overestimate the speed of it. The observed weights of the contacts between sheep are highly heterogeneous, with many low weighted links, but the well connected nature of the flocks leads to only small differences between models that distribute the weights more homogeneously. Since sheep flocks are probably amongst the most heterogeneously stocked livestock in the UK and Europe, the application of such simplified compartmental models is also well justified for other domestic species.

6.2 Background

Livestock diseases present a challenge to global food security and are of socioeconomic importance both in industrialised nations [97] and the developing world [99]. It is important to understand the spread of pathogens amongst animal hosts both for livestock health and productivity and potentially for human health directly, since the majority of emerging infectious diseases are of zoonotic origin [58, 115].

Epidemiological models have already been applied to a number of important diseases, such as foot-and-mouth disease (FMD) [31, 56, 62, 64, 118], bluetongue [46, 49], brucellosis [28] and classical swine fever [6]. Most, however, only consider disease transmission explicitly on a large scale i.e. between premises, making use of livestock movement data and holding records, while actual transmission data is generally restricted to small scale experiments between a few animals. Although infection between individuals is therefore reasonably well understood for a number of pathogens, it is fallacious to assume that groups of animals will respond in the same way; key temporal factors such as the latent, incubation and infectious periods are likely to be different for herds and flocks than for individual animals.

Group level dynamics will be driven by the pattern of interactions between susceptible and infectious hosts, as well as intrinsic properties of the pathogens.

How these relate to individual dynamics can be non trivial, especially if behaviour is not homogeneous. The number and relative strength of connections between individuals impacts on the basic reproduction number for an outbreak [66]. These properties, as well as factors such as group size and heterogeneity, determine what theoretical structures (mathematical models) are appropriate in different settings. For example, human contact patterns have been found to be more heterogeneous than assumed by classic homogeneous-mixing models, but not as variable as some have speculated [9].

It is of practical value to determine what level of model complexity is required to adequately describe a realistic scenario, and where approximating assumptions do not undermine the validity of results. Here detailed field data is applied to a series of models to identify the most suitable model structure for representing disease transmission amongst what are probably the least intensively farmed - and thus least homogeneously mixed - domestic animals in the UK and most of Europe.

In this chapter the most appropriate formulation for domestic sheep flocks is investigated, as determined by the level of contact between individuals. Previous observations have found age-dependent behaviour amongst sheep, as well as behaviour driven by parenthood [33, 95]. Norton *et al.* [94] demonstrated a clear difference in the rate of contact between and amongst ewes and lambs, and showed that this changed with the age of offspring.

There exist a number of detailed studies on the nature and composition of flocks [33, 95]. The rate of contact is a key factor in determining the force of transmission between individuals or groups: explicitly, it is weighted by the probability that a given contact is between a susceptible individual and an infected individual and the probability that it results in transmission. Here available contact data [94] is considered directly to simulate the potential for disease transmission within the flocks observed, and compared with predictions made

using suitable state transition models, with particular emphasis on the effect of observed seasonal differences [33, 94].

6.3 Modelling methodology

6.3.1 Disease dynamics

As there is significant variability in the dynamics of different sheep diseases, results derived here are kept as general as possible. Where appropriate foot-and-mouth disease (FMD), a viral disease with a fast recovery rate of 7-8 days in sheep (see Alexandersen *et al.* [2]), and brucellosis, a bacterial disease with a slow recovery rate of approximately 3 weeks in sheep (see England *et al.* [28]) are considered as exemplars, with the parameter ranges presented chosen to encompass their respective values.

To provide estimates of p, the per-contact transmission probability for the exemplar FMD, the experimental data of Orsel *et al.* [96] is considered. This provides the infection status, at the end of a 14-day trial period, of six groups of four unvaccinated lambs, two of which were initially infected (by inoculation), the other two being susceptible individuals [96].

6.3.2 Contact rates based on field observations

Contact data used in this chapter are derived from field observations by Norton *et al.* [94] for three different conventionally managed flocks: one with young (newborn) lambs and their mothers; one with older (nearly weaned) lambs and their mothers; and one with ewes only. The observed flocks consisted of N_e ewes and N_l lambs, giving $N = N_e + N_l$ sheep in total (between 25 and 30 in practice); for details of data collection see Norton *et al.* [94].

Contact data are in the form of adjacency matrices $C = \{c_{ij}\}_{1 \leq i,j \leq N}$ that record the frequency of physical contacts between individuals per day. The re-

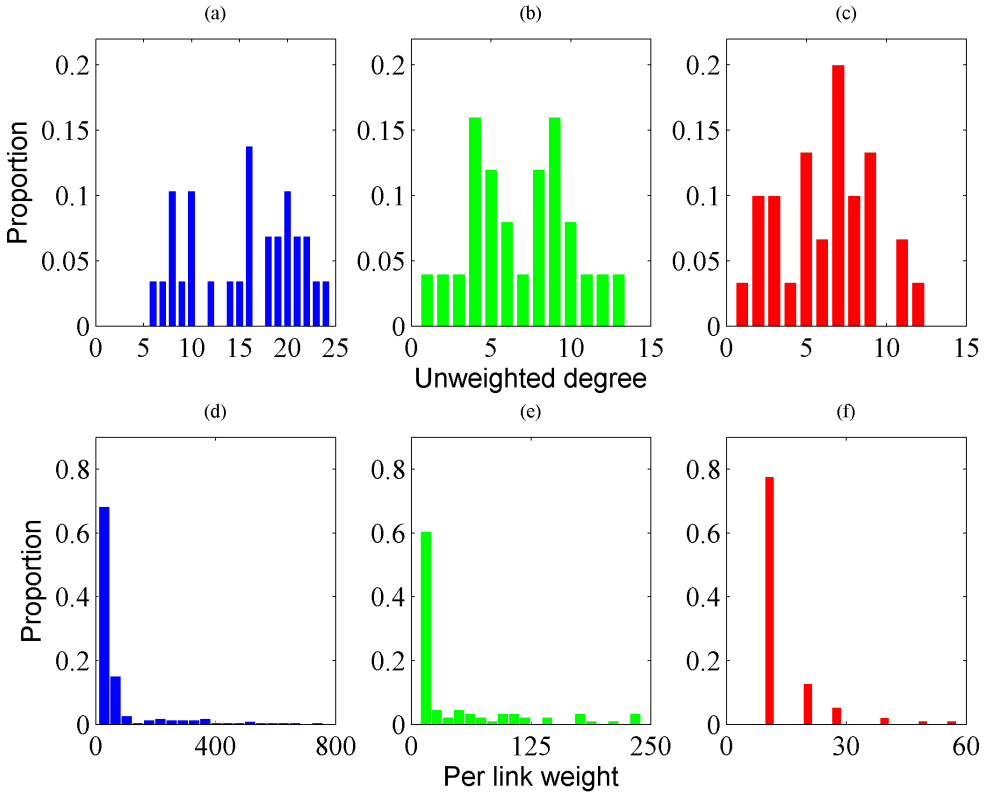

Figure 6.1: The degree distribution (top row) and per-link weight distribution (bottom row) for the three flocks: ewes and newborn lambs (blue: first column), ewes and nearly-weaned lambs (green: second column); and ewes only (red: third column).

sulting matrix is symmetric due to a contact initiated by sheep i to sheep j contributing to both c_{ij} and c_{ji} . This is an appropriate assumption when considering disease transmission, since it is the contact alone that is important. Where there is no contact between two sheep, the entry is zero (including c_{ii} for $i = 1, \ldots, N$). This matrix of weighted contacts can be interpreted as a weighted network, where the strength of a link c_{ij} is simply equal to the frequency of contacts between individual i and j (for the purpose of the analysis, all rates have been scaled to units corresponding to the expected number of contacts per day). The networks, in all three situations, are relatively well connected with individuals having a high number of links and with a per-link weight distribution that is skewed towards smaller weights, as shown in Fig. 6.1.

Flock	Contacts	Parameter	Estimated daily rate
Ewes with newborn lambs	ewe $\leftrightarrow$ ewe	c_e	0.8 ± 2.7
	ewe $\leftrightarrow$ lamb	c_m	49.7 ± 131.6
	lamb $\leftrightarrow$ lamb	c_l	41.7 ± 74.8
	any $\leftrightarrow$ any	c	39.6 ± 102.7
Ewes with nearly weaned lambs	ewe $\leftrightarrow$ ewe	c_e	1.3 ± 5.5
	ewe $\leftrightarrow$ lamb	c_m	17.0 ± 47.7
	lamb $\leftrightarrow$ lamb	c_l	14.3 ± 32.0
	any $\leftrightarrow$ any	c	13.5 ± 38.6
Ewes only	ewe with ewe	c	2.8 ± 6.7

Table 6.1: Daily rate of physical contacts between individuals of different types, with the total population level weight of contact averaged over all possible links, thus assuming a fully connected network within each population. The values given (mean $\pm$ standard deviation) are calculated from the raw observational data available in the supplementary materials section of Schley *et al.* [110] and is explored further in Norton *et al.* [94].

The weighted contact matrix $C = \{c_{ij}\}_{1 \leq i,j \leq N}$ will be the building block for a range of within-flock models and will be used to define (i) individual based stochastic network models and (ii) compartmental ODE models at the group (ie ewes and lambs) or flock level. How the full contact data feed into both the stochastic simulation and ODE models is clearly defined below.

6.3.3 Network models

In this Chapter, the following four increasingly homogeneous network models are considered:

1. The fully weighted heterogeneous network model, with rates given by the full adjacency matrix C (See Fig. 6.2 and the supplementary materials in Schley *et al.* [110]),

2. A homogeneous-weight network model, with the full network structure preserved but with each link weighted equally with mean c_G, as given by Eq. (6.1),

3. A semi-homogeneous two-class fully connected network model, with all con-

	G1	G1a	G1b	G2	G2a	G2b	G3	G3a	G3b	G4	G4a	G4b	G5	G5a	G5b	B1	B1a	B1b	B2	B2a	B3	B3a	B4	B4a	B5	B5a	B8	B8a	B8b
G1	0	585.6	384	0	0	28.8	0	9.6	0	0	0	0	0	0	0	0	19.2	19.2	0	9.6	0	0	0	9.6	0	0	0	0	0
G1a	585.6	0	249.6	38.4	9.6	57.6	28.8	48	28.8	0	19.2	0	9.6	9.6	38.4	19.2	28.8	105.6	0	0	48	19.2	0	0	0	19.2	0	0	9.6
G1b	384	249.6	0	57.6	19.2	67.2	9.6	28.8	9.6	0	48	9.6	0	19.2	48	19.2	9.6	57.6	0	86.4	0	76.8	19.2	19.2	0	0	0	76.8	38.4
G2	0	38.4	57.6	0	345.6	681.6	9.6	9.6	0	0	9.6	0	0	19.2	48	0	0	0	0	19.2	0	0	0	9.6	0	0	0	0	28.8
G2a	0	9.6	19.2	345.6	0	307.2	0	0	0	374.4	28.8	38.4	0	76.8	28.8	0	9.6	9.6	0	0	19.2	9.6	9.6	0	0	0	0	9.6	9.6
G2b	28.8	57.6	67.2	681.6	307.2	0	9.6	9.6	57.6	0	28.8	28.8	0	67.2	19.2	0	9.6	0	0	57.6	0	38.4	9.6	38.4	19.2	57.6	0	9.6	19.2
G3	0	28.8	9.6	9.6	0	9.6	0	758.4	441.6	0	0	9.6	0	28.8	0	0	0	9.6	0	182.4	9.6	19.2	9.6	28.8	0	9.6	0	0	19.2
G3a	9.6	48	28.8	9.6	0	9.6	758.4	0	316.8	96	48	38.4	67.2	48	28.8	9.6	105.6	9.6	28.8	28.8	19.2	28.8	9.6	48	0	0	0	9.6	9.6
G3b	0	28.8	9.6	0	0	57.6	441.6	316.8	0	38.4	0	9.6	9.6	76.8	19.2	0	9.6	19.2	0	0	0	19.2	0	9.6	0	19.2	0	0	9.6
G4	0	0	0	0	374.4	0	0	96	38.4	0	547.2	624	0	9.6	0	0	9.6	0	0	0	0	9.6	0	38.4	0	0	0	0	9.6
G4a	0	19.2	48	9.6	28.8	28.8	0	48	0	547.2	0	230.4	0	9.6	9.6	0	9.6	48	9.6	19.2	0	38.4	9.6	76.8	0	9.6	0	0	28.8
G4b	0	0	9.6	0	38.4	28.8	9.6	38.4	9.6	624	230.4	0	0	28.8	9.6	0	0	0	19.2	0	0	0	0	19.2	19.2	9.6	28.8	0	0
G5	0	9.6	0	0	0	0	0	67.2	9.6	0	0	0	0	355.2	288	0	9.6	28.8	0	0	0	28.8	0	0	0	9.6	9.6	0	0
G5a	0	9.6	19.2	19.2	76.8	67.2	28.8	48	76.8	9.6	9.6	28.8	355.2	0	480	0	28.8	57.6	0	19.2	0	38.4	0	28.8	57.6	9.6	0	0	0
G5b	0	38.4	48	48	28.8	19.2	0	28.8	19.2	0	9.6	9.6	288	480	0	0	28.8	105.6	0	19.2	0	0	0	28.8	0	0	0	0	86.4
B1	0	19.2	19.2	0	0	0	0	9.6	0	0	0	0	0	0	0	0	268.8	288	0	0	0	9.6	0	0	0	9.6	0	0	38.4
B1a	19.2	28.8	9.6	0	9.6	9.6	0	105.6	9.6	9.6	9.6	0	9.6	28.8	28.8	268.8	0	518.4	0	38.4	0	144	0	0	0	48	0	0	67.2
B1b	19.2	105.6	57.6	0	9.6	0	9.6	9.6	19.2	0	48	0	28.8	57.6	105.6	288	518.4	0	19.2	28.8	19.2	48	9.6	48	0	0	57.6	57.6	28.8
B2	0	0	0	0	0	0	0	28.8	0	0	9.6	19.2	0	0	0	0	0	19.2	0	384	0	0	9.6	19.2	0	0	0	0	9.6
B2a	9.6	0	86.4	19.2	0	57.6	182.4	28.8	0	0	19.2	0	0	19.2	19.2	0	38.4	28.8	384	0	9.6	19.2	28.8	19.2	9.6	28.8	38.4	0	9.6
B3	0	48	0	0	19.2	0	9.6	19.2	0	0	0	0	0	0	0	0	0	19.2	0	9.6	0	230.4	0	0	0	0	0	0	0
B3a	0	19.2	76.8	0	9.6	38.4	19.2	28.8	19.2	9.6	38.4	0	28.8	38.4	0	9.6	144	48	0	19.2	230.4	0	9.6	28.8	19.2	48	28.8	9.6	76.8
B4	0	0	19.2	0	9.6	9.6	9.6	9.6	0	0	9.6	0	0	0	0	0	0	9.6	9.6	28.8	0	9.6	0	499.2	0	9.6	0	9.6	9.6
B4a	9.6	0	19.2	9.6	0	38.4	28.8	48	9.6	38.4	76.8	19.2	0	28.8	28.8	0	0	48	19.2	19.2	0	28.8	499.2	0	0	249.6	9.6	0	57.6
B5	0	0	0	0	0	19.2	0	0	0	0	0	19.2	0	57.6	0	0	0	0	0	9.6	0	19.2	0	0	0	211.2	0	0	0
B5a	0	19.2	0	0	0	57.6	9.6	0	19.2	0	9.6	9.6	9.6	9.6	0	9.6	48	0	0	28.8	0	48	9.6	249.6	211.2	0	19.2	182.4	163.2
B8	0	0	0	0	0	0	0	0	0	0	0	28.8	9.6	0	0	0	0	57.6	0	38.4	0	28.8	0	9.6	0	19.2	0	412.8	336
B8a	0	0	76.8	0	9.6	9.6	0	9.6	0	0	0	0	0	0	0	0	0	57.6	0	0	0	9.6	9.6	0	0	182.4	412.8	0	211.2
B8b	0	9.6	38.4	28.8	9.6	19.2	19.2	9.6	9.6	9.6	28.8	0	0	0	86.4	38.4	67.2	28.8	9.6	9.6	0	76.8	9.6	57.6	0	163.2	336	211.2	0

Figure 6.2: Expected number of physical contacts per day in a flock of ewes with newborn lambs. Here letter-number combinations (e.g. G1, B3) refer to individual ewes with suffix letters (e.g. a,b) referring to their respective lambs. This data was collected through field observations and is reproduced from the supplementary materials of Schley *et al.* [110], where similar tables can be found for flocks comprising ewes with nearly-weaned lambs and flocks comprising ewes only.

tact rates replaced by the group-level means c_e, c_l and c_m, as given by Eq. (6.2),

4. A completely homogeneous one-class fully connected network, with all contact rates equal to the flock mean c, leading to random mixing.

For each of the three different flocks under consideration, comparison of these network models allows us to determine the effect of the group and population level heterogeneity implicit in the field data.

In the first model, the weighted adjacency matrix contains rich individual level data from which we define the full stochastic weighted network simulation model (network model 1), and this matrix is shown for the flock with lambs and ewes in Fig. 6.2. Further details can be found in the supplementary materials section of Schley *et al.* [110]. In addition to an explicitly defined contact network, the two main features of this full stochastic model are the heterogeneity in link weight and

the modular, or group-like, structure of the populations. The detailed, individual level data given by C can be aggregated at either group or population level and then used to parameterise a range of stochastic network models. These models allow us to investigate the impact of the weighted and modular structure of the full population on the spread of disease.

Secondly, a homogeneous-weight network model (network model 2) that preserves the full network structure but remove link-weight heterogeneity can be parameterised by finding the ratio of link weight to link frequency:

$$c_G = \frac{1}{|L|} \sum_{i=1}^{N} \sum_{j=1}^{N} c_{ij}, \qquad L = \{c_{ij} : c_{ij} \neq 0\} \tag{6.1}$$

Thirdly, The impact of the group-like structure of the population can be investigated by removing the network structure entirely by assuming a fully connected network (network model 3). This model can be parameterised by calculating the mean daily contact rate between any two ewes c_e, between any two lambs c_l and between any ewe and lamb c_m.

Finally, the mean rate of contact between any two individuals c can also be calculated, which can be used to parameterise a fourth model that assumes random mixing between all animals (network model 4). These group and population level means can be calculated following Norton *et al.* [94] as follows:

$$\begin{aligned} c_e &= \frac{1}{N_e(N_e-1)} \sum_{i \in C_e} \sum_{j \in C_e} c_{ij}, \qquad c_l = \frac{1}{N_l(N_l-1)} \sum_{i \in C_l} \sum_{j \in C_l} c_{ij}, \\ c_m &= \frac{1}{N_l N_e} \sum_{i \in C_l} \sum_{j \in C_e} c_{ij}, \qquad c = \frac{1}{N(N-1)} \sum_{i=1}^{N} \sum_{j=1}^{N} c_{ij}, \end{aligned} \tag{6.2}$$

where C_e and C_l are the set of indices in each matrix for ewes and lambs respectively. The actual values used in the stochastic network models are calculated from C by Schley *et al.* [110] and are summarised in Table 6.1.

6.3.4 Compartmental ODE models

In a compartmental SIR formulation, the force of infection is the product of the rate of contact k an individual has with the rest of the group, the probability that any given contact is between a susceptible individual and an infectious individual - here assumed to be frequency dependent and equal to I/N - and the probability p that such a contact successfully results in transmission [14]. In addition to being used to parameterise stochastic network models, the field-data can also be used to parameterise these compartmental ODE models. For compartmental models, however, a different method is needed to calculate the appropriate rates from the raw data given by adjacency matrix C. In this case it is the total contact an individual has with *all members of each group* that determines the contact rate. For a flock of ewes and lambs the rate of contact a ewe has with other ewes k_{ee}, a ewe has with lambs k_{el}, a lamb has with ewes k_{le} and a lamb has with other lambs k_{ll}, together with the equivalent single-group parameter representing the amount of contact any individual has with the rest of the flock, k, are calculated as follows:

$$\begin{aligned} k_{ee} &= \frac{1}{N_e}\sum_{i\in C_e}\sum_{j\in C_e} c_{ij}, \qquad k_{el} = \frac{1}{N_e}\sum_{i\in C_e}\sum_{j\in C_l} c_{ij}, \\ k_{le} &= \frac{1}{N_l}\sum_{i\in C_l}\sum_{j\in C_e} c_{ij}, \qquad k_{ll} = \frac{1}{N_l}\sum_{i\in C_l}\sum_{j\in C_l} c_{ij}, \end{aligned} \tag{6.3}$$

where C_e and C_l are the set of indices in each matrix for ewes and lambs respectively. The actual values used in the ODE models are calculated from C by Schley *et al.* [110] and are summarised in Table 6.2.

The observed flocks lend themselves to being modelled using a two-class system of ODEs. In addition, the clear differences in the contact rates within and between lamb and ewe groups [94] suggest that the assumption of homogeneous contact required by a single class model are not appropriate for breeding flocks. Building on work by Kiss *et al.* [72], where a two-group preferential mixing model

was formulated from a contact network point of view, a two-class SIR model representing ewes and lambs is constructed. The system utilizes the group-level contact rates described above and is given by:

$$\dot{S}_e = -p\left(k_{ee}\frac{I_e}{N_e} + k_{el}\frac{I_l}{N_l}\right)S_e, \tag{6.4}$$

$$\dot{S}_l = -p\left(k_{le}\frac{I_e}{N_e} + k_{ll}\frac{I_l}{N_l}\right)S_l, \tag{6.5}$$

$$\dot{I}_e = p\left(k_{ee}\frac{I_e}{N_e} + k_{el}\frac{I_l}{N_l}\right)S_e - \gamma I_e, \tag{6.6}$$

$$\dot{I}_l = p\left(k_{le}\frac{I_e}{N_e} + k_{ll}\frac{I_l}{N_l}\right)S_l - \gamma I_l, \tag{6.7}$$

$$\dot{R}_e = \gamma I_e, \tag{6.8}$$

$$\dot{R}_l = \gamma I_l, \tag{6.9}$$

where the subscripts e and l refer to the ewe and lamb populations. A single-class ODE can be obtained by ignoring the class distinctions and is also valid in the case of the ewe-only flock.

$$\dot{S} = -pk\frac{I}{N}S, \tag{6.10}$$

$$\dot{I} = pk\frac{I}{N}S - \gamma I, \tag{6.11}$$

$$\dot{R} = \gamma I. \tag{6.12}$$

Although it is assumed that parameters derived from the contact data are applicable to all flock sizes of more than three or four animals [94], the underlying assumptions of these deterministic models are only truly valid in the limit of large N. Since here disease dynamics are firstly considered amongst a conventional sized flock of only about 30 animals, it is important to compare the deterministic ODE results to results from stochastic network simulations and consider any significant difference carefully.

Flock	Contacts	Parameter	Estimated daily rate
Ewes with newborn lambs	ewe with ewes	k_{ee}	8.7 ± 9.1
	ewe with lambs	k_{el}	895.4 ± 475.0
	lamb with ewes	k_{le}	547.2 ± 193.6
	lamb with lambs	k_{ll}	749.9 ± 213.4
	any with all	k	1148.0 ± 386.6
Ewes with nearly weaned lambs	ewe with ewes	k_{ee}	13.4 ± 21.8
	ewe with lambs	k_{el}	254.4 ± 99.9
	lamb with ewes	k_{le}	169.6 ± 67.6
	lamb with lambs	k_{ll}	213.8 ± 121.3
	any with all	k	337.1 ± 121.0
Ewes only	ewe with ewes	k	83.8 ± 52.5

Table 6.2: Daily rate of physical contacts for individual members of different groups with any other members of a group (mean ± standard deviation). Distributions are skewed with high variability. These rates are calculated from the raw observational data available in the supplementary materials section of Schley *et al.* [110] and is explored further in Norton *et al.* [94].

Flock	R_0
Ewes with newborn lambs	$1171p/\gamma$
Ewe with nearly weaned lambs	$344p/\gamma$
Ewes only	$84p/\gamma$

Table 6.3: Estimated R_0 of whole flock based on the average number of physical contacts per day. Here γ is the recovery rate and p is the probability of a given SI contact resulting in transmission.

6.4 Results

We can analytically derive the basic reproductive number, R_0, by using a next generation approach [21], whereby we separate different states into either disease or disease free and consider transitions into and out of the disease states when the system is at disease free equilibrium, for the two-class ODE we find that

$$F = p \begin{bmatrix} k_{ee} & k_{el}\frac{N_e}{N_l} \\ k_{le}\frac{N_l}{N_e} & k_{ll} \end{bmatrix} \text{ and } V = \begin{bmatrix} \gamma & 0 \\ 0 & \gamma \end{bmatrix},$$

where F describes all the rates of transition from disease-free to disease states and V describes all the rates of transitions out of disease states. For example, the top left entry of the F matrix is related to how the rate at which individuals leave

S_e and enter I_e changes with respect to I_e, given that we are starting from the disease free equilibrium (DFE). From Eq. (6.4) it is clear that individuals enter state I_e from S_e at rate $p(k_{ee}I_e/N_e + k_{el}I_l/N_l)S_e$. We differentiate with respect to I_e and evaluate at the DFE where $S_e = N_e$, $S_l = N_l$ and all other states are empty. This leads to the entry in F of pk_{ee}. All other entries in F and V are found in a similar way. From here R_0 is given by the leading eigenvalue of FV^{-1}:

$$R_0 = \frac{p}{\gamma}\frac{k_{ee} + k_{ll} + \sqrt{(k_{ee} - k_{ll})^2 + 4k_{el}k_{le}}}{2}$$

whereas for the single-class ODE we simply find $R_0 = (p/\gamma)k$. The estimated values of R_0, as function of the recovery rate γ and the probability of a contact (between and infected individual and a susceptible one) resulting in transmission p for each of the trials are given explicitly in Table 6.3, but of greatest interest is the relative magnitude of the basic reproduction number within the flock at different times of the year, as the lambs are born, weaned and leave the flock. This is independent of p and γ, and shows that the presence of lambs significantly increases the susceptibility to an outbreak and that this is worst when lambs are young:

$$\frac{R_0^{\text{with newborns}}}{R_0^{\text{ewes only}}} = 16.1, \qquad \frac{R_0^{\text{with weaned}}}{R_0^{\text{ewes only}}} = 4.6. \tag{6.13}$$

Note that using the conventional (single class) form for these ratios would be smaller in magnitude (13.7 and 4.0 respectively).

The final epidemic size R^∞ is the proportion of the flock that become infected (i.e. does not remain in the susceptible population). For the mixed-model this can be calculated following the methods used by Kiss *et al.* [72]. Firstly, Eqs. (6.4-6.7) are rewritten for ease of notation to give

$$\dot{S_m} = -S_m \sum_{n\in\{e,l\}} pk_{mn}\frac{I_n}{N_n}, \qquad m \in \{e, l\}, \tag{6.14}$$

$$\dot{I_m} = S_m \sum_{n\in\{e,l\}} pk_{mn}\frac{I_n}{N_n} - \gamma I_m, \qquad m \in \{e,l\}. \tag{6.15}$$

We let $\lambda_m = \sum_{n\in\{e,l\}} pk_{mn}I_n/N_n$ and solve the ODE in Eq. (6.14) with initial conditions $S_m(0) = N_m$ and $I_m(0) = 0$ to find

$$S_m(t) = N_m \exp(-\Phi_m(t)), \qquad m \in \{e,l\}, \tag{6.16}$$

where

$$\Phi_m(t) = \int_0^t \lambda_m(s)\ \mathrm{ds}. \tag{6.17}$$

Next, we can sum Eqs. (6.14-6.15), integrate from 0 to ∞ and use initial conditions $S_m(0) = N_m$, $I_m(\infty) = 0$ and $I_m(0) = 0$ to obtain

$$-\gamma \int_0^\infty I_m(s)\mathrm{ds} = S_m(\infty) - N_m, \qquad m \in \{e,l\}. \tag{6.18}$$

By noting that $S_m(\infty) = S_m^\infty = N_m - R_m^\infty$ the following expression for R_m^∞ is obtained:

$$R_m^\infty = \gamma \int_0^\infty I_m(s)\ \mathrm{ds}, \qquad m \in \{e,l\}. \tag{6.19}$$

Also, by taking the limit as $t \to \infty$ of Eq. (6.17), and then using Eq. (6.19) it follows that

$$\begin{aligned}
\Phi_m(\infty) = \Phi_m^\infty &= \int_0^\infty \sum_{n\in\{e,l\}} pk_{mn}\frac{I_n(s)}{N_n}\ \mathrm{ds} \\
&= \sum_{n\in\{e,l\}} \frac{pk_{mn}}{N_n}\int_0^\infty I_n(s)\ \mathrm{ds} \\
&= \sum_{n\in\{e,l\}} \frac{pk_{mn}}{N_n}\frac{1}{\gamma}R_n^\infty.
\end{aligned} \tag{6.20}$$

By again noting that $S_m^\infty = N_m - R_m^\infty$ and using Eq. (6.16) in the limit as $t \to \infty$ we find that

$$R_m^\infty = N_m\left(1 - \exp(-\Phi_m^\infty)\right), \qquad m \in \{e,l\}, \tag{6.21}$$

and as $R^\infty = R_e^\infty + R_l^\infty$, it follows that

$$R^\infty = N_e\left(1 - \exp(-\Phi_e^\infty)\right) + N_l\left(1 - \exp(-\Phi_l^\infty)\right). \tag{6.22}$$

where

$$\Phi_e^\infty = \frac{p}{\gamma}\left(k_e(1 - \exp(-\Phi_e^\infty)) + k_m(1 - \exp(-\Phi_l^\infty))\right), \tag{6.23}$$

$$\Phi_l^\infty = \frac{p}{\gamma}\left(k_m(1 - \exp(-\Phi_e^\infty)) + k_l(1 - \exp(-\Phi_l^\infty))\right). \tag{6.24}$$

For the ewe only flock the standard implicit formula holds:

$$R^\infty = (1 - \exp(-(p/\gamma)kR^\infty))N. \tag{6.25}$$

Although the final number of infected individuals does not depend on the total population size N, it is affected by the proportion of the population that is ascribed to each group. The final epidemic size as a consequence of physical contact, as a function of the probability of successful transmission p, is shown as a proportion of the population $r^\infty = R^\infty/N$ in Fig. 6.3. This is done by fixing γ and solving the parametric system of equations given by Eqs. (6.22-6.24) for a range of values of p. Results indicate that an epidemic is much more likely to take off in a flock with lambs, increasingly so with younger lambs, and that only in an all adult flock is it likely that some individuals will remain uninfected. Note that unless the recovery rate γ is exceptionally high, only a very low probability of successful transmission per contact is required to sustain the disease.

Epidemic length t^0 is the time between the infection of the first case and the recovery of the last, whereas the time of peak infectiousness t^* is defined as the time when the largest number of animals are infectious: these may be extracted from simulations by considering the duration for which $I \geq 0$ (or, more precisely for the continuous model, some strictly positive threshold value) and the time

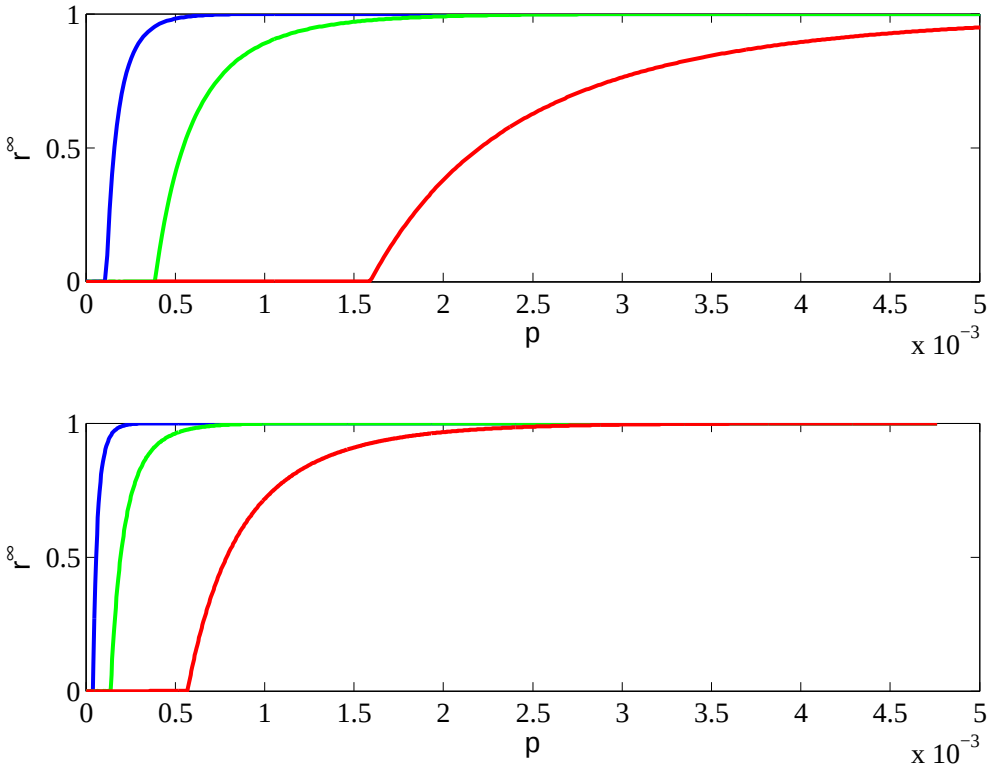

Figure 6.3: Final epidemic size r^{∞}, as a function of the transmission probability p for physical contacts amongst a flock with (top) a fast recovery rate similar to FMD ($\gamma = 2/15$) and (bottom) a slower recovery similar to brucellosis ($\gamma = 1/21$) for: ewes with newborn lambs (blue), ewes with nearly weaned lambs (green) and ewes only (red) flocks in a conventional group with two lambs per ewe on average.

when $\max\{I(t) : t \geq 0\}$ are attained respectively. For the single-class model given by Eqs. (6.10) - (6.12), an analytical solution exists:

$$t^* = \frac{1}{\gamma}\int_0^{1-\frac{1}{R_0}-I(t^*)} \frac{dR}{1-R-S(0)\exp(-R_0 R)} \tag{6.26}$$

$$I(t^*) = 1 - \frac{1}{R_0}\left(1 + \ln(R_0 S(0))\right) \tag{6.27}$$

Differences in the rates of contact within each flock impact on the length of the outbreak, although the interaction between the probability of infection and the rate of recovery is perhaps more significant, as shown in Fig. 6.4. As can be seen, for flocks with lambs infection will only die out without a minor outbreak (or full epidemic) if the probability of successful transmission on contact p is very low,

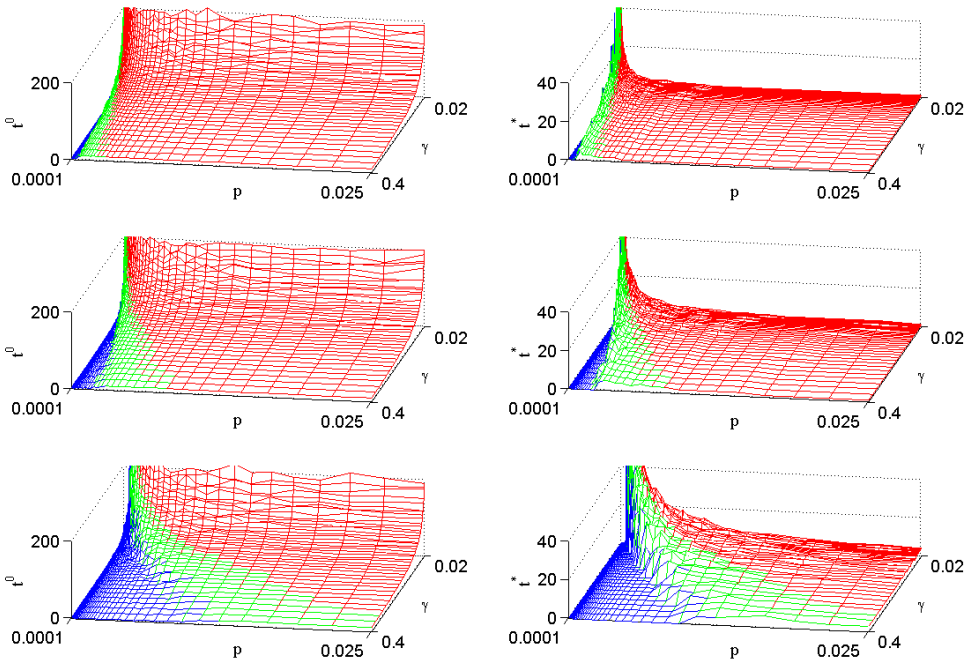

Figure 6.4: Epidemic length t^0 (left column) and time of peak infectiousness t^* (right column) in days, as a function of the recovery rate γ and the transmission probability p for physical contacts amongst a flock of 30 sheep consisting of: 10 ewes with 20 newborn lambs (top), 10 ewes with 20 nearly weaned lambs (middle) and 30 ewes only (bottom), based on initial infection of a single ewe. Results are derived from numerical simulations of the deterministic system, and distinguished according to whether infections die out (blue), result in partial outbreaks (green) or cause epidemics that infect the entire flock (red). When infection dies out, peak infectiousness occurs at the outset of the outbreak ($t^* = 0$) by definition.

while for the ewe only flock the parameter landscape is dominated by self-limiting outbreaks unless the disease recovery rate is very slow.

Results from network simulations also indicate a strong seasonal effect (i.e. differences between flock types as lambs are born, weaned and eventually leave the flock) as shown in Fig. 6.5. The presence of lambs facilitates a much quicker spread of the disease and such flocks have a much higher chance of experiencing an epidemic. This is to be expected, given the presence of lambs that are more highly connected and who have a much greater frequency of repeat contacts [94], which more than compensates for the reduction in connection between ewes that

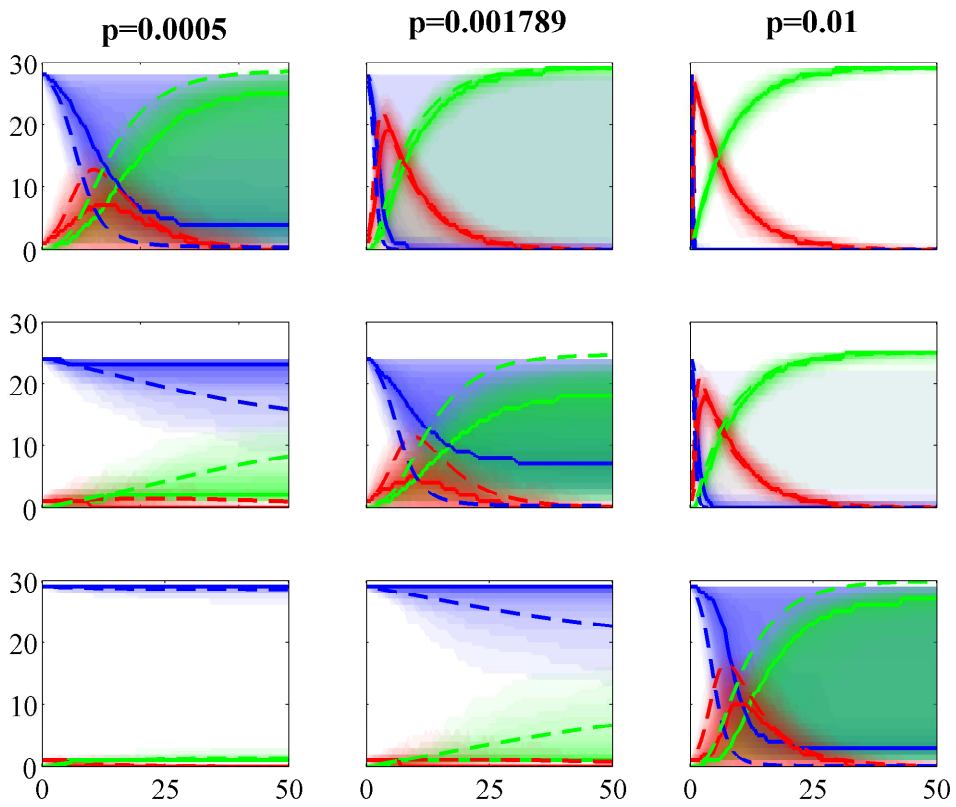

Figure 6.5: The time evolution (in days) of a potential outbreak amongst the three different flocks (top row: ewes with new-born lambs; middle row: ewes with nearly weaned lambs; bottom row: ewes only). Here $\gamma = 2/15$, appropriate for FMD, and results are presented for three different values of p, the probability of transmission occurring during contact: that estimated for FMD (middle column) and values an order of magnitude smaller (left column) and larger (right column) than this. The total number of susceptible (blue), infected (red) and recovered (green) individuals is plotted as a function of time: the solid lines show the median values from stochastic simulations of the full weighted network, with the shaded bands showing confidence intervals in steps of 5%. The dashed line shows results from the two-class ODE system.

is seen in breeding flocks compared to ewe-only groups. The number and strength of links decreases as lambs grow older, and amongst mature animals, a per contact probability of transmission of an order of magnitude bigger is required in order to achieve an outbreak similar to that observed in a flock with newborn lambs, as demonstrated in Fig 6.5. Explicitly, for our estimated parameter values the system results in die-out amongst mature ewes, a partial outbreak amongst ewes

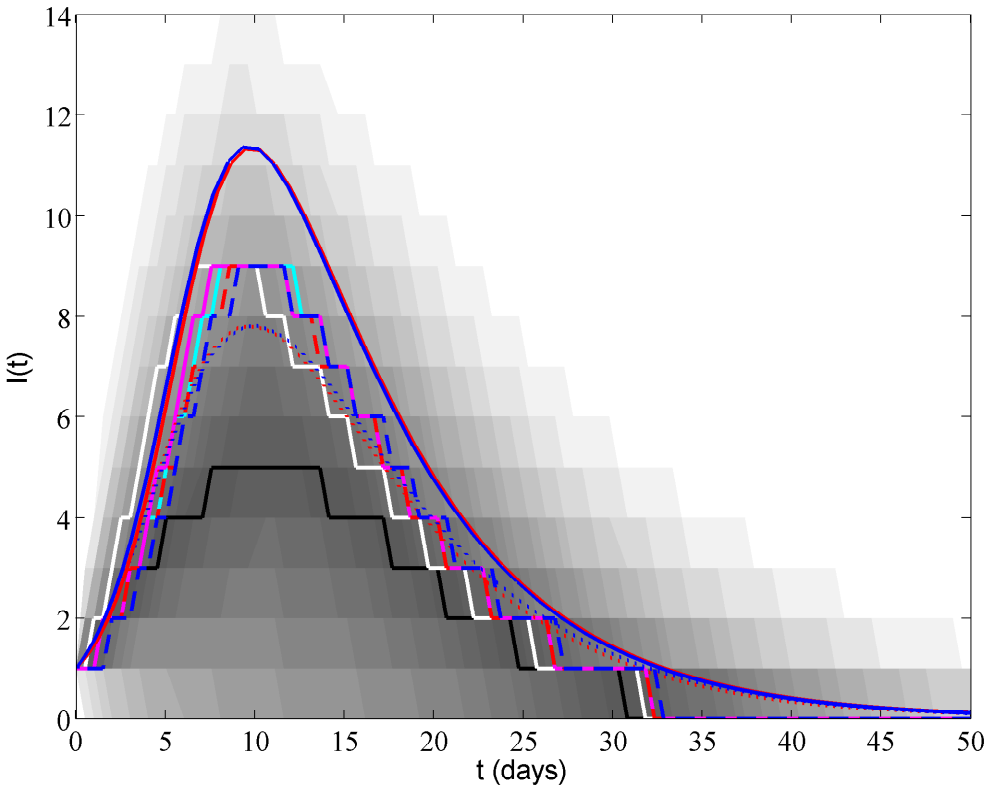

Figure 6.6: Time evolution of the number of infected for ewes with nearly-weaned lambs for $N = 25$, $\gamma = 2/15$ and $p = 1.789x10^{-3}$, the estimated recovery rate and probability of transmission per contact respectively for FMD. For all network models, the median number of infected individuals is shown: the black line shows the results from simulations on the full weighted network, with the shaded bands showing confidence intervals in steps of 5%; the white line represents simulations on the homogeneous-weight network model, the magenta line shows results a semi-homogeneous two-class fully connected network model, the cyan line shows results from a homogeneous fully connected network model. The blue and red lines represent results from the two-class one-class ODE models respectively, with a solid line for the deterministic solution, a dashed line for the median of the stochastic results and a dotted line for the mean of the stochastic results.

with nearly-weaned lambs and an epidemic amongst ewes with new-born lambs on the full weighted network, as shown in Fig 6.4.

6.4.1 Model comparison

Fig. 6.5 shows predicted epidemic from the two-class ODE system: results from the compartmental model vary in their agreement with simulation results for

different flock compositions and different values of p.

In Fig. 6.6, all four network models and the two ODE models are compared on the same figure. All of the network models that remove heterogeneity in some way predict very similar results to each other, and are all much closer to the ODE outputs than to the output from the full weighted network simulation. Thus Fig. 6.5 suggests that the heterogeneity in the contact rates acts to slow down the spread of diseases. The lack of difference between the one-class and two-class ODEs is due to the very high rates of mixing between the groups (see Norton *et al.* [94]), which agrees with previous findings [72].

6.5 Discussion

Results from one-class and two-class epidemic models have been presented, with each class representing ewes or lambs in sheep flocks. These results include the derivation of important epidemiological parameters such as the basic reproduction ratio and the final outbreak size, in terms of the disease recovery rate, contact rates between individuals and the probability of successful transmission when a contact between an susceptible and infected individual occurs. Application of field data indicates that the basic reproduction ratio increases dramatically in the presence of lambs, an effect that decreases with the age of lambs, as might be expected. Furthermore, it has been shown that for realistic contact rates based on field observations, this increase is underestimated if a conventional (single class) formulation of R_0 is used. Flock demographics influence not only how quickly a disease spreads, but also the final epidemic size. It is clear from Fig. 6.3 that the absence of lambs contributes significantly to reducing the overall size of the outbreak.

It appears that differences in contact structure and difference in the weight of contacts can always be compensated for in this network by adjustments in the per-contact probability of infection, to produce similarly behaving outbreaks in

different flocks. This is illustrated by the subplots on the main diagonal of Fig. 6.5 where the time evolution of the epidemics is very similar. This suggests that the fundamental structure of the networks is similar, despite the variability in the weight of each contact.

In general, as networks become more densely connected, the results from stochastic simulations on networks tend to approach the mean-field approximation, given by ODE models [113], which is exactly the situation shown in Figs. 6.5 & 6.6. As expected, for unrealistically high per-link probability of infection, the differences are less significant as in this case almost all individuals become infected rapidly. It is interesting to note that the full network simulation is more markedly different from the mean-field result than the homogeneous, or semi-homogeneous network models. Since the main difference between the various network models lies in the distribution of contacts, it seems reasonable to assume that the observed differences shown in Fig. 6.6 are being driven by this hetergeneity. The difference between the output from homogeneous and heterogeneous network models can be explained intuitively as follows: links with high weight are relatively rare and hence they will play a minor role in the overall dynamics, which is going to be dominated by links with low weights. This leads to slower dynamics and smaller epidemics. However, when the contribution of highly weighted links is spread evenly across all links, the previously numerous low-weight links become more potent in transmitting the infection and this leads to both faster and larger epidemics.

Although individual-based simulations on networks are usually regarded as the most accurate type of model, there are a number of considerations that need to be taken into account when assessing their appropriateness. Firstly, networks are very good at describing situations in which contact patterns between individuals are well defined. For this to be the case, what constitutes a contact, in addition to who contacts whom, needs to be well defined. It is clear from the

observational data [94] that what constitutes a contact that could potentially lead to the transmission of the disease is unclear. For example, the rates given in the full contact matrix are the estimates for the expected number of short lived contacts between two sheep, regardless of the type of contact (for example, was the contact a nuzzle or a mount - see Norton *et al.* [94] for a full breakdown of the different types of between-sheep contacts that were observed and recorded). This differs from a sexual contact network, in which the contact between two individuals that could result in disease transmission is more clearly defined.

Modelling using networks assumes frequency dependent contact, which is independent of population size [14]. Whether a frequency or density dependent approach should be used depends heavily on the flock setup and how the flock is managed. For example, if the flock is roaming on open hillside then a frequency dependent approach seems suitable. However, if the flock was rounded up and kept in a tight pen, then a density dependent approach would seem more suitable, as the number of contacts an individual could expect to have would depend upon how many sheep were in the pen.

In conclusion, seasonal variability in the structure and resultant connectivity of conventionally managed sheep flocks, as lambs are born, weaned and eventually leave the flock, can have a significant impact on the potential spread of directly-transmitted ovine diseases. While full network simulations best capture the observed heterogeneity of contacts amongst animals, simple compartmental models describe the key features of an outbreak. Although these models over-predict the speed and scale of an outbreak, they do fall within the 95% confidence intervals predicted by full stochastic network simulations, and as such could prove to be a useful tool for modelling real-world flocks. Since sheep are probably the least intensively farmed livestock in the UK and much of Europe, it is likely that results will be even more favourable for other more intensively farmed (and hence more homogeneously mixed) species of livestock.

Chapter 7

Discussion

This thesis is concerned primarily with modelling the spread of epidemics on networks. In this final chapter, we highlight some of the results of this thesis and examine their limitations in more detail. We also propose future lines of enquiry where appropriate.

In Chapter 2, we proved that the previously well known equations governing the population level expectations of individuals and pairs are exact. Until now these equations were derived using only heuristic reasoning, whereas in this thesis these are rigorously derived from the full Kolmogorov equations for SIS type epidemics on an arbitrary network.

In Chapter 3, we start with these exact but unclosed equations and proceed to apply three different closure approximations. Firstly, we assume homogeneous random mixing between all individuals, and hence approximate the number of pairs in terms of the number of individuals in the system. This strong assumption leads to the well known mean-field approximation, which overestimates the size of epidemics when compared to results from stochastic simulation. We proceed to prove that this crude mean-field approximation becomes exact in the limit of a large, fully connected network.

We also examine the performance of two distinct pairwise closures, the original pairwise closure (OPA) [61] and an improved pairwise closure (IPA) [52].

Both deal with triple motifs - both open and closed triples - and we show that, unsurprisingly, they perform best on networks that have been re-wired to remove large-scale network structures and replace them with the local clustering captured by the closures. An interesting avenue for future work would be to develop bespoke closure approximations for use with different network topologies, although the development of a pairwise closure that captures large-scale network properties is unrealistic, due to the local assumptions required to construct the approximations and the limited amount of network information that can be included at the level of pairs.

In Chapter 4 we introduce the effective degree (ED) modelling framework, proposed by Linquist *et al.* [83]. They show that the static ED model is ideally suited for modelling epidemics on simple random networks, with results from ODEs agreeing closely to those from stochastic simulation. However, the static ED model is unable to account for clustering or degree correlations. This inability to account for local clustering follows from the assumption of star-like structures as its core motifs. Hence, a pairwise model is better suited to modelling epidemics on networks that have a high degree of clustering or are assortatively mixed.

Comparing the ED model to an unclustered pairwise model reveals two different approaches to the problem of moment closure. For the standard pairwise closure with no clustering, Keeling [61] defines that $Q_i(B|A)$ is the number of neighbours of disease state B surrounding node i, given that node i is in state A. It is comprised of two parts: the expected value $\bar{Q}$ and an associated error σ which is not necessarily small:

$$Q_i(B|A) = \bar{Q}(B|A) + \sigma_i(B|A) = \frac{[AB]}{[A]} + \sigma_i(B|A).$$

By assuming a distribution for the Q_i, and hence the σ_i, expressions can be produced for triples in terms of pairs and singles. Keeling assumes a multinomial

error distribution

$$\begin{aligned}
[ABC] &= \sum_{j,B_j=1} Q_j(A|B)Q_j(C|B) \\
&= \sum_{j,B_j=1} \left(\frac{[AB]}{[B]} + \sigma_j(A|B)\right)\left(\frac{[BC]}{[B]} + \sigma_j(C|B)\right) \\
&= \frac{[AB][BC]}{[B]} + \sum_{j,B_j=1} \sigma_j(A|B)\sigma_j(C|B) \\
&= \left(\frac{n-1}{n}\right)\frac{[AB][BC]}{[B]}.
\end{aligned}$$

Here $\sum_{j,B_j=1} \sigma_j(A|B)\sigma_j(C|B)$ is the covariance of two multinomial distributions. In general, $\mathrm{Cov}(X_i, X_j) = -np_ip_j$. Here $p_i = P_{AB} = \frac{AB}{nB}$ and $p_j = P_{CB} = \frac{CB}{nB}$. Hence

$$\sum_{j,B_j=1} \sigma_j(A|B)\sigma_j(C|B) = -\frac{1}{n}\frac{[AB][BC]}{[B]}$$

as required.

Using the same idea, but with the effective degree model:

$$\begin{aligned}
[ABC] &= \sum_{j,B_j=1} Q_j(A|B)Q_j(C|B) \\
&= \sum_{k}\sum_{j+l=k} jlS_{jl}.
\end{aligned}$$

At first glance, it may appear that no assumptions are needed on the state of a given node's neighbours. However this is not the case, for in the ED model the closure lies in placing assumptions on the rate at which a given node's neighbours change their disease state, which depends upon the rate at which they come into contact with other infectious individuals. The ED model assumes that the rate at which an individual's neighbours come into contact with others follows the homogeneous random mixing assumption, as given by the term

$$\beta\frac{\sum_{k=1}^{M}\sum_{j+l=k} jlS_{jl}}{\sum_{k=1}^{M}\sum_{j+l=k} jS_{jl}}(s+1)S_{s+1,i-1}$$

in Eq. (4.2), for example. So, in the case of the static ED model, the dynamics are primarily driven by two key assumptions: (1) the network is comprised of star-like motifs and (2) the rate at which individuals mix between these core motifs is via homogeneous random mixing.

Lindquist *et al.* [83] point out that the ED modelling framework for static networks is suited to adaptation for modelling epidemics on dynamic networks. This is due to the explicit notation denoting the expected number and type of a node's neighbours, along with the strong random mixing assumption. Hence it would be expected to perform well on dynamic networks with random link activation/deletion. In this thesis, we test this claim and the main result of Chapter 4 was the adaptation of the static ED model to deal with dynamic networks that have locally constrained random link activation and deletion. We showed that this new model, given by Eqs. (4.4-4.5), closely agrees with simulations results for both the evolution of the disease and network. Furthermore, we derived a next-generation calculation of R_0 and showed that in the context of a dynamically changing network, it is possible for epidemics to take off with $R_0 < 1$ and die out with $R_0 > 1$.

The dynamic ED model could be extended to allow for type dependent dynamics, as well as relaxing the local constraint. Below, a few different models are proposed that begin to address this. The most general form of the dynamic ED model, adapted for type dependent link activation and deletion, is described by the following set of $(M+1)(M+2)$ equations

$$\begin{aligned}
\dot{S_{s,i}} &= -\beta i S_{s,i} + \gamma I_{s,i} + \gamma[(i+1)S_{s-1,i+1} - iS_{s,i}] \\
&\quad + \beta \frac{\sum_{k=1}^{M}\sum_{j+l=k} jlS_{jl}}{\sum_{k=1}^{M}\sum_{j+l=k} jS_{jl}}[(s+1)S_{s+1,i+1} - sS_{s,i}] \\
&\quad - \omega_{SS} s S_{s,i} - \omega_{SI} i S_{s,i} + \omega_{SI}(i+1)S_{s,i+1} + \omega_{SS}(s+1)S_{s+1,i} \\
&\quad - (M-(s+i))(P_S\alpha_{SS} + P_I\alpha_{SI})S_{s,i} + \alpha_{SS}(M-(s-1+i))P_S S_{s-1,i} \\
&\quad + \alpha_{SI}(M-(s+i-1))P_I S_{s,i-1},
\end{aligned} \tag{7.1}$$

$$
\begin{aligned}
\dot{I_{s,i}} &= \beta i S_{s,i} - \gamma I_{s,i} + \gamma[(i+1)I_{s-1,i+1} - iI_{s,i}] \\
&+\beta \frac{\sum_{k=1}^{M}\sum_{j+l=k} l^2 S_{jl}}{\sum_{k=1}^{M}\sum_{j+l=k} jI_{jl}}[(s+1)I_{s+1,i+1} - sI_{s,i}] \\
&-\omega_{SI} s I_{s,i} - \omega_{II} i I_{s,i} + \omega_{SI}(s+1)I_{s+1,i} + \omega_{II}(i+1)I_{s,i+1} \\
&-(M-(s+i))(\alpha_{s,i}P_S + \alpha_{II}P_I)I_{s,i} + \alpha_{SI}(M-(s-1+i))P_S I_{s-1,i} \\
&+\alpha_{II}(M-(s+i-1))P_I I_{s,i-1},
\end{aligned} \tag{7.2}
$$

for $\{(s,i) : s,i \geq 0, 0 \leq k = s+i \leq M\}$ and where $P_X = \frac{\sum_{k=0}^{M}\sum_{j+l=k}(M-(j+l))X_{jl}}{\sum_{k=0}^{M}\sum_{j+l=k}(M-(j+l))(S_{jl}+I_{jl})}, X \in \{S, I\}$ and is the probability of picking a stub belonging to a node of type X.

Clearly by setting $\alpha_{SI} = \alpha_{II} = \alpha_{SS} = \alpha$, a model that describes type dependent link deletion, but random link activation can be recovered. This model could have intuitive modelling merit, as it could be argued that an individual would not be aware of the state of another individual until after a link between them has been established. Type dependency is preserved in the model through the variable link deletion rates, whereby a high ω_{SI} would ensure that an SI link was active for less time than links of other types. Furthermore, by setting $\omega_{SI} = \omega_{II} = \omega_{SS} = \omega$, the original random link model, described by Eqs. (4.4-4.5), is recovered.

By setting $M = N - 1$, the model becomes unconstrained. However, due to the system size of Eqs. (4.4-4.5) being defined by M, setting $M = N - 1$ would result in systems too large to solve for $N \gtrsim 25$. This can be overcome by calculating the mean degree at equilibrium. For the case with type independent cutting, Eqs. (4.5-4.4), this is given by Eq. (4.6).

So, for example, with values of $\alpha = 0.005$, $\omega = 0.995$, $N = 1000$ and $M = N - 1 = 999$ gives $\langle k \rangle^* = 4.995$. As the degree distribution at equilibrium is Poisson, the probability that a node has a certain degree, D, is given by

$$
P(Degree = D) = \frac{\left(\langle k \rangle^*\right)^D e^{-(\langle k \rangle^*)}}{D!}. \tag{7.3}
$$

For the example given above, $P(Degree = 20) = O(10^{-7})$. This means we can confidently limit our system size by a parameter D, for which there is a very small probability that there will ever be nodes that exceed that degree.

However, if we decide to proceed with an unconstrained model, a far simpler fully-type dependent model can be constructed by recognising that a node of type $X_{s,i}$ has $([S]-s)$ susceptible nodes and $([I]-i)$ infected nodes to which it is currently *not* connected. As the model is unconstrained and hence could potentially describe a fully connected network, we know that each of these inactivate links could be activated at rates α_{XS} and α_{XI} respectively (where $X \in \{S, I\}$), without the need for the probability parameters P_S and P_I, which were previously required. This gives rise to the following model:

$$\begin{aligned}
\dot{S_{s,i}} =& -\beta i S_{s,i} + \gamma I_{s,i} + \gamma[(i+1)S_{s-1,i+1} - iS_{s,i}] \\
&+ \beta \frac{\sum_{k=0}^{M}\sum_{j+l=k} jlS_{jl}}{\sum_{k=0}^{M}\sum_{j+l=k} jS_{jl}}[(s+1)S_{s+1,i-1} - sS_{s,i}] \\
&- \omega_{SS} s S_{s,i} - \omega_{SI} i S_{s,i} + \omega_{SI}(i+1)S_{s,i+1} + \omega_{SS}(s+1)S_{s+1,i} \\
&- \alpha_{SS}([S]-s)S_{s,i} - \alpha_{SI}([I]-s)S_{s,i} \\
&+ \alpha_{SS}([S]-(s-1))S_{s-1,i} + \alpha_{SI}([I]-(i-1))S_{s,i-1}, \\
\dot{I_{s,i}} =& \beta i S_{s,i} - \gamma I_{s,i} + \gamma[(i+1)I_{s-1,i+1} - iI_{s,i}] \\
&+ \beta \frac{\sum_{k=1}^{M}\sum_{j+l=k} l^2 S_{jl}}{\sum_{k=1}^{M}\sum_{j+l=k} jI_{jl}}[(s+1)I_{s+1,i-1} - sI_{s,i}] \\
&- \omega_{SI} s I_{s,i} - \omega_{II} i I_{s,i} + \omega_{II}(i+1)I_{s,i+1} + \omega_{SI}(s+1)I_{s+1,i} \\
&- \alpha_{SI}([S]-s)I_{s,i} - \alpha_{II}([I]-i)I_{s,i} \\
&+ \alpha_{SI}([S]-(s-1))I_{s-1,i} + \alpha_{II}([I]-(i-1))I_{s,i-1}.
\end{aligned}$$

Another adaptation of the dynamic ED model follows from the argument that rates such as α_{SI} have little real world relevance. How are people to know the state of another individual until a link has been created? The creation rates could

be better described by half-rates such as α_S, whereby the rate at which new links are created depends on the state of the individual, not the link. This has the added advantage of reducing the number of parameters by two. This kind of behaviour is described by the following model:

$$\begin{aligned}
\dot{S_{s,i}} &= -\beta i S_{s,i} + \gamma I_{s,i} + \gamma[(i+1)S_{s-1,i+1} - iS_{s,i}] \\
&\quad + \beta \frac{\sum_{k=1}^{M}\sum_{j+l=k} jlS_{jl}}{\sum_{k=1}^{M}\sum_{j+l=k} jS_{jl}}[(s+1)S_{s+1,i+1} - sS_{s,i}] \\
&\quad - \omega_{SS} s S_{s,i} - \omega_{SI} i S_{s,i} + \omega_{SI}(i+1)S_{s,i+1} + \omega_{SS}(s+1)S_{s+1,i} \\
&\quad - \alpha_S(M-(s+i))S_{s,i} + \alpha_S(M-(s-1+i))\tilde{P_S}S_{s-1,i} \\
&\quad + \alpha_S(M-(s+i-1))\tilde{P_I}S_{s,i-1}, \qquad (7.4) \\
\dot{I_{s,i}} &= \beta i S_{s,i} - \gamma I_{s,i} + \gamma[(i+1)I_{s-1,i+1} - iI_{s,i}] \\
&\quad + \beta \frac{\sum_{k=1}^{M}\sum_{j+l=k} l^2 S_{jl}}{\sum_{k=1}^{M}\sum_{j+l=k} jI_{jl}}[(s+1)I_{s+1,i+1} - sI_{s,i}] \\
&\quad - \omega_{SI} s I_{s,i} - \omega_{II} i I_{s,i} + \omega_{SI}(s+1)I_{s+1,i} + \omega_{II}(i+1)I_{s,i+1} \\
&\quad - \alpha_I(M-(s+i))I_{s,i} + \alpha_I(M-(s-1+i))\tilde{P_S}I_{s-1,i} \\
&\quad + \alpha_I(M-(s+i-1))\tilde{P_I}I_{s,i-1}, \qquad (7.5)
\end{aligned}$$

where $\tilde{P_X} = \frac{\sum_{k=0}^{M}\sum_{j+l=k}(M-(j+l))\alpha_X X_{jl}}{\sum_{k=0}^{M}\sum_{j+l=k}(M-(j+l))(\alpha_S S_{jl}+\alpha_I I_{jl})}, X \in \{S, I\}$. Indeed a whole range of different models can be created this way, and are easily captured by systems of ODEs. However, as there are now more complex feedback mechanisms between the disease and network dynamics, care must be taken that these ODEs are consistent with simulation results, which are challenging to produce.

In Chapter 5, we extend the work of Kiss *et al.* [74], who propose a model that allows for individuals to be either responsive or non-responsive to the possibility of an epidemic outbreak, with responsive individuals becoming infected at a lower rate than non-responsive individuals. Individuals can move from one awareness class to another as they respond to information about the disease and then slowly forget over time. Whereas the model proposed by Kiss *et al.* [74] is a simple

compartmental model, our model proposed in Chapter 5 is a full pairwise model that accounts for multiple sources of information generation and transmission. We show that peer-to-peer dissemination of information is more effective than a global dissemination of information for a range of different values of τ. The pairwise nature of the model allows us to look at the correlations of responsive and non-responsive individuals, something not possible in a simple compartmental model. We show that peer-to-peer information transmission leads to a non-trivial disease-free steady state, whereby responsiveness is endemic even though the disease dies out. This leaves the population more resistant to re-infection than would otherwise be the case. Future work may expand on the work by Hatzopoulos *et al.* [48] and model the effects of having information and disease travel on sperate networks. The degree of overlap between these networks can be adjusted, and this type of model could be used to account for the difference between virtual and physical links, for example.

An interesting open question brings together Chapter 4 and Chapter 5. Both models aim to investigate the control of an epidemic via behavioral response. For the information model, control is through the modification of disease transmission parameters, with the contact network unchanged, but for the dynamic ED model, control is through the removal of links. It would be interesting to consider how these two approaches are similar, especially if the dynamic ED model was changed to reflect preferential link deletion. Both aim to prevent an epidemic, but both consider two very different approaches. Which is more effective could depend upon the virulence of a disease, or of the particular structure of a host population. The ability to be able to compare these two approaches in a meaningful way would allow public health officials to make informed decisions about whether an awareness raising campaign would be sufficient to reduce the likelihood of an outbreak, or whether more direct measures, such as the closure of public services, curfews or quarantines, are required.

In summary, this thesis contributes a number of significant results to the field of epidemiology. Mathematical modelling of epidemics plays a key role in understanding the risks of disease outbreaks and the effectiveness of different intervention strategies. The field of epidemiology is best described as multi-disciplinary. Closer collaboration between the medical, social and mathematical communities will allow us to better infer disease parameters, to develop a deeper understanding of how real-world networks can be described, as well as being able to include these in realistic models that will allow informed health choices to be made by both individuals and public health bodies.

Bibliography

[1] R. Albert and A.-L. Barabási. Statistical mechanics of complex networks. *Rev. Mod. Phys*, 74:47–97, 2002.

[2] S. Alexandersen et al. Quantities of infectious virus and viral RNA recovered from sheep and cattle experimentally infected with foot-and-mouth disease virus O UK 2001. *J. Gen. Viro.*, 83:1915–1923, 2002.

[3] R. M. Anderson et al. Epidemiology, transmission dynamics and control of SARS: the 2002-2003 epidemic. *Phil. Trans. R. Soc. B*, 359(1447):1091–1105, 2004.

[4] R. M. Anderson and R. M. May. *Infectious diseases of humans: dynamics and control*. Oxford University Press, Oxford, 1991.

[5] H. Andersson. Epidemic models and social networks. *Math. Sci.*, 24:128–147, 1999.

[6] J. Backer et al. Modelling the effectiveness and risks of vaccination strategies to control classical swine fever epidemics. *J. R. Soc. Interface*, 6(39):846–861, 2008.

[7] N. Bailey. *The mathematical theory of infectious diseases and its applications*. Charles Griffin and Company, London, 1975.

[8] F. Ball, D. Sirl, and P. Trapman. Analysis of a stochastic SIR epidemic

on a random network incorporating household structure. *Math. Biosci.*, 224(2):53–73, 2010.

[9] S. Bansal, B. T. Grenfell, and L. A. Meyers. When individual behaviour matters: homogeneous and network models in epidemiology. *J. R. Soc. Interface*, 4:879–891, 2007.

[10] C. Bauch. The spread of infectious diseases in spatially structured populations: An invasory pair approximation. *Math. Biosci.*, 198(2):217–237, 2005.

[11] C.T. Bauch. Imitation dynamics predicting vaccinating behaviour. *Proc. R. Soc. B.*, 272:1669–1675, 2005.

[12] C.T. Bauch and D.J.D Earn. Vaccination and the theory of games.. *PNAS*, 101(36):13391–13394, 2004.

[13] M.H Becker and J.G. Joseph. AIDS and behavioral change to reduce risk: a review. *American Journal of Public Health*, 78(4):395–410, 1988.

[14] M. Begon et al. A clarification of transmission terms in host-microparasite models: numbers, densities and areas. *Epidemiology and Infection*, 129:147–153, 2002.

[15] J.T. Bertrand et al. Systematic review of the effectiveness of mass communication programs to change HIV/AIDS-related behaviors in developing countries. *Health Educ.Res.*, 21(4):567–597, 2006.

[16] F. Brauer and P. van den Driessche. *Mathematical Epidemiology*. Springer, Berlin, 2008.

[17] T. Britton and P. D. O'Neill. Bayesian inference for stochastic epidemics in populations with random social structure. *Scan. J. Stat.*, 29(3):375–390, 2002.

[18] D. J. Daley and J. Gani. *Epidemic modelling: An Intoduction*. Cambridge University Press, Cambridge, 1999.

[19] C E. Dangerfield, J. V. Ross, and M. J. Keeling. Integrating stochasticity and network structure into an epidemic model. *J. R. Soc. Interface*, 6(38):761–774, 2009.

[20] L. Danon et al. Networks and the epidemiology of infectious disease. *Interdiscip. Perspect. Infect. Dis.*, 2011:284909, 2011.

[21] O. Diekmann and J. A. P. Heesterbeek. *Mathematical Epidemiology of Infectious Diseases*. Wiley, New York, 2000.

[22] A. d'Onofrio, P. Manfredi, and E. Salinelli. Vaccinating behaviour, information, and the dynamics of SIR vaccine preventable diseases. *Theor.Pop.Biol.*, 71:301–317, 2007.

[23] R. Durrett. *Random graph dynamics*. Cambridge University Press, 2007.

[24] K. T. D. Eames. Contact tracing strategies in heterogeneous populations. *J. R. Soc. Interface*, 3:55–62, 2006.

[25] K. T. D. Eames. Modelling disease spread through random and regular contacts in clustered populations. *Theor. Pop. Biol.*, 73:104–111, 2007.

[26] K. T D Eames and M. J Keeling. Modeling dynamic and network heterogeneities in the spread of sexually transmitted diseases. *PNAS*, 99(20):13330–13335, 2002.

[27] K. T D Eames and M. J Keeling. Contact tracing and disease control. *Proc Roy Soc B*, 270(1533):2565–71, Dec 2003.

[28] T. England et al. A simulation model of brucellosis spread in British cattle under several testing regimes. *Prev. Vet. Med.*, 63:63–73, 2004.

[29] J.M. Epstein, J. Parker, D. Cummings, and R.A. Hammond. Coupled contagion dynamics of fear and disease: mathematical and computational explorations. *PLoS ONE*, 3(12):e3955, 2008.

[30] N. M. Ferguson. Capturing human behaviour. *Nature*, 446:733, 2007.

[31] N. M. Ferguson, C. A. Donnelly, and R. M. Anderson. Transmission intensity and impact of control policies on the foot and mouth epidemic in Great Britain. *Nature*, 413:542–548, 2001.

[32] N. M. Ferguson et al. Strategies for mitigating an influenza pandemic. *Nature*, 442:448–452, 2006.

[33] A. Fisher and L. Mathews. The social behaviour of sheep. In L. J. Keeling and H. W. Gonyou, editors, *Social behaviour in farm animals*, pages 211–245. CABI, 2001.

[34] S. Funk, E. Gilad, and V.A.A. Jansen. Endemic disease, awareness and local behavioural response. *J.Theor.Biol.*, 264(2):501–509, 2010.

[35] S. Funk, E. Gilad, C. Watkins, and V.A.A. Jansen. The spread of awareness and its impact on epidemic outbreaks. *PNAS*, 106(16):6872, 2009.

[36] S. Funk., M. Salathe, and V.A.A. Jansen. Modelling the influence of human behaviour on the spread of infectious diseases: a review. *J. R. Soc. Interface*, 7(50):1247–1256, 2010.

[37] G. F. Gensini, M. H. Yacoub, and A. A. Conti. The concept of quarantine in history: from plague to SARS. *J. Infect.*, 49:257–261, 2004.

[38] D. T. Gillespie. Exact stochastic simulation of coupled chemical reactions. *J. Phys. Chem.*, 81:2340 – 2361, 1977.

[39] J. P. Gleeson. High-accuracy approximation of binary-state dynamics on networks. *Phys. Rev. Lett.*, 107, 2011.

[40] J. Goldenberg, B. Libai, and E. Muller. Talk of the network: A complex-systems look at the underlying process of word-of-mouth. *Market Lett.*, 12(3):211, 2001.

[41] D. M. Green and I. Z. Kiss. Large scale properties of clustered networks: implications for disease dynamics. *J. Biol. Dyn.*, 4:431–445, 2010.

[42] G. Gregson et al. HIV decline associated with behaviour change in Eastern Zimbabwe. *Science*, 311(5761):664–666, 2006.

[43] P. Grindrod and D. J. Higham. Evolving graphs: dynamical models, inverse problems and propagation. *Proc. R. Soc. A*, 466:753, 2010.

[44] T. Gross and B. Blasius. Adaptive coevolutionary networks: a review. *J. R. Soc. Interface*, 5(20):259–271, 2008.

[45] T. Gross, C. J. Dommar D'Lima, and B. Blasius. Epidemic dynamics on an adaptive network. *Phys. Rev. Lett.*, 96:208701, 2006.

[46] S. Gubbins et al. Assessing the risk of bluetongue to UK livestock: uncertainty and sensitivity analyses of a temperature-dependent model for the basic reproduction number. *J. R. Soc. Interface*, 5:363, 2008.

[47] L. Gustafsson and M. Sternad. Consistent micro, macro and state-based population modelling. *Math. Biosci.*, 225:94–107, 2010.

[48] V. Hatzopoulos, M. Taylor, P. L. Simon, and I. Z. Kiss. Multiple sources and routes of information transmission: Implications for epidemic dynamics. *Math. Biosci.*, 231:197–209, 2011.

[49] G. Hendricks et al. A wind density model to quantify the airborne spread of culicoides species during north-western Europe bluetongue epidemic. *Prev. Vet. Med.*, 87:162–181, 2008.

[50] T. D. Hollingsworth, N. M. Ferguson, and R. M. Anderson. Will travel restrictions control the international spread of pandemic influenza? *Nat. Med.*, 12:497–499, 2006.

[51] T. House, G. Davies, L. Danon, and M. J. Keeling. A motif-based approach to network epidemics. *Bull. Math. Biol.*, 71:1693–1706, 2009.

[52] T. House and M. J. Keeling. The impact of contact tracing in clustered populations. *PLoS Comput. Biol.*, 6(3): e1000721, 2010.

[53] T. House and M. J. Keeling. Insights from unifying modern approximations to infections on networks. *J. R. Soc. Interface*, 8:67–73, 2011.

[54] W. Hundsdorfer and J. G. Verwer. *Numerical solution of time-dependent advection-diffusion-reaction equations*. Springer, 2003.

[55] M. N. Jacobi and O. Görnerup. A spectral method for aggregating variables in linear dynamical systems with application to cellular automata renormalization. *Advances in Complex Systems*, 12:1–25, 2009.

[56] C. P. Jewell, M. J. Keeling, and G. O. Roberts. Predicting undetected infections during the 2007 foot-and-mouth disease outbreak. *J. R. Soc. Interface*, 6:1145–1151, 2009.

[57] C. P. Jewell, T. Kypraios, P. Neal, and G. O. Roberts. Bayesian analysis for emerging infectious diseases. *Bayesian Analysis*, 4:465–496, 2009.

[58] K. Jones et al. Global trends in emerging infectious diseases. *Nature*, 451:990–993, 2008.

[59] S.C. Kalichman and L.C. Simbayi. HIV testing attitudes, AIDS stigma, and voluntary HIV counselling and testing in a black township in Cape Town, South Africa. *Sex.Transm.Infect.*, 79:442–447, 2003.

[60] R. R. Kao. Evolution of pathogens towards low R0 in heterogeneous populations. *J. Theor. Biol.*, 242:634–642, 2006.

[61] M. J. Keeling. The effects of local spatial structure on epidemiological invasions. *Proc. R. Soc. Lond. B*, 266:859–867, 1999.

[62] M. J. Keeling. Models of foot-and-mouth disease. *Proc. R. Soc. B - Bio. Sci.*, 272:1195–1202, 2005.

[63] M. J. Keeling and K. T. D. Eames. Networks and epidemic models. *J. R. Soc. Interface*, 2:295–307, 2005.

[64] M. J. Keeling et al. Dynamics of the 2001 UK foot and mouth epidemic: Stochastic dispersal in a heterogeneous landscape. *Science*, 294:813–817, 2001.

[65] M. J. Keeling et al. Modelling vaccination strategies against foot-and-mouth disease. *Nature*, 421:136–142, 2003.

[66] M. J. Keeling and B. T. Grenfell. Individual-based perspectives on R0. *J. Theo. Biol.*, 203:51–61, 2000.

[67] M. J. Keeling and P. Rohani. *Modeling Infectious Diseases in Humans and Animals*. Princeton University Press, 2008.

[68] M. J. Keeling and J. V. Ross. On methods for studying stochastic disease dynamics. *J. R. Soc. Interface*, 5:171–181, 2008.

[69] J. G. Kemney and J. L. Snell. *Finite Markov Chains, 2nd edition*. Springer, New York, 1976.

[70] W. O. Kermack and A. G. McKendrick. A contribution to the mathematical theory of epidemics. *Proc. R. Soc. A*, 115:700–721, 1927.

[71] I. Z. Kiss, D. M. Green, and R. R. Kao. Infectious disease control using contact tracing in random and scale-free newtworks. *J. R. Soc. Interface*, 3:55–62, 2006.

[72] I. Z. Kiss, P. L. Simon, and R. R. Kao. A contact-network-based formulation of a preferential mixing model. *Bulletin of Mathematical Biology*, 71:888–905, 2009.

[73] I.Z. Kiss, M. Broom, and P.G. Craze. Can epidemic models describe the diffusion of topics across disciplines? *J. Informetr.*, 4:74–82, 2010.

[74] I.Z. Kiss, J. Cassell, M. Recker, and P.L. Simon. The effect of information transmission on epidemic outbreaks. *Math.Biosci.*, 225(1):1, 2009.

[75] A. Kleczkowski and S. Maharaj. Stay at home, wash your hands: epidemic dynamics with awareness of infection. In *2010 Summer Simulation Multiconference*, pages 141–146, 2010.

[76] A. Kleczkowski, K. Oles, E. Gudowska-Nowak, and C. A. Gilligan. Searching for the most cost-effective strategy for controlling epidemics spreading on regular and small-world networks. *J. R. Soc. Interface*, 9(66):158–169, 2012.

[77] J. Kleinberg. Cascading behaviour in networks: algorithmic and economic issues. In N. Nisan, T. Roughgarden, and É. Tardos, editors, *Algorithmic Game Theory*, chapter 24. Cambridge University Press, 2007.

[78] J. Klotz. Statistical inference in Bernoulli trials with dependence. *Annals of Statistics*, 1:373–379, 1973.

[79] A. S. Klovdahl. Social networks and the spread of infectious diseases: the AIDS example. *Soc. Sci. Med.*, 21(11):1203–1216, 1985.

[80] T. G. Kurtz. Limit theorems for sequences of jump Markov processes approximating ordinary differential processes. *J. Appl. Prob.*, 8:344–356, 1971.

[81] J. Leskovec, L.A. Adamic, and B.A. Huberman. The dynamics of viral marketing. *ACM Trans.Web*, 1(1):5, 2007.

[82] F. Liljeros et al. The web of human sexual contacts. *Nature*, 411:907, 2001.

[83] J. Lindquist, J. Ma, P. van den Driessche, and F. H. Willeboordse. Effective degree network disease models. *J. Math. Biol.*, 62:143–164, 2010.

[84] N. Low et al. Effectiveness of chlamydia screening: systematic review. *Int. J. Epidemiol.*, 38:435–448, 2009.

[85] V. Marcaeu et al. Adaptive networks: coevolution of disease and topology. *Phys. Rev. E*, 82:036116, 2010.

[86] R. M. May and R. M. Anderson. Transmission dynamics of hiv infection. *Nature*, 326(6109):137–142, 1987.

[87] N. Meade and T. Islam. Modelling and forecasting the diffusion of innovation - a 25-year review. *Int.J.Forecasting*, 22:519, 2006.

[88] L. A. Meyers, B. Pourbohloul, M. E. J. Newman, D. M. Skowronski, and R. C. Brunham. Network theory and SARS: predicting outbreak diversity. *J. Theo. Biol.*, 232:71–81, 2005.

[89] J. C. Miller. A note on a paper by Erik Volz: SIR dynamics in random networks. *J. Math. Biol.*, 62:349–358, 2009.

[90] I. Nåsell. The quasi-stationary distribution of the closed endemic SIS model. *Adv. Appl. Probab*, 28:895–932, 1996.

[91] M. E. J. Newman. Spread of epidemic disease on networks. *Phys. Rev. E*, 66, 2002.

[92] M. E. J. Newman. Properties of highly clustered networks. *Phys. Rev. E*, 68:026121, 2003.

[93] M. E. J. Newman. The structure and function of complex networks. *SIAM Rev.*, 45:167–256, 2003.

[94] E. Norton et al. Seasonal variations in physical contact amongst domestic sheep and the implications for disease transmission. *Livestock Science*, 145:34–43, 2012.

[95] R. Nowak et al. Behaviour and the welfare of the sheep. In C. M. Dwyer, editor, *The Welfare of Sheep*, pages 81–135. Springer, 2008.

[96] K. Orsel et al. Quantification of foot and mouth disease virus excretion and transmission within groups of lambs with and without vaccination. *Vaccine*, 25:2673–2679, 2007.

[97] P. Paarlberg, A. Seitzinger, J. Lee, and K. Mathews Jr. Economic impacts of foreign animal disease. *Economic Research Report*, 57, 2008.

[98] A. Perisic and C.T. Bauch. Social contact networks and disease eradicability under voluntary vaccination. *PLoS. Comput. Biol.*, 5(2), 2009.

[99] B. Perry and D. Grace. The impacts of livestock diseases and their control on growth and development processes that are pro-poor. *Phil. Trans. R. Soc. B*, 364:2643, 2009.

[100] J.E. Phelps, R. Lewis, L. Mobilio, D. Perry, and N. Raman. Viral marketing or electronic word-of-mouth advertising: examining consumer responses and motivations to pass along email. *J. Advert. Res.*, 44(4):333, 2005.

[101] P. Picard. Sur les modèles stochastique logistiques en démographie. *Ann. Inst. Henri Poincaré B II*, pages 151 – 172, 2004.

[102] P. Poletti, B. Caprile, M. Ajelli, A. Pugliese, and S. Merler. Spontaneous behavioural changes in response to epidemics. *J.Theor.Biol.*, 260:31–40, 2009.

[103] D. A. Rand. Correlation equations and pair approximations for spatial ecologies. In Jacqueline McGlade, editor, *Advanced Ecological Theory*, pages 100–142. Blackwell Science, Oxford, 1999.

[104] J. M. Read, K.T.D. Eames, and W.J. Edmunds. Dynamic social networks and the implications for the spread of infectious disease. *J. R. Soc. Interface*, 5:1001, 2008.

[105] J. M. Read and M. J. Keeling. Disease evolution on networks: the role of contact structure. *Proc. R. Soc. Lond. B*, 270:699–708, 2003.

[106] T. Rehle et al. National HIV incidence measures-new insights into the South African epidemic. *S.Afr.Med.J.*, 97:194–199, 2007.

[107] S. Riley et al. Transmission dynamics of the etiological agent of SARS in Hong Kong: Impact of public health interventions. *Science*, 300(5627):1961–1966, 2003.

[108] M. Roberts and H. Heesterbeek. Bluff your way in epidemic models. *Trends in Microbiology*, 1(9):343–348, 1993.

[109] K. Sato, H. Matsuda, and A. Sasaki. Pathogen invasion and host extinction in lattice structured populations. *J. Math. Biol.*, 32:251–268, 1994.

[110] D. Schley, S. Whittle, M. Taylor, and I. Z. Kiss. Models to capture the potential for disease transmission in domestic sheep flocks. *Prev. Vet. Med.*, 106:174–184, 2012.

[111] Y. Schwarzkopf, A. Rákos, and D. Mukamel. Epidemic spreading in evolving networks. *Phys. Rev. E*, 82, 2010.

[112] K. J. Sharkey. Deterministic epidemiological models at the individual level. *J. Math. Biol.*, 57:311–331, 2008.

[113] P. L. Simon, M. Taylor, and I. Z. Kiss. Exact epidemic models on graphs using graph automorphism driven lumping. *J. Math. Biol.*, 62:479–508, 2011.

[114] S. H. Strogatz. Exploring complex networks. *Nature*, 410:268–276, 2001.

[115] L. Taylor, S. Latham, and M. Woolhouse. Risk factors for human disease emergence. *Phil. Trans. R. Soc. B*, 356:983, 2001.

[116] M. Taylor, P. L. Simon, D. M. Green, T. House, and I. Z. Kiss. From Markovian to pairwise epidemic models and the performance of moment closure approximations. *J. Math. Biol.*, 64:1021–1042, 2012.

[117] M. Taylor, T. J. Taylor, and I. Z. Kiss. Epidemic threshold and control in a dynamic network. *Phys. Rev E*, 85:016103, 2012.

[118] M. J. Tildesley et al. Optimal reactive vaccination strategies for a foot-and-mouth outbreak in the UK. *Nature*, 440:83–86, 2006.

[119] M. J. Tildesley and M. J. Keeling. Is R_0 a good predictor of final epidemic size: Foot-and-mouth disease in the UK. *J. Theo. Biol.*, 258:623–629, 2009.

[120] P. Trapman. On analytical approaches to epidemics on networks. *Theor. Popul. Biol*, 71:160–173, 2007.

[121] T.W. Valente and R. Fosados. Diffusion of innovations and network segmentation: the part played by people in promoting health. *Sex.Transm.Dis*, 33(7):23, 2006.

[122] M. van Baalen. Pair approximations for different spatial geometries. In Ulf Dieckmann and Richard Law, editors, *The geometry of ecological interactions*, pages 359–387. Cambridge University Press, Cambridge, 2000.

[123] S. van Segbroeck, F.C. Santos, and J.M. Pacheco. Adaptive contact networks change effective disease infectiousness and dynamics. *PLoS Comp. Biol.*, 6:e1000895, 2010.

[124] E. Volz. SIR dynamics in random networks with heterogeneous connectivity. *J. Math. Biol.*, 56:293–310, 2008.

[125] E. Volz and L. A. Meyers. Susceptible-infected-recovered epidemics in dynamic contact networks. *Proc. Roy. Soc. B*, 74:2925–2933, 2007.

[126] E. Volz and L. A. Meyers. Epidemic threshold in dynamic contact networks. *J. Roy. Soc. Interface*, 6:233–241, 2009.

[127] E. Volz, J. C. Miller, A. Galvani, and L. A. Meyers. The effects of heterogeneous and clustered contact patterns on infectious disease dynamics. *PLoS Comput. Biol.*, 7:e1002042, 2011.

[128] D. J. Watts. The "new" science of networks. *Annu. Rev. Sociol.*, 30:243–270, 2004.

[129] D.H. Zanette and S. Risau-Gusmán. Infection spreading in a population with evolving contacts. *J. Biol. Phys.*, 34:135, 2008.